Rapid FTIR analysis for respirable crystalline silica monitoring in coal mines using readily available sampling equipment

Garek C. Elie

Thesis submitted to the faculty of the Virginia Polytechnic Institute and State University in partial fulfillment of the requirements for the degree of

Master of Science

In

Mining Engineering

Emily A. Sarver, Chair

Rohit Pandey

Setareh Afrouz

May 23rd, 2024

Blacksburg, Virginia

Keywords: Respirable, Coal, RCMD, Quartz, Silica, RCS, direct-on-filter, DOF, FTIR, Monitoring, Sampling

Rapid FTIR analysis for respirable crystalline silica monitoring in coal mines using readily available sampling equipment

Garek C. Elie

Technical Abstract

In coal mines, workers can be exposed to respirable coal mine dust (RCMD) in conjunction with respirable crystalline silica (RCS). Overexposure can pose serious health risks, including development of coal workers' pneumoconiosis (CWP) (also known as "black lung"). CWP has the potential to progress to a more consequential form known as progressive massive fibrosis (PMF), for which a dramatic resurgence has been observed among US miners since the early 2000's. Recent rules promulgated by the Mine Safety and Health Administration (MSHA) have lowered the permissible exposure limit (PEL) of RCMD and RCS, but the nuances of dust monitoring are complicated. For RCMD, frequent monitoring is required using the continuous personal dust monitor (CPDM), which enables real time data—but the physical sample collected by the CPDM cannot currently be used for RCS analysis. For RCS monitoring, filter samples are still collected with the traditional coal mine dust personal sampling unit (CMDPSU)—but the standard RCS analysis must be done in a centralized lab and there is considerable lag time between sampling and data availability.

To enable rapid RCS analysis of filter samples, NIOSH has developed a direct-on-filter (DOF) Fourier transform infrared (FTIR) spectroscopy method for use with CMDPSU filter samples. It can be performed in the field with a portable instrument. NIOSH has also developed a compatible software called the Field Analysis of Silica Tool (*FAST*), which simplifies processing of the FTIR spectral data to yield RCS mass results. While not allowed to demonstrate regulatory compliance with the RCS PEL, this method could be quite useful for routine non-regulatory monitoring (e.g., to support research or engineering studies). However, adoption of the method may hinge on a variety of factors such as costs, ease-of-use, and the usability and reliability of generated data. This thesis reports a field study designed to demonstrate how the DOF FTIR method (with *FAST*) might be used by mines with relatively low-cost, off-the-shelf sampling components for the CMDPSU. The field study also demonstrates how the *percentage* of RCS in RCMD (in addition to RCS mass) can be estimated by simply pairing a CPDM with the CMDPSU during sampling. Understanding RCS percentage may be important for a variety of research or engineering applications.

While the DOF FTIR method can work well for CMDPSU samples, it is recognized that RCS analysis of CPDM samples would be ideal. However, the materials and construction of the filter assembly used by the CPDM is not conducive to DOF analysis. As part of an effort to develop a simple method for CPDM sample recovery, redeposition, and analysis by FTIR, the second study in this thesis focused on establishing the recovery procedure—and corrections to account for sample mass and RCS content attributed to any residue sourced from the CPDM filter assembly itself. Using blank CPDM filters and blank CPDM filters spiked with well characterized respirable

dust, results show that the mass and RCS content of the CPDM residue may be quite small. Moreover, using field CPDM samples, results show that dust recovery can be quite high. Taken together, these are promising findings and suggest that a method for RCS analysis of CPDM samples is possible.

Rapid FTIR analysis for respirable crystalline silica monitoring in coal mines using readily available sampling equipment

Garek C. Elie

General Audience Abstract

In coal mines, workers can be exposed to respirable coal mine dust (RCMD) in conjunction with respirable crystalline silica (RCS). Overexposure can pose serious health risks, including development of coal workers' pneumoconiosis (CWP) (also known as "black lung"). CWP has the potential to progress to a more consequential form known as progressive massive fibrosis (PMF), for which a dramatic resurgence has been observed among US miners since the early 2000's. There have been rules and regulations set by the Mine Safety and Health Administration (MSHA) to lower the permissible exposure limits of RCMD and RCS, however dust monitoring can be complicated. RCMD is monitored in real-time using a continuous personal dust monitor (CPDM) by mine operators, but it cannot be currently used to monitor RCS. RCS is monitored using filter sample from a traditional coal mine dust personal sampling unit (CMDPSU), with there being a delay to obtain results due to lab analysis time.

To enable rapid RCS analysis of filter samples, NIOSH has developed a direct-on-filter (DOF) Fourier transform infrared (FTIR) spectroscopy method for use with CMDPSU filter samples. It can be performed in the field with a portable instrument. NIOSH has also developed a compatible software called the Field Analysis of Silica Tool (*FAST*), which simplifies processing of the data to determine RCS results. The first study of this thesis demonstrates the use of portable FTIR with *FAST* to determine RCS masses and concentrations using affordable sampling equipment. Additionally, the study shows how the RCS percentages were estimated with paired CPDMs and CMDPSUs.

Though the method used in the first study works with samples from CMDPSUs, it would be ideal for the analysis to work with samples from CPDMs since they are the prominent type of sampling equipment at coal mines. However, the materials that make-up the CPDM filters interfere with DOF FTIR analysis methods and as a result, cannot be directly used. The second part of this study provides a CPDM sample recovery, redeposition, and analysis procedure. RCS data was determined from CPDM filters with different dust sources. Using blank CPDM filters, potential interference was also corrected in the dust laden samples. From the findings of the study, it suggests that the use of CPDM samples for RCS analysis is possible as there was good dust recovery and little CPDM filter material interference in the analysis.

Acknowledgements

I would like to provide a sincere thank you to my advisor, Dr. Emily Sarver for all of her motivation and guidance in my time at Virginia Tech and for this thesis. Her support has been both invaluable and indispensable in my development to becoming a mining engineer.

A great appreciation must also be extended to Dr. Rohit Pandey and Dr. Setareh Afrouz for their keenness to serve on my committee and for all they have taught me at Virginia Tech to improve my skills and education as a mining engineer.

I am very grateful to August Greth for his encouragement and guidance in my lab experiments, writing, and data analyzation for my thesis. He has always been a great help and a great friend during my time as a master's student.

I am also very grateful to my parents who have provided me with an abundance of support to complete my college degrees and get where I am today.

A thank you must additionally be expressed to the Mine 28 engineers, health and safety team, and miners for their assistance and support in the data collection for this thesis.

Finally, I would like to thank the NIOSH Capacity Building Project [grant number: 75D30119C05529] for providing the funding to complete my thesis work at Virginia Tech.

Table of Contents

Table of Figures

Table of Tables

1 Introduction

1.1 Research Motivation

Occupational exposure to respirable coal mine dust (RCMD) can lead to coal workers' pneumoconiosis (CWP), also known as "black lung", which is a debilitating and irreversible disease. For more than 50 years, Federal regulations have sought to control RCMD exposures in the United States. However, beginning in the late 1990s, there has been an alarming rise in black lung cases—especially in central Appalachia (Hall et al., 2019). For workers with 25 or more years of underground mining tenure in this region, recent data indicates that roughly 4.5% are impacted by the advanced form of CWP, progressive massive fibrosis (PMF). This is the highest prevalence of disease since federal regulations were implemented (Figure 1.1), prompting calls for new research and government actions (National Academies Press, 2018). It is increasingly apparent that this resurgence of disease is, to a large extent, associated with exposure to respirable crystalline silica (RCS) (Hall et al., 2019). RCS is just one constituent of RCMD, and the predominant RCS mineral in coal mines is α-quartz (Ainsworth, 2005).

Figure 1.1: Black lung cases spiked starting around 1980 before falling to its lowest right before 2000. After which, a surge in cases occurs to what was seen around 1970 (Hall et al., 2019).

1.2 Standard RCMD Sampling and Monitoring

Respirable coal mine dust (RCMD) is the fraction of airborne dust in the mine atmosphere that is fine enough to enter the gas exchange region of the lung. For the purposes of sampling and monitoring, this

fraction is usually defined as the particles finer than about 10 µm, with a size distribution following the "respirable convention" (ISO, 1995). Sampling is conducted using a specific size selector (typically a cyclone) operating at a specific flow rate to match the respirable convention. To demonstrate compliance with US regulations, the US Mine Safety and Health Administration (MSHA) defines the sampling equipment and parameters (Lowering Miners' Exposure, 2014). For collection of filter samples—which can be used to determine both RCMD concentration and quartz content (as a proxy for RCS)—the Coal Mine Dust Personal Sampling Unit (CMDPSU) is required. It consists of a personal air sampling pump operating at 2.0 L/min with a 10-mm Dorr Oliver cyclone, and collects the respirable dust particles onto a pre-weighed 37-mm polyvinyl chloride (PVC) filter. For PVC filters collected using the CMDPSU, the sample mass is multiplied by 1.38 to convert to the Mining Research Establishment (MRE) equivalent values (Lowering Miners' Exposure, 2014).

Using a filter sample, the MRE corrected RCMD mass concentration (mg/m^3) can be determined gravimetrically. For compliance samples, the filter is sent to an MSHA-approved lab to measure the post-weight, and then the time-weighted average MRE corrected RCMD concentration is determined per Equation 1:

$$C_{RCMD} = \frac{M_{RCMD}}{T \times F} \times 1000 \left(\frac{L}{min}\right) \qquad \text{Equation 1}$$

where, M_{RCMD} is the MRE corrected respirable dust mass by the 1.38 MRE factor (mg); T is the sampling time (min); and F is the sampling flowrate (L/min).

If quartz analysis is also to be conducted on a compliance sample, following the gravimetric analysis the sample is analyzed by MSHA Method P-7 using infrared (IR) spectroscopy (MSHA P-7, 2013). For this, a low-temperature radio-frequency asher is used to burn the coal and filter matrix, and then the residue is redeposited on a vinyl acrylic copolymer (VAC) filter. The IR analysis of the sample is conducted using a Fourier Transform infrared spectrometer (FTIR), using a spectrum range of 1000 cm^{-1} and 700 cm^{-1} for quantification of quartz and kaolinite. Similarly to the MRE calculation for sample mass, the identified quartz mass from the IR analysis must also be multiplied by the 1.38 factor to be MRE equivalent. Note that kaolinite can interfere with quartz determination, so a correction must be applied before calculating the quartz mass (W_Q) and the quartz percentage of the sample using Equation 2 (MSHA P-7, 2013).

$$Q_{\%} = \frac{M_Q}{M_{RCMD}} \times 100 \qquad \text{Equation 2}$$

Where, M_Q is the MRE corrected quartz mass of the sample by the 1.38 MRE factor (mg) and M_{RCMD} is the MRE corrected respirable dust mass by the 1.38 MRE factor (mg).

As discussed below in more detail, historically, all RCMD sampling for compliance was done using the CMDPSU. However, in 2016, MSHA mandated that mine-operator sampling begin using a continuous personal dust monitor (CPDM) for much of the required RCMD monitoring. This instrument enables near real-time monitoring of RCMD concentration, however the sample it collects cannot be used for quartz analysis by any standard method. Thus, for quartz sampling, filter samples must still be collected by CMDPSUs—and these samples are virtually all collected by MSHA inspectors (i.e., not in tandem with CPDM monitoring by mine operators).

1.3 Overview of Federal RCMD Regulations

The Coal Mine Health and Safety Act of 1969 (CMHSA) first established Federal regulations for the control of airborne respirable coal mine dust (RCMD). The goal of these regulations was to prevent workers from developing disabilities or injuries from CWP. CMHSA went into effect on June 30, 1970, and set the permissible exposure limit (PEL) for RCMD at 3.0 mg/m^3 (National Academies Press, 2018). On December 30, 1972, the original 3.0 mg/m^3 PEL was reduced to 2.0 mg/m^3, and an indirect exposure limit was also set for quartz. As mentioned, quartz is the predominant form of RCS in coal mines (NIOSH, 2002). If the quartz content in RCMD is greater than 5%, the CMHSA requires that the standard PEL is further reduced to effectively achieve a quartz PEL of 0.1 mg/m^3 (100 µg/m^3) (National Academies Press, 2018).

In September of 1995, the National Institute of Occupational Safety and Health (NIOSH) released a criteria document about the occupational exposure to RCMD and RCS (NIOSH, 1995). The document stated that a reduction in the RCMD PEL from the CMHSA-required 2.0 mg/m^3 to 0.5 mg/m^3 would be expected to significantly reduce the risk of damage to lung function in coal mine workers. Nevertheless, considering a variety of other factors, NIOSH recommended that RCMD PEL should be limited to 1 mg/m^3 as a time-weighted average for miners working 10 hours/day in a 40-hour work week. For RCS, NIOSH recommended that PEL should be limited 0.05 mg/m^3 (50 µg/m^3)—so half the effective limit set by CMHSA. Around the same time, the Secretary of Labor also created an *Advisory Committee on the Elimination of Pneumoconiosis Among Coal Mine Workers*. This committee established a report which made several recommendations to MSHA based on the latest recommendations from NIOSH and the best available science at the time. Like the NIOSH criteria document, these recommendations included reduced PELs for RCMD and RCS, and direct regulation of RCS exposure (i.e., rather than continuing to use the indirect approach whereby the effective RCMD limit is determined by quartz content in the dust) (Academies Press, 2018). The report also recommended a balance between exposure monitoring strategies for compliance sampling at coal mines. These strategies were broken down into three categories: Personal Monitoring (on the individual), Occupational Monitoring (designated occupations expected to have the highest exposure risks), and Environmental Monitoring (designated areas in a mine expected to represent exposure environments of interest) (Academies Press, 2018). However, no immediate action was taken.

It was previously seen that when averaging over consecutive shifts, the samples taken by MSHA after the first day were systematically lower in dust. The first-day samples were the only days that MSHA showed up to a mining operation unannounced, and therefore the samples collected on the first day were found to be the most accurate representation of the dust conditions at a mine operation (Weeks, 2003). This developed a joint proposal between NIOSH and MSHA in 2000, which required that compliance sampling for RCMD concentration relied on a single, full-shift sample (i.e., rather than the average of multiple samples, typically collected during consecutive shifts). Simultaneously, development of the continuous personal dust monitor (CPDM) was ongoing, and prototypes were being field tested. But again, no immediate action was taken. In 2010, NIOSH and MSHA established requirements to evaluate any commercialized version of the CPDM (Academies Press, 2018).

In 2014, MSHA promulgated its New Dust Rule, which included several key changes for RCMD exposure standards that were implemented in 2016 (Lowering Miners' Exposure, 2014). First, it reduced the PEL for RCMD from 2.0 to 1.5 mg/m^3. The new rule also limited the RCMD concentration in intake airways

where Part 90 miners are exposed to 0.5 mg/m^3; Part 90 workers are those who have already been diagnosed with CWP and invoked their right under the 1969 CMHSA to be assigned work in a less dusty environment. Importantly, the new rule did not change the indirect PEL for quartz concentration, which remains at 100 µg/m^3.

Regarding RCMD sampling and monitoring, the new dust rule required that compliance sampling is conducted over a full shift of work (rather than 8 hours) and when mine production is at least 80% of its normal production (rather than 50%). Further, for mine-operator monitoring, it mandates that compliance sampling must be conducted using the CPDM and it increased the frequency of that monitoring (i.e., 15 consecutive shifts per quarter on each designated occupation). Training was required to be provided by mine operators to all miners in wearing a CPDM. To be certified in the calibration and maintenance of CPDMs at a mine site, an MSHA course and exam must also be taken (Academies Press, 2018). However, the transition to CPDMs for mine-operator monitoring meant that these samples were no longer used for quartz analysis. Indeed, the sample collected by the CPDM is not compatible with standard methods for quartz analysis. Since 2016, the only quartz sampling is done by mine inspectors. While that sampling is only required on a quarterly basis, MSHA has increased its sampling frequency at some mines (Lowering Miners' Exposure, 2023). Nevertheless, the quartz sampling is not conducted in tandem with the operator RCMD sampling.

Over the past several years, evidence linking the resurgence of CWP and PMF in US miners to RCS exposure has continued to grow (Hall et al., 2019, Cohen et al., 2022, Almberg et al. 2023, Hua et al., 2023). In 2022, pathologic and mineralogical research concluded that RCS exposure has been a primary cause of CWP resurgence (Cohen et al., 2022). While the New Dust Rule appears to be having beneficial impacts on reducing RCMD exposures, the latency of disease means it may be another decade before the effects can be reliably assessed (National Academies, 2018). Thus, there continue to be calls to reduce the RCS (quartz) PEL.

Notably, in 2017 the Occupational Safety and Health Administration (OSHA) reduced the PEL for RCS for general industry from 250 to 50 µg/m^3, measured as an 8-hour time-weighted average (Standard 1910.1053(c)). This has put additional pressure on MSHA to act for the protection of miners, who do not fall under OSHA standards. In 2022, MSHA announced new enforcement efforts related to RCS (MSHA, 2022), and in 2023 the administration published a draft of proposed new RCS standard (Lowering Miners' Exposure, 2023). It would set the quartz PEL for *all* miners to 50 µg/m^3, based on a full shift sample and calculated as an 8-hour time-weighted average. It would also increase the frequency of required quartz sampling—presumably using CMDPSUs to collect filter samples for laboratory analysis. As of April 2024, MSHA issued its ruling to lower the PEL of respirable crystalline silica to its initially proposed 2023 limit of 50 µg/m^3 (Lowering Miners' Exposure, 2024).

1.4 RCS Analysis by Direct-on-Filter FTIR

Parallel to calls for a reduced RCS exposure limit, there has been an impetus to develop improved RCS monitoring capabilities. While real time silica monitoring is certainly the most preferred option, proven technologies are not currently available. However, researchers in the NIOSH Mining Research Division have been working since the early 2000s on a method that uses direct-on-filter (DOF) FTIR spectrometry with a portable instrument (Ashely, 2003, Miller et al., 2012, Cauda et al., 2016). This may prove to be a valuable tool for "end-of-shift" or rapid, on-site analysis of quartz (i.e., as a proxy for RCS). The DOF method uses the same type of filter sample used for Method P-7 (i.e., a 37-mm PVC filter collected using

a CMDPSU), however it does not require filter preparation. This means the analysis can be done in the field. In essence, the PVC filter is placed directly into the portable FTIR and scanned to generate the absorbance spectra; a blank PVC filter is also scanned to enable "blank correction," eliminating any filter interference for the samples that do contain dust. The method has been designed to use a single scan (6-mm) in the center of the filter.

NIOSH's Field Analysis of Silica Tool (*FAST*) software was developed to be paired with portable FTIR to simplify and standardize data analysis (Cauda et al., 2018). The software is freely accessible online, such that anyone can process FTIR spectral data, given compatible file formats. The absorbance spectra from the FTIR are downloaded into a CSV file template, which is input into *FAST*. Shown in Figure 1.2, there are eight different models available in *FAST*; and the user should select the model which matches their conditions (i.e., cyclone, cassette, flow rate). Each model uses a unique calibration factor to essentially extrapolate the spectral peak areas measured on a single, center scan on the sample filter to predict quartz mass for the entire filter. The model calibration factors vary based on characteristic dust deposition patterns yielded by specific sampling conditions. In addition to inputting FTIR spectral data for each sample, *FAST* has input fields for sampling flow rate, duration, filter size and sample weight (if measured). *FAST* can return quartz mass (µg) based only on the FTIR spectral data and model factor; but it can also return MRE corrected quartz mass concentrations (µg/m^3) if the sampling time and flowrate, and appropriate sampling model are entered per Equation 3:

$$C_Q = \frac{M_Q}{T \times F} \times 1000 \left(\frac{L}{min}\right) \qquad \text{Equation 3}$$

where, M_Q is the MRE corrected quartz mass by the 1.38 MRE factor (µg); T is the sampling time (min); and F is the sampling flowrate (L/min).

In addition to enabling end-of-shift quartz measurement, the DOF FTIR method could also support a wide range of research and engineering studies. However, to use *FAST* for data analysis, it important to consider the sampling conditions. Of the eight models currently included in *FAST*, only two were established for RCMD sampling: (1) the 'CMDPSU with coal dust sampling cassette', and (2) the 'CMDPSU with conductive four-piece cassette'. Both of these models use 10-mm nylon (Dorr Oliver) cyclones which are standard for RCMD sampling and incorporate the standard MRE correction to match the approach of Method P7; but they were developed for use with sampling cassettes that might not be practical or preferable for some applications. The 'coal dust sampling cassette' is sometimes referred to as an 'MSA cassette' based on the historical vendor, Mine Safety Appliances (Pittsburgh, PA). This cassette type was specifically designed for compliance RCMD and quartz sampling in coal mines, and is still required by MSHA for this purpose, but it is not commonly used otherwise—presumably due to expense and to avoid confusion between sampling for compliance and other purposes. The 'four-piece cassette' was designed for use with the DOF FTIR method to maximize predictability of the dust deposition pattern on the filter (Chubb et al., 2021), however these cassettes are only available from a single vendor and are still relatively expensive. For research and engineering studies or other non-compliance purposes, generic cassettes which are inexpensive and widely available may be preferred—so long as their deposition pattern is also predictable.

The deposition pattern of respirable dust onto the filter can be influenced by cassette type, pump flow rate, and the type of cyclone-cassette connection used. The cassette type used creates differences in deposition pattern as well as deposition consistency such as in the contrast of coal dust sampling

cassettes and three-piece cassettes. Three-piece cassettes had more predictable and radial deposition patterns compared to the coal dust sampling cassettes (Pampena et al., 2020). Additionally, cyclones using couplers that wrap around the cassette inlet as a connection deposit dust in a wider area on the filter, whereas cyclones using a built-in-fitting that is inserted into the cassette inlet as a connection have a more center-heavy dust deposition. A cyclone-cassette connection using a coupler does not have as strong of a hold as one with a built-in-fitting, and therefore data collection with the built-in-fittings could be useful due to its security.

Figure 1.2: *FAST* software sampling cyclones.

Depending on the application, the ability to estimate quartz content (mass percentage) in an RCMD sample might also be important. As discussed above, the quartz content of RCMD has historically been the metric on which indirect regulation of quartz exposures has been based. Thus, for mine operators and others working in RCMD sampling and monitoring, there may be considerable reference data available. Moreover, quartz content could also be of value in efforts to correlate RCMD composition with geology or mining conditions, or studies to evaluate the effectiveness of dust controls. In any case, to determine quartz content from the PVC filter sample, both the quartz mass and the total RCMD sample mass must be measured (i.e., Equation 2). The DOF FTIR method can only measure quartz mass. Traditionally a microbalance is used to measure the RCMD sample mass (i.e., as described for the MSHA Method P7), but this sort of equipment is not portable and therefore unlikely to be present outside of a centralized laboratory. An alternative approach could be to pair a CPDM with the CMDPSU during sampling. In essence, the CPDM's accumulated mass data (i.e., from the time interval corresponding to the PVC filter sample collection with the CMDPSU) could be used to yield an estimate for the CMDPSU's RCMD sample mass per Equation 4:

$$M_{RCMD\_CPDM} = M_{CPDM-2} - M_{CPDM-1} \qquad \text{Equation 4}$$

where, M_{CPDM-2} is the CPDM filter mass at time 2 (mg), and M_{CPDM-1} is the CPDM filter mass at time 1 (mg).

Notably, since the CPDM was designed to match the CMDPSU in terms of RCMD mass concentration, Equation 4 must include the MRE factor. Further, using the CMDPSU sampling time and respective

flowrates for both samplers, Equation 5 could be used to estimate the RCMD mass concentration for the PVC filter sample.

$$C_{RCMD\_CPDM} = \frac{M_{RCMD\_CPDM}}{T \times F} \times 1000 \left(\frac{L}{min}\right) \qquad \text{Equation 5}$$

Where, M_{RCMD_CPDM} is the accumulated CPDM dust mass (mg); T is the sampling time (min); and F is the flowrate (L/min).

With an estimate of RCMD sample mass per Equation 4 or mass concentration per Equation 5, and quartz mass or mass concentration from the *FAST* output, Equation 6 or 7 could be applied to estimate quartz content. However, this approach has not yet been demonstrated in the field. Equation 2 could still be applied.

$$Q_{\%\_est} = \frac{M_Q}{M_{RCMD\_CPDM}} \times 100 \qquad \text{Equation 6}$$

Where, M_Q is the MRE corrected quartz mass by the 1.38 MRE factor (mg) and M_{RCMD_CPDM} is the accumulated CPDM dust mass (mg).

$$Q_{\%-est} = \frac{C_Q}{C_{RCMD\_CPDM}} \times 100 \qquad \text{Equation 7}$$

Where, C_Q is the MRE corrected quartz concentration by 1.38 factor (mg/m^3), and C_{RCMD_CPDM} is the estimated RCMD concentration from the CPDM accumulated mass (mg/m^3).

1.5 Toward Future Rapid RCS Analysis of CPDM Samples

As explained earlier, one effect of the 2014 'New Dust Rule' has been that mine-operator compliance sampling for RCMD has transitioned from using CMDPSUs to using CPDMs. Since most mine-operator sampling is for compliance purposes, many mines do not even still have or maintain CMDPSU samplers. This is an obvious challenge for adoption of the rapid RCS analysis by DOF FTIR as described above. However, if the FTIR method could be adapted for use with CPDM samples, it would enable the CPDM to be used for both RCMD and quartz monitoring.

The primary hindrance of FTIR analysis of CPDM samples is due to the composition and construction of the filter stubs used by the CPDM instrument. They consist of a borosilicate fiberglass and polytetrafluoroethylene (PTFE) filter with woven glass backing (Chow et al., 2022), which is mounted to a polypropylene (PP) stub. The filter materials directly interfere with the IR spectra peaks of quartz, and the filter cannot be easily detached from the stub. Indeed, studies of direct FTIR analysis on the CPDM filters/filter assemblies using absorbance and diffuse reflectance have demonstrated the interference problem (Tuchman, 2008).

However, until now, there are no reports of attempts to perform FTIR analysis on dust recovered from the CPDM. One possible method could include dust recovery and redeposition onto a suitable substrate (e.g., PVC). To develop such a method, a range of experimental work is required to establish reliable procedures for the dust recovery, redeposition, and FTIR scanning—as well as accurate models for converting the raw FTIR spectral data to quartz mass. One important element of this work is understanding the potential for interference from any contamination attributed to the CPDM filter stub itself (i.e., which could be recovered along with the dust sample). If a sample recovery procedure can be developed which yields minimal—or at least predictable—CPDM residue mass and composition, then

the issue of possible interference can be addressed or accounted for in the FTIR spectra-to-quartz mass model.

1.6 Thesis Scope

Portable FTIR could be a powerful new tool for rapid, onsite analysis of RCS (quartz). NIOSH has fully developed a standardized method for end-of-shift analysis using DOF FTIR, which includes a user-friendly software called *FAST* for data analysis. However, to make the method more practical for research and engineering studies, two key issues need to be addressed:

- *FAST*'s underlying models for determining quartz in RCMD have been developed for specific sampling conditions—i.e., combination of specific cyclone and cassette used at a specific flowrate. However, *FAST*'s models are limited to two conditions which might not be practical for research and engineering studies, because the required cassettes tend to either only be used for compliance sampling and/or are relatively expensive.
- Moreover, the FTIR can measure quartz mass on an RCMD sample, but an understanding of quartz content (mass percentage) might be more valuable for research and engineering studies. This requires a complementary measurement of RCMD sample mass.

Using a field study, the objective of Chapter 2 was to demonstrate how both issues can be addressed. CMDPSU sampling was conducted with generic 3-piece cassettes, which are widely available and inexpensive in comparison to the four-piece cassettes. All samples were analyzed by DOF FTIR, and a subset was sent off for analysis by the standard NIOSH Method 7603 (i.e., analogous to MSHA Method P7). This enabled the development of correction factor for *FAST*-derived quartz values. Moreover, the CMDPSU samplers were paired with CPDMs, and the CPDM data was used as a proxy to estimate the CMDPSU sample masses. When combined with the DOF FTIR measurements of quartz mass, this enabled estimation of quartz percentage on the CMDPSU samples.

DOF-FTIR analysis requires PVC filters, which are paired with CMDPSUs. The transition towards CPDMs for RCMD monitoring has resulted in a lack of CMDPSUs availability at mines, with the CPDMs using borosilicate fiberglass filters for dust collection within the unit. These filters interfere with current IR analysis for quartz by creating false positives, and thus cannot currently be used for DOF-FTIR analysis as a result.

The purpose of Chapter 3 was to identify a redeposition process paired with DOF-FTIR to address the CPDM filter material interference during analysis. A series of blank CPDM filters were placed into test tubes with isopropyl alcohol (IPA) and shaken on a shaker table to remove material from the filters. The IPA mixed with CPDM filter material was then redeposited onto 25-mm PVC filters for DOF-FTIR analysis. Based on the masses of CPDM filter residue and quartz mass found on the 25-mm filters, a potential correction for CPDM filter interference of field samples redeposited in the same manner could be applied. Estimation of quartz in mine field samples may then be possible using DOF-FTIR analysis.

1.7 References

Hall, N. B., Blackley, D. J., Halldin, C. N., & Laney, A. S. (2019). Current review of pneumoconiosis among US coal miners. *Current environmental health reports*, *6*, 137-147.

National Academies of Sciences, Medicine Division, Division on Earth, Life Studies, Board on Health Sciences Policy, Board on Environmental Studies, ... & Committee on the Study of the Control of Respirable Coal Mine Dust Exposure in Underground Mines. (2018). Monitoring and sampling approaches to assess underground coal mine dust exposures.

Ainsworth, S. M. (2005). *Infrared analysis of respirable coal mine dust for quartz: thirty-five years*. ASTM International.

International Standard ISO. (1995). ISO 7708 Air Quality – Particle size fraction definitions for health-related sampling. https://www.iso.org/standard/14534.html

Lowering Miners' Exposure to Respirable Coal Mine Dust, Including Continuous Personal Dust Monitors, 79 F.R. 24814-24994 (May 1, 2014). https://arlweb.msha.gov/regs/fedreg/final/2014finl/2014-09084.asp

Department of Labor, Mine Safety and Health Administration. (2013). Infrared Determination of Quartz in Respirable Coal Mine Dust, MSHA Method P-7. https://arlweb.msha.gov/Techsupp/pshtcweb/MSHA%20P7.pdf

NIOSH (2002). Health effects of occupational exposure to respirable crystalline silica.

NIOSH (1995). Criteria for a Recommended Standard: Occupational exposure to respirable coal mine dust.

Weeks, J. L. (2003). The fox guarding the chicken coop: monitoring exposure to respirable coal mine dust, 1969–2000. *American Journal of Public Health*, *93*(8), 1236-1244.

Lowering Miners' Exposure to Respirable Crystalline Silica and Improving Respiratory Protection, 88 F.R. 54961 (August 14, 2023). https://www.federalregister.gov/documents/2023/08/14/2023-17370/lowering-miners-exposure-to-respirable-crystalline-silica-and-improving-respiratory-protection#:~:text=On%20July%2013%2C%202023%2C%20MSHA,Protection%20(88%20FR%2044852).

Cohen, R. A., Rose, C. S., Go, L. H., Zell-Baran, L. M., Almberg, K. S., Sarver, E. A., ... & Green, F. H. (2022). Pathology and mineralogy demonstrate respirable crystalline silica is a major cause of severe pneumoconiosis in US coal miners. *Annals of the American Thoracic Society*, *19*(9), 1469-1478.

Almberg, K. S., Halldin, C. N., Friedman, L. S., Go, L. H., Rose, C. S., Hall, N. B., & Cohen, R. A. (2023). Increased odds of mortality from non-malignant respiratory disease and lung cancer are highest among US coal miners born after 1939. *Occupational and environmental medicine*, *80*(3), 121-128.

Hua, J. T., Zell-Baran, L. M., Moore, C. M., & Rose, C. S. (2024). Racial Differences in Respiratory Impairment, Pneumoconiosis, and Federal Compensation for Western US Indigenous Coal Miners. *Annals of the American Thoracic Society*, *21*(4), 551-558.

Mine Health and Safety Administration. (2022). *Silica Enforcement Initiative*. https://www.msha.gov/safety-and-health/safety-and-health-initiatives/2022/06/08/silica-enforcement-initiative

Lowering Miners' Exposure to Respirable Crystalline Silica and Improving Respiratory Protection, 89 F.R. 28218-28485 (April 18, 2024). https://www.federalregister.gov/documents/2023/08/14/2023-17370/lowering-miners-exposure-to-respirable-crystalline-silica-and-improving-respiratory-protection#:~:text=On%20July%2013%2C%202023%2C%20MSHA,Protection%20(88%20FR%2044852).

Ashley, K. (2003). Field-portable spectroscopy. *Applied Occupational and Environmental Hygiene*, *18*(1), 10-15.

Miller, A. L., Drake, P. L., Murphy, N. C., Noll, J. D., & Volkwein, J. C. (2012). Evaluating portable infrared spectrometers for measuring the silica content of coal dust. *Journal of Environmental Monitoring*, *14*(1), 48-55.

Cauda, E., Miller, A., & Drake, P. (2016). Promoting early exposure monitoring for respirable crystalline silica: Taking the laboratory to the mine site. *Journal of occupational and environmental hygiene*, *13*(3), D39-D45.

Cauda, E., Chubb, L., Britton, J., Fritz, J., & Cole, G. (2018). *CDC - Mining - FAST - Field Analysis of Silica Tool - NIOSH*. Centers for Disease Control and Prevention. https://www.cdc.gov/niosh/mining/works/coversheet2056.html

Chubb, L. G., & Cauda, E. G. (2021). A novel sampling cassette for field-based analysis of respirable crystalline silica. *Journal of occupational and environmental hygiene*, *18*(3), 103-109.

Pampena, J. D., Cauda, E. G., Chubb, L. G., & Meadows, J. J. (2020). Use of the field-based silica monitoring technique in a coal mine: A case study. *Mining, metallurgy & exploration*, *37*(2), 717-726.

Chow, J. C., Watson, J. G., Wang, X., Abbasi, B., Reed, W. R., & Parks, D. (2022). Review of filters for air sampling and chemical analysis in mining workplaces. *Minerals*, *12*(10), 1314.

Tuchman, D. P., Volkwein, J. C., & Vinson, R. P. (2008). Implementing infrared determination of quartz particulates on novel filters for a prototype dust monitor. *Journal of environmental monitoring*, *10*(5), 671-678.

2 Chapter 2: Direct-on-filter FTIR analysis of respirable crystalline silica: a field study to demonstrate utility for routine non-regulatory monitoring in coal mines

Garek Elie, Emily Sarver

2.1 Abstract

Miners are exposed to respirable coal mine dust (RCMD) in combination with respirable crystalline silica (RCS) which can lead to debilitating health risks. Mine operators lack the technology for efficient non-regulatory quartz monitoring for on-site analysis. The use of direct-on-filter (DOF) Fourier transform infrared (FTIR) analysis provides a potential rapid, end-of-shift quartz analysis for research or engineering studies by mine operators. Paired with the Field Analysis of Silica Tool (*FAST*) developed by the National Institute of Occupational Safety and Health (NIOSH), inexpensive sampling equipment can be used to determine quartz mass and quartz concentration. A subset of sample filters can be sent to a contract lab to undergo a NIOSH Method 0600 and NIOSH Method 7603 study, with the resulting dust and quartz data used to calibrate the DOF FTIR results at a mine. The use of a coal mine dust personal sampling unit (CMDPSU) paired with a continuous personal dust monitor (CPDM) could provide alternative weighing methods for dust mass in the determination of quartz percentages when a microbalance is not available.

2.2 Introduction

Respirable crystalline silica (RCS) is a serious yet ubiquitous hazard in many occupational environments. In coal mines, RCS is one of many constituents of the total respirable coal mine dust (RCMD) (Sarver et al., 2021), and it predominantly presents as α-quartz (termed "quartz" from here) (NIOSH, 2002). RCS has been linked to resurgence of disease in US coal mine workers (Hall et al., 2019, Cohen et al., 2022). Federal monitoring data suggests RCS levels have been gradually declining in coal mines (Lowering Miners' Exposure, 2024), especially since the US Mine Safety and Health Administration (MSHA) reduced the personal exposure limit for RCMD and mandated new monitoring technology as part of a 2014 rule (Lowering Miners' Exposure, 2014). However, to better protect workers in all US mining sectors, MSHA recently published a 'new RCS rule' which lowers the personal exposure limit. The new limit is 50 $\mu g/m^3$ for a full work shift, calculated as an 8-hr time-weighted average (TWA).

Currently, RCS is monitored in coal mines by collecting RCMD filter samples and sending them to a certified lab for analysis of quartz (Figure 2.1); and this will continue to be the approach for regulatory monitoring under MSHA's 'new RCS rule'. Briefly, the procedure can be summarized in the following steps: First, the filter (37-mm polyvinyl chloride, PVC, with nominal 5 µm pore size) is pre-weighed. This requires a sensitive microbalance in the laboratory, and in most cases pre-weights are measured by the filter vendor, prior to loading the filter (and filter support) into the sampling cassette. Then, the RCMD sample is collected in the field, typically using a coal mine dust personal sampling unit (CMDPSU). The CMDPSU consists of an air pump with a cyclone pre-selector (to remove oversized particles) to pull the respirable dust directly onto the filter housed within a closed cassette. For compliance RCS sampling in US coal mines, a 10-mm nylon cyclone (Dorr-Oliver type) is required with a sampling flow rate of 2.0 L/min. The sampling time is recorded, such that the total volume of air sampled can be determined. Next, the sample is sent to a lab for analysis. This includes post-weighing the filter to enable determination of total RCMD sample mass, and then analysis by a standard Fourier transform infrared (FTIR) method to determine quartz mass[1]. Using the quartz mass and sampled air volume, the quartz concentration can be computed; and the same can be done to determine RCMD mass concentration. Finally, using the ratio of the quartz and RCMD concentrations, the quartz percentage can be computed.

[1] For monitoring in US coal mines, both RCMD mass and quartz mass are multiplied by a factor of 1.38 to determine 'MRE equivalent' values. This convention stems from the fact that coal mine dust regulations in the US were historically based on data derived from sampling with an MRE sampler (i.e., which was designed by the Mining Research Establishment). The MRE sampler collects a slightly different size fraction of dust than the CMDPSU samplers approved for compliance sampling in US mines, so CMDPSU measurements are corrected to be MRE-equivalent (see Tomb, *et al.*, 1973).

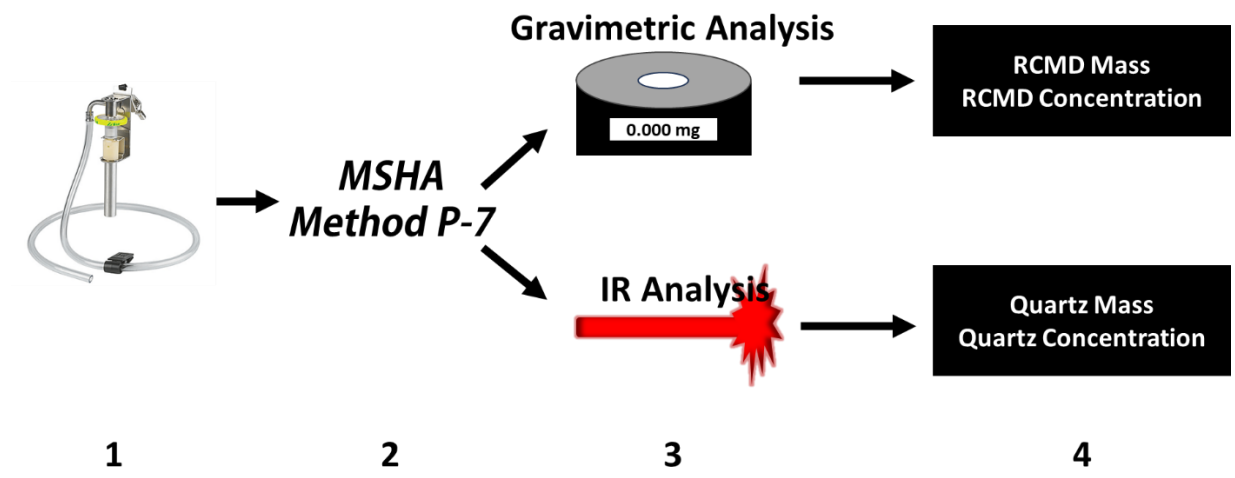

Figure 2.1: Sample collection and analysis process. Samples are collected using the CMDPSU with coal mine dust cassette (1) (image taken from Zefon.com) and sent to a contract lab to be analyzed (2). In the MSHA Method P-7, the filter undergoes a gravimetric and infrared (IR) analysis (3). From the gravimetric analysis, the RCMD mass and RCMD concentration is determined, while the IR analysis provides the quarts mass and quartz concentration of the sample (4).

Notably, the standard methods for quartz analysis of coal mine samples—MSHA Method P7 for regulatory compliance sampling and/or NIOSH Method 7603 for non-regulatory sampling—require careful preparation of the sample prior to the FTIR analysis. The preparation involves ashing the sample to remove the filter and combustible material, and then the residue is redeposited for the FTIR analysis (MSHA P-7, 2013, NIOSH, 2020). In all, the time from sampling to results may be days to weeks. Not only is this unfavorable for correcting overexposures indicated by personal samples, it is also unfavorable for routine monitoring to support engineering work (e.g., to track RCS trends with mining conditions, evaluate controls, etc.) Moreover, the standard analysis is relatively expensive. The net result is that, at present, RCS monitoring is typically limited to that which is required for regulatory compliance. However, especially considering the implications of the 'new RCS rule', there is both a need and desire to do more.

2.2.1 RCS Analysis by Direct-on-filter FTIR

While real time RCS monitoring would be ideal, there are currently no proven technologies for this in coal mines (National Academies Press, 2018). However, NIOSH has developed and standardized a method for direct-on-filter (DOF) spectroscopy FTIR analysis (NIOSH, 2022, Miller et al., 2012, Cauda et al., 2016, Ashley et al., 2020) (Figure 2.2). It uses the same type of filter sample that would be collected for the lab-based analysis described above—but if the DOF method is done with a portable FTIR spectrometer, it can enable rapid and field-based analysis. Further, NIOSH has developed a free software called the *Field Analysis of Silica Tool* (*FAST*) to simplify data processing (Cauda et al, 2018). In essence, *FAST* takes the user-inputted FTIR spectrum and sampling conditions (i.e., target flowrate, cyclone/cassette combination) and outputs the computed quartz mass; with user-inputted sampling time and flowrate, the quartz mass concentration is also output. However, since weighing the sample filter in the field is not practical (i.e., microbalance is not available), the quartz percentage cannot be directly determined.

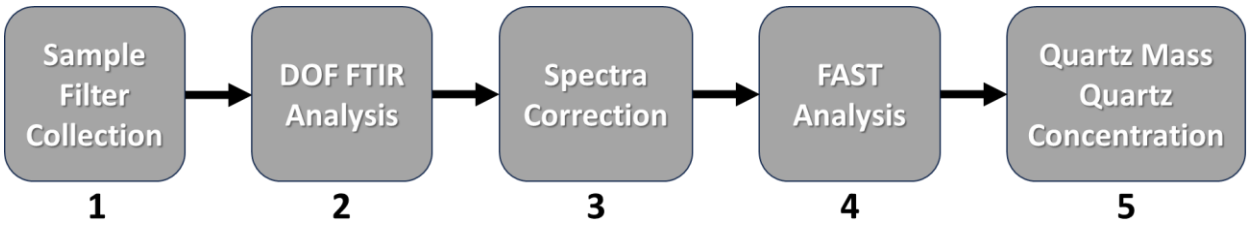

Figure 2.2: Sample analysis process using NIOSH's DOF FTIR method. Sample collection is first performed using sampling equipment (1). The filter is then placed into the portable FTIR (2) and a scan of the filter is performed with a correction applied to the spectra (3). Following the scanning procedure, the data is imported into NIOSH's *FAST* software (4) which calculates the quartz masses and quartz concentrations of the sample based on the spectra file as well as the sampling equipment and conditions (5).

Importantly, for DOF analysis, sampling conditions are important for translating the FTIR spectral results to quartz mass. To explain: the analysis is conducted on a small, central area of the filter, but the result must be extrapolated across the entire filter area (Miller et al., 2013, NIOSH, 2022, Cauda et al., 2016, Ashley et al. 2020). The extrapolation model is dependent on the expected dust deposition pattern, which is dependent on the geometry of the cassette and inlet airflow conditions (i.e., sampling flow rate and the effective inlet diameter, which depends on how the cassette is connected to the cyclone pre-selector). Thus, for accurate quartz measurements using the DOF FTIR method, the extrapolation model must be specific to the sampling conditions.

With an eye toward eventual capabilities for end-of-shift personal RCS monitoring in coal mines, NIOSH has developed and included in *FAST* two models for RCMD samples collected with CMDPSUs (Figure 2.3). One is for use with traditional coal mine sampling cassettes (Figure 2.3a, sometimes called 'MSA' cassettes due to the historical vendor), which are the type used by MSHA for compliance RCS sampling. The other model is for use with a special 4-piece conductive cassette (Figure 2.3b), which NIOSH specifically designed for the DOF FTIR analysis (Chubb et al., 2021). Notably, both models include the MRE-equivalency conversion, and both assume the cassette was connected to the cyclone using a holder assembly that includes a coupler. (This is sometimes referred to as the "mining" or "IH" style holder assembly as shown in Figure 2.3d and Figure 2.3e, respectively.)

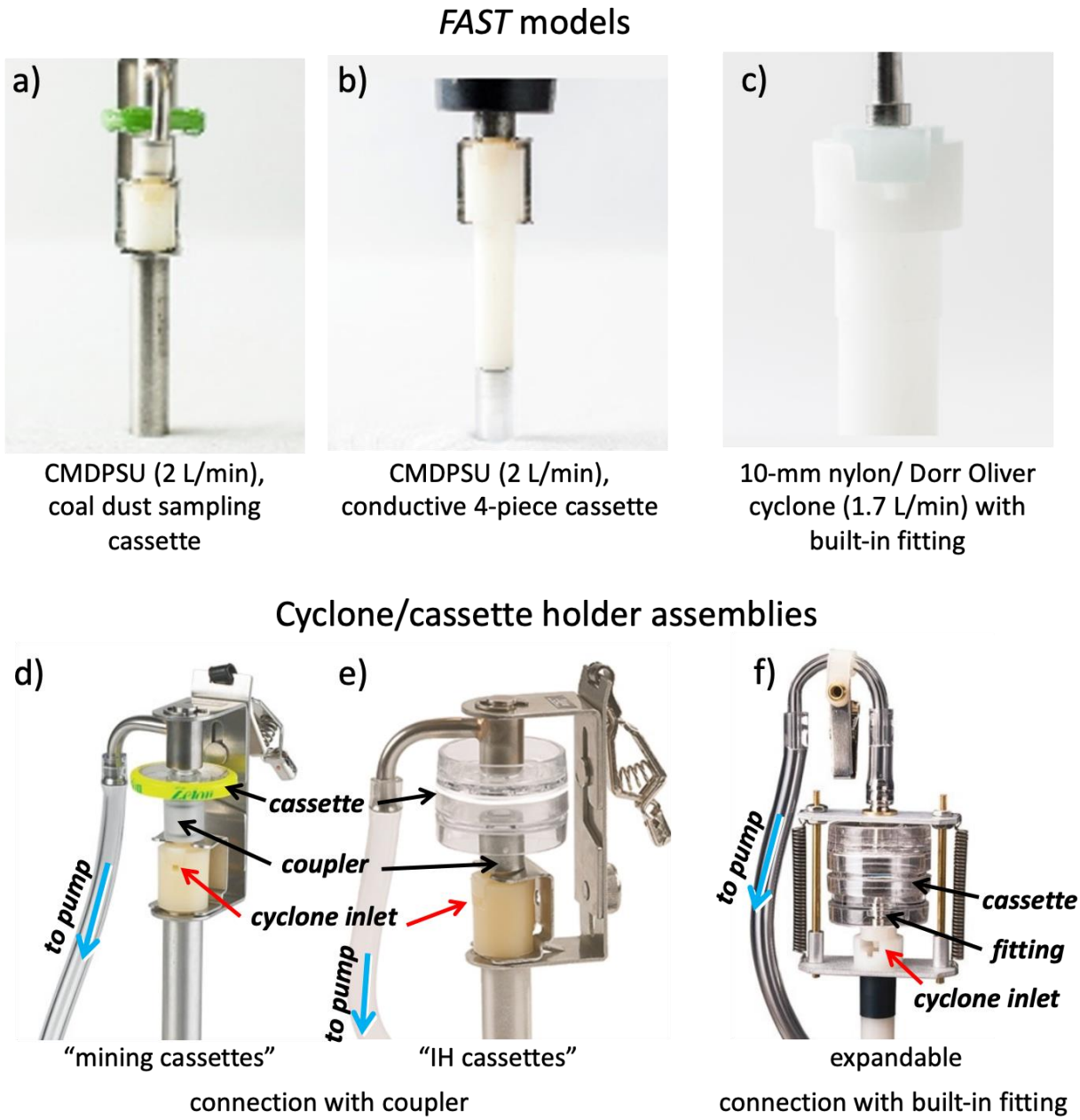

Figure 2.3: Example respirable mine dust sampling cyclone and cassette combinations; all combinations use a 10-mm Dorr Oliver cyclone, but they differ in terms of the cassette and cyclone-cassette assembly. The top row shows combinations that have been modeled in NIOSH's Field Analysis of Silica Tool (*FAST*) (images taken as screenshots from the *FAST* user interface), and the bottom row shows standard cyclone-cassette assemblies (images taken from Zefon.com). For coal mine dust (sampled at 2.0 L/min), the *FAST* models assume a cyclone-cassette assembly that uses a coupler: Model a) is for a 'coal dust sampling cassette', which would be sampled using the assembly shown in d). Model b) is for a special 4-piece conductive cassette, which presumably would be sampled with a modification of the assembly shown in e); per photos in Chubb et al. (2021), which details design of the cassette, it appears the top of the holder assembly would be removed to accept the height of the 4-piece cassette. *FAST* also includes Model c) for a cyclone-cassette assembly with a built-in fitting instead of the coupler (i.e., as shown in e), which can fit a 3- or 4-piece cassette), however the assumed sampling flow rate is 1.7 L/min. (Note: the *FAST*-output quartz mass is MRE-equivalent for Models a) and b), but not for c).)

Pampena et al. (2020) field tested the DOF FTIR method with the coal mine sampling cassettes and found variable accuracy (against MSHA Method P7 as reference), which was attributed to variable dust deposition pattern on the sample filter. This finding was consistent with earlier findings by Miller et al. (2013). On the other hand, the 4-piece cassette yields a reproducible deposition pattern, with heavier loading in the filter center that gradually dissipates radially toward the filter edge (Chubb et al., 2021). This pattern enables an accurate extrapolation model. Moreover, the 4-piece design of the cassette enables the DOF FTIR analysis with minimal sample handling due to two main features. First, the filter support is a stainless steel ring, which is fully open in the center to allow FTIR beam transmission. Second, the filter and support are sandwiched between the middle two pieces of the cassette, such that this assembly can serve as the filter holder during FTIR analysis; the top and bottom (outer) pieces can simply be removed. Though the 4-piece design doesn't require filter handling by the user, a study by Miller et al. (2017) utilized coal dust sampling cassettes and handled the filters to be placed into a stainless steel holder, similar to that used in this study for FTIR analysis.

2.2.2 Considerations for Routine Non-regulatory Monitoring

While the DOF FTIR method has primarily been considered in the context of personal RCS exposure monitoring, application for environmental monitoring is a more likely entry point for coal mines. To gain experience and confidence with this new capability, mines might want to use it for routine non-regulatory monitoring, for example in fixed or standardized locations to track RCS trends with operational or geological conditions, or to evaluate dust controls. For these sorts of applications, data utility and costs are obvious considerations.

With respect to data, one issue could be the inability to directly determine quartz percentage using the DOF FTIR method. As noted, this metric is readily determined with standard lab analysis of RCMD filter samples (i.e., because the filter is weighed prior to preparation for the quartz analysis by FTIR). Thus, most coal mines have considerable knowledge of the typical quartz percentages in their RCMD, and this data could be quite useful for a range of engineering purposes (e.g., to evaluate RCS generation from various geological features). However, the DOF FTIR method only determines quartz mass (and mass concentration). While it is impractical to weigh the filter sample in the field, an alternative approach could be to estimate the RCMD sample mass by pairing the CMDPSU with a continuous personal dust monitor (CPDM) during sampling. The CPDM was developed, and is now mandated, for RCMD monitoring in US coal mines. In essence, it tracks (MRE-equivalent) mass concentration on 1-minute intervals over its entire sampling period. Thus, if a CPDM is paired with the CMDPSU, the quartz percentage could be estimated using the quartz concentration derived from DOF FTIR analysis of the filter sample and the CPDM's RCMD concentration.

Regarding costs, adoption of the DOF FTIR method represents an investment. In terms of equipment, a portable FTIR spectrometer is needed, though operators with multiple mines might consider a single instrument that could be shared across sites. Other equipment costs should be limited to CMDPSUs (and perhaps related calibration accessories), which some mines may still own since these samplers were required for RCMD compliance monitoring prior to implementation of the CPDM in 2016. (Lowering Miners' Exposure, 2014). For consumables, sampling supplies (i.e., cassettes, filters and filter supports) are expected to be the main costs. While the special 4-piece conductive cassettes have been designed to minimize sample handling, mines could opt to use generic 3-piece styrene cassettes for routine non-regulatory monitoring. This option would require sample handling since the filter cannot be scanned while still inside the cassette; but, at the time of publication, 3-piece cassettes were about 7× less

expensive than the 4-piece cassettes[2]. Notably, the 3-piece cassettes were the basis of NIOSH's early work to develop the DOF FTIR method (e.g., see Miller et al., 2013). They have essentially the same deposition pattern (and pattern reproducibility) as the special 4-piece cassette (Chubb et al., 2021), and therefore the *FAST* model for coal mine samples collected with a 4-piece cassette should also be accurate for samples collected with a 3-piece cassette—so long as the same cyclone-cassette holder assembly is used.

Indeed, the cyclone-cassette holder type is a critical parameter for the DOF FTIR data analysis. As mentioned, the *FAST* model for use with 4-piece cassettes assumes that sampling was conducted with a CMDPSU with the IH style holder that uses a coupler to connect the cyclone and cassette (Figure 2.3e); the coupler is like a sleeve that fits around the outside diameter of the cyclone outlet and cassette inlet, thereby enabling airflow through the full diameter of the cassette inlet tube. However, this particular cyclone-cassette holder, as designed, is not compatible with the 4-piece cassette—and can even be challenging to use with a 3-piece cassette. This is because, as shown in Figure 2.3e (with a 2-piece cassette), the holder uses a metal frame to secure the cyclone-cassette connection. However, the height of the 4-piece cassette is too tall to fit within the frame, and a 3-piece cassette does not fit easily. Thus, the assembly would either require modification or the cassette would be unsecured (i.e., with top portion of frame removed). An alternative option is shown in Figure 2.3f, which is an assembly with a spring-enabled expandable frame that can easily fit the 4- or 3-piece cassette to secure it. As designed though, this holder assembly uses a built-in fitting to connect the cyclone outlet to the cassette inlet. Since the fitting goes inside the cassette inlet tube, it effectively reduces the airflow diameter and thereby increases the velocity, which can alter the dust deposition pattern on the sample filter. NIOSH has included a model in *FAST* to cover this condition for samples collected at 1.7 L/min (see Figure 2.3c), which would be appropriate for metal/nonmetal mine samples (note that data output is not MRE-equivalent). However, there is no model in *FAST* to cover this condition at 2.0 L/min for coal mine dust samples.

Based on the motivations described above, the aim of this field study was to demonstrate the DOF FTIR method for RCS monitoring in coal mines, specifically using (a) low-cost yet practical consumables (i.e., pre-loaded 3-piece styrene cassettes), (b) cassette-cyclone holder assemblies that can be used off-the-shelf, as-designed (i.e., the expandable type shown in Figure 2.3e), and (c) paired CPDM instruments to enable estimation of quartz percentage (in addition to quartz mass).

[2] From Zefon International (Ocala, FL), which manufacturers the 4-piece cassettes: for pre-loaded cassettes (37 mm PVC filter and support), styrene 3-piece cassettes were just under $2/each ($94.50 per box of 50), whereas conductive 4-piece cassettes were just under $14/each ($138 per box of 10).

2.3 Methods and Materials

2.3.1 Mine sampling

This field study was conducted in an underground room and pillar mine (called "Mine 28" from here) located in the Illinois coal basin. At the time of sampling, Mine 28 was producing coal from the Indiana V seam. Sampling was conducted in two different sections (MMU1 and MMU3), both of which had 11 entries and operated with a split air, blowing ventilation design. In general, the roof strata in MMU1 consisted of highly fractured shale, whereas the roof in MMU3 was a structurally stronger limestone.

Dust sampling was conducted during 10 separate events (Table A1); each event refers to sampling in a particular MMU on a particular day. For each event, relative heights of coal and roof rock being mined in the section were recorded, and airflow quantities were estimated in each sampling location based on airway dimensions and velocities measured using a 4-inch anemometer (Davis, Hayward, CA). Production was at typical levels for Mine 28 during all events (i.e., there was not significant downtime of equipment).

Events 1, 2, 6, and 9 were conducted in MMU1 and Events 3, 4, 5, 7, 8, and 10 were conducted in MMU3. During each event, samples were simultaneously collected in standardized locations (Figure 2.4). In all events, Location 1 was in the return of the continuous miner and Location 2 was in the section return (last open crosscut in the return entry). In Events 1 and 2, samples were collected in two additional locations; Location 3 was in the return of the roof bolter (upwind the continuous miner) and Location 4 was in the section intake.

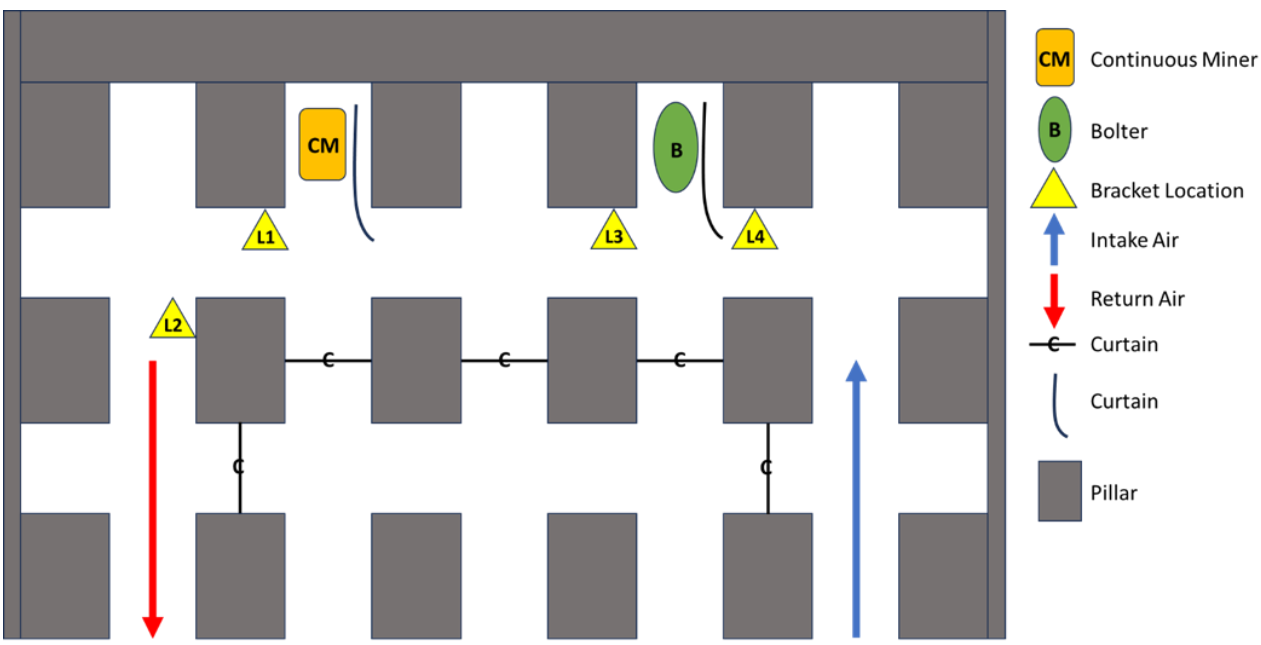

Figure 2.4: General sampling locations where each 'set' was placed.

In each event, a 'set' of RCMD filter samples were collected in each location; across all events and locations, there were a total of 24 sets (see Table A1 in the Appendix). Each set included three filter samples (triplicates) collected with CMDPSUs (72 samples total). Additionally, paired with the CMDPSUs in each set were either one (Events 1-2) or two CPDMs (Events 3-10); the only exception was Event 2 in

Location 3, for which no CPDM was available. In all, this yielded a total of 39 CPDM data logs (i.e., one log per CPDM in each unique sampling event and location). All sampling equipment was attached to an angled-steel frame, such that the air inlets were oriented in the same direction (Figure 2.5). Within each sample set, the CMDPSUs were switched on and off simultaneously, and the start and stop times were recorded to determine the total sampling duration. However, the CPDM has a substantial warm-up time, so these instruments were turned on prior to being transported into the mine.

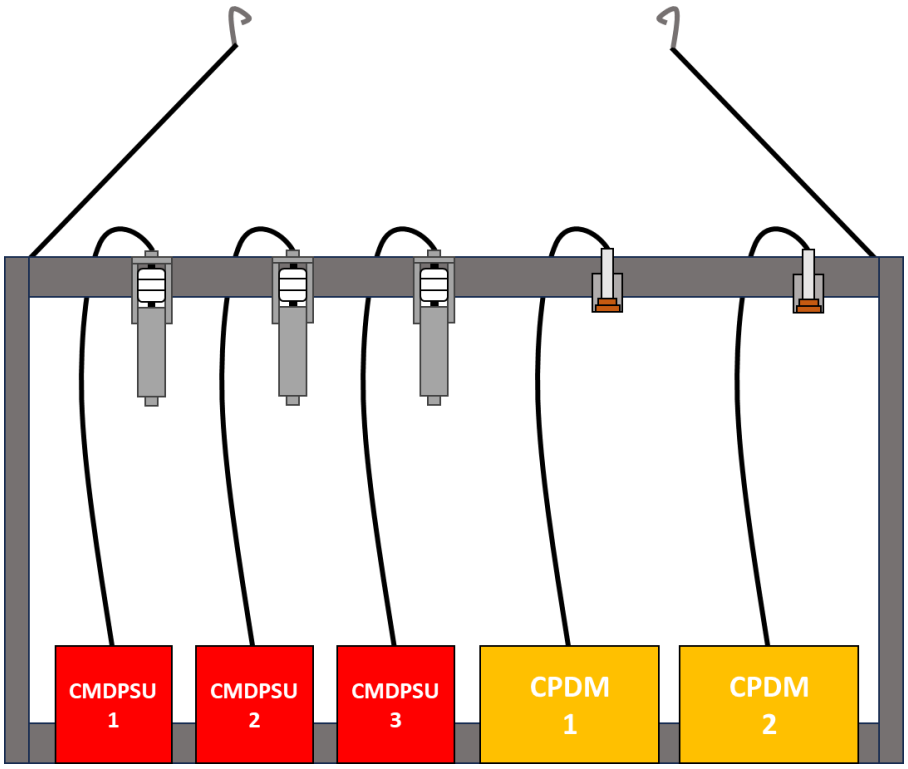

Figure 2.5: Schematic of equipment used to collect a 'set' of RCMD samples (i.e., each event x location).

Each CMDPSU consisted of an Escort ELF air pump operating at 2.0 L/min, a 10-mm nylon Dorr Oliver cyclone, and a 3-piece styrene cassette loaded with a pre-weighed 37-mm PVC filter and cellulose support pad. The cyclone-cassette assembly was of expandable type shown in Figure 2.3f. (All CMDPSU parts were purchased from Zefon International, Ocala, FL.) Pump flowrates were checked and calibrated prior to each event using a Gilian Gilibrator-2 (Sensidyne, St. Petersburg, FL). The CMDPSU filter samples were analyzed gravimetrically to determine RCMD mass and TWA RCDM concentration, and by FTIR to determine quartz mass and TWA quartz concentration (see below).

The CPDMs were Thermo Scientific PDM3700 Personal Dust Monitors, operated at 2.2 L/min with a Higgins-Dewell cyclone (which has a similar penetration efficiency to the Dorr Oliver cyclone at 2.0 L/min). Each monitor was cleaned and calibrated prior to each sampling event. The CPDM collects a dust sample on a special filter stub, which is attached to a tapered element oscillating microbalance (TEOM). As dust accumulates on the filter, the TEOM tracks changes in oscillation frequency and uses a calibration factor to determine the MRE-equivalent dust mass deposited on a 1-minute time interval (logged in the instrument's data file); under typical use, the instrument uses the mass accumulation to continuously compute and display mass concentration (i.e., as a rolling 15-minute average or the current full-shift equivalent). For this study, the CPDM's data log was downloaded following each sampling event and the

sample mass accumulated during the specific time interval corresponding to the paired CMDPSUs was used to derive an estimate of the TWA RCMD concentration during this time. This concentration was considered as an alternate to the value that can be determined from the CMDPSU filters gravimetrically—since such gravimetric analysis is impractical in the field.

In both of the mine sections studied, grab samples of primary dust source materials were also collected. These included raw coal (MMU and MMU3) and roof rock (shale, MMU1), which were hand-picked from the production belt, and a sample of the limestone rock dusting product the mine uses. Since very little roof rock was being cut in MMU3 during the study, a sample of the material from the roof bolter dust collection system was taken to represent dust generated from the roof in this section. Each material was used to generate respirable dust samples (triplicates) in the laboratory to gain insights to the quartz content. Briefly, this was done by aerosolizing a small mass of each source material within a small enclosure, and collecting the respirable dust using the same CMDPSU apparatus used for the mine sampling. (For these samples, the PVC filters were placed in 2-piece rather than 3-piece cassettes.) The filters were pre- and post-weighed to determine the sample mass. Notably, while the roof bolter material and the rock dust product were already very fine, the raw coal and rock materials were pulverized in the lab and sieved (to minus 200 µm) before generating the respirable dust samples.

2.3.2 Gravimetric Analysis

Filter samples collected with CMDPSUs were pre-weighed and post-weighed in the authors' Virginia Tech laboratory using a Cubis MSE6.6S microbalance (Sartorius, Gottingen, Germany) which has a readability of 2 µg. For each sample, the MRE-equivalent RCMD mass (mg) was determined using Equation 1, and the TWA concentration (mg/m^3) was determined using Equation 2:

$$M_{RCMD\_filter}\ (\mathrm{mg}) = 1.38\ \times\ (F_2 - F_1)\ (\mathrm{mg}) \qquad \text{Equation 1}$$

$$C_{RCMD\_filter}\ \left(\frac{\mathrm{mg}}{\mathrm{mg}^3}\right) = \frac{M_{RCMD\_filter}\ (\mathrm{mg})}{2.0\left(\frac{\mathrm{L}}{\mathrm{min}}\right) \times t\ (\mathrm{min})} \times \frac{1000\ \mathrm{L}}{\mathrm{m}^3} \qquad \text{Equation 2}$$

where, F_1 and F_2 are the filter pre- and post-weight (mg), respectively; 1.38 is the constant MRE-equivalency factor; t is the sampling duration (min); and 2.0 L/min is the sampling flow rate for the CMDPSU.

To derive estimated RCMD mass (mg) and TWA concentration (mg/m^3) values from the CPDM data, Equations 3 and 4, respectively, were used:

$$M_{RCMD\_CPDM}\ (\mathrm{mg}) = (S_2 - S_1)\ (\mathrm{mg}) \qquad \text{Equation 3}$$

$$C_{RCMD\_CPDM}\ \left(\frac{\mathrm{mg}}{\mathrm{mg}^3}\right) = \frac{M_{RCMD\_CPDM}\ (\mathrm{mg})}{2.2\left(\frac{\mathrm{L}}{\mathrm{min}}\right) \times t\ (\mathrm{min})} \times \frac{1000\ \mathrm{L}}{\mathrm{m}^3} \qquad \text{Equation 4}$$

where, S_1 and S_2 are the CPDM's recorded values for filter stub mass (mg) at the start time and stop time of the paired CMDPSU samplers, respectively; t is again the sampling duration (min) of the CMDPSU samplers; and 2.2 L/min is the sampling flow rate for the CPDM (L/min). (Note the 1.38 MRE-equivalency factor is not needed in Equation 3 because the CPDM is programmed to record MRE-equivalent mass.)

For the respirable dust samples that were lab-generated from the dust source materials collected in Mine 28, the filters were pre- and post-weighed (using the same microbalance as above). The sample mass (mg) was determined by simple difference using Equation 5:

$$M_{RD}(\text{mg}) = (F_2 - F_1)\ (\text{mg}) \qquad \text{Equation 5}$$

2.3.3 DOF FTIR Analysis

The PVC filter samples collected with CMDPSUs were analyzed by DOF FTIR using an Alpha II Compact spectrometer and OPUS software (Bruker Optics, Billerica, MA), and then the data was inputted into NIOSH's *FAST* software. To scan the filter, it needed to be removed from its respective 3-piece cassette. The filter was carefully grabbed on the edge using steel tongs so as not to disturb any dust collected on the filter, and then placed into the body of a 4-piece cassette which contained a stainless-steel ring as a support backing. This was then placed into a 4-piece cassette cradle developed by NIOSH, and slid into the FTIR to be scanned.

Analysis with the FTIR instrument was conducted following the method outlined by NIOSH (2022). Briefly, the center (6-mm diameter area) of each sample filter was scanned to measure the absorbance spectrum between 4000-cm^{-1} and 400-cm^{-1} (NIOSH, 2022); a blank PVC filter was also scanned. Specifically, the instrument was set to obtain 16 consecutive scans using Blackman-Harris 3-term apodization with a 4-cm^{-1} resolution. Using a NIOSH-developed macro for the OPUS software, distortions were removed from the spectrum with a 'rubber band baseline correction' that includes 64 baseline points; and then the blank filter spectrum was used to correct each sample spectrum by simple blank subtraction (NIOSH, 2022). The macro output is the integrated peak area for each sample in two regions: 767 to 816 cm^{-1} corresponds to the characteristic peak area for (alpha) quartz, and 900 to 930 cm^{-1} corresponds to the primary peak area for kaolinite. (Notably, kaolinite also has a secondary peak that interferes with the quartz peak area. However, the secondary peak occurs in near constant proportion with the primary peak, and *FAST* has been programmed to correct for this.)

The integrated peak areas for quartz and kaolinite were output as a CSV file, which was then imported to the *FAST* software. As explained earlier, *FAST* does not include a model for the specific sampling conditions used in this study (i.e., cyclone-cassette assembly with built-in fitting as shown in Figure 2.3f, with airflow at 2.0 L/min). However, it does include a model for the same hardware at 1.7 L/min—called '10-mm nylon Dorr Oliver cyclone (with built-in fitting)' as shown in Figure 2.3c. This model was selected to analyze the mine filter sample data, and a subset of the samples were also analyzed by a standard method for reference (see below). The *FAST*-output quartz mass (called 'silica mass' in the software) was recorded for each filter sample and used to compute TWA quartz concentration using Equation 6:

$$\text{C}_{Q\_FAST}\ \left(\frac{\mu\text{g}}{\text{mg}^3}\right) = \frac{1.38 \times M_{Q\_FAST}\ (\mu\text{g})}{2.0\left(\frac{\text{L}}{\text{min}}\right) \times t\ (\text{min})} \times \frac{1000\ \text{L}}{\text{m}^3} \qquad \text{Equation 6}$$

Where, M_{Q_FAST} is the quartz mass (µg) output by *FAST*; 1.38 is the constant MRE-equivalency factor; *t* is the sampling duration (min) for the CMDPSU; and 2.0 L/min is the sampling flow rate for the CMDPSU. Notably, for quartz measurements determined with the portable FTIR instrument on 37-mm PVC filters, *FAST* considers the limit of detection (LOD) and limit of quantification (LOD) to be 5 µg and 16 µg, respectively (NIOSH, 2022). These limits are based on analysis of blank filters (Cauda et al., 2016), and the software notifies the user if the measured value for a sample is below the LOD or LOQ.

The respirable dust samples generated in the lab from Mine 28 dust source materials were also analyzed by the portable FTIR instrument, using the same procedure described above to measure the integrated areas for the quartz and primary kaolinite peaks (i.e., following baseline and blank filter corrections). However, to determine quartz mass on each filter, an internally developed algorithm was used rather than *FAST*. This is because the lab-generated filter samples were collected (a) using 2-piece cassettes from (b) a high-concentration enclosure. The combination of these two factors leads to a deposition pattern that is substantially more center-heavy than the pattern which occurs with 3-piece (and 4-piece) cassettes in a typical mine environment, and therefore none of the *FAST* models are expected to accurately predict quartz mass. The internal algorithm to determine quartz mass on these filters essentially had two steps: First, the measured quartz peak area was corrected for kaolinite interference per Pokhrel et al., (2022). Second, the corrected quartz peak area was translated to quartz mass using the calibration curve given by Keles et al. (2022). Equation 7 combines these two steps to compute quartz mass on the 2-piece lab filters:

$$M_{Q\_2PC}\ (\mu\text{g}) = \frac{(P_Q - \frac{P_K}{3.8})}{0.00695\ (\mu\text{g}^{-1})} \qquad \text{Equation 7}$$

where, P_Q and P_K are the integrated areas (arbitrary units) of the quartz and primary kaolinite peaks, respectively; 3.8 is a constant ratio between the primary and secondary kaolinite peak areas (Pokhrel et al., 2022); and 0.00695 (arbitrary units/µg) is the slope of a calibration curve for (kaolinite-corrected) integrated quartz peak area versus measured quartz mass, determined in the laboratory for filter samples collected in 2-piece cassettes at high dust concentration (Keles et al. 2022).

2.3.4 Reference Quartz Analysis

Ten of the Mine 28 filter samples were selected for analysis by standard NIOSH Method 7603; this analysis was conducted by RJ Lee Group (Pittsburgh, PA). These samples were selected to represent a range of sampling events and sample masses. Prior to performing the Method 7603 analysis, the contracted lab weighed each filter (i.e., to re-measure F_2 and determine M_{RCMD_filter} using the F_1 values provided by the authors.) Figure 2.6 shows that sample loss and/or contamination was unlikely during transport.

The contract lab reported the 7603-derived quartz mass (µg) for each of the 10 filters, and then the (MRE-equivalent) TWA quartz concentration was computed using Equation 8 (analogous to Equation 6 for the *FAST*-derived quartz mass values).

$$\text{C}_{Q\_7603}\ \left(\frac{\mu\text{g}}{\text{mg}^3}\right) = \frac{1.38 \times M_{Q\_7603}\ (\mu\text{g})}{2.0\left(\frac{\text{L}}{\text{min}}\right) \times t\ (\text{min})} \times \frac{1000\ \text{L}}{\text{m}^3} \qquad \text{Equation 8}$$

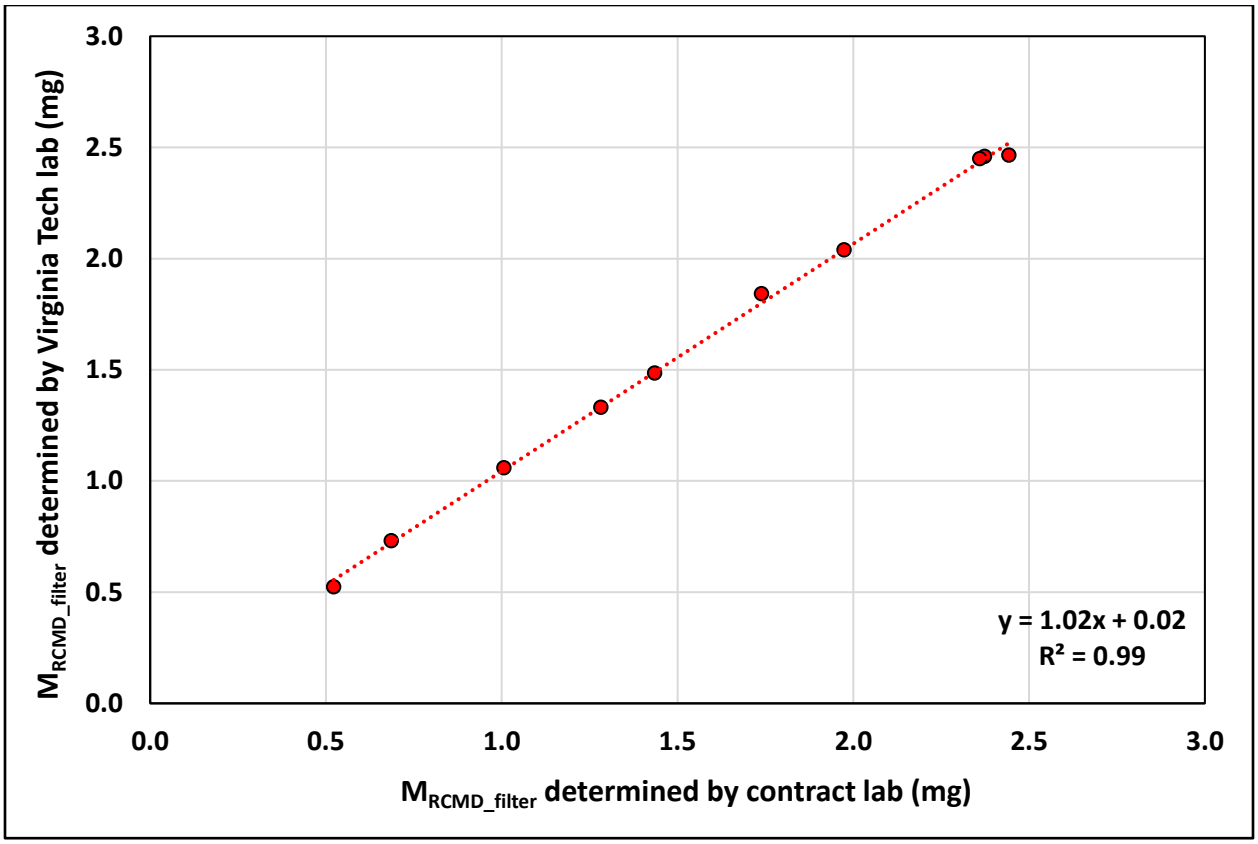

Figure 2.6: MRE-equivalent RCMD mass determined by the authors versus the contract lab for 10 filter samples selected for Method 7603 analysis.

2.3.5 Quartz Percentage

For the Mine 28 filter samples, quartz percentage was determined as the ratio of quartz concentration to RCMD concentration per Equation 9:

$$Q_{RCMD}(\%) = 100\% \times \frac{C_Q(\frac{\mu g}{m^3})}{C_{RCMD}(\frac{mg}{m^3})} \times \frac{mg}{1000\ \mu g} \qquad \text{Equation 9}$$

where, C_Q (µg/m³) is the TWA quartz concentration that is derived either from the DOF FTIR method or 7603-derived; and C_{RCMD} (mg/m³) is the TWA RCMD concentration that is either derived from gravimetric analysis of the filter sample or estimated from the paired CPDM instrument(s).

For the respirable dust samples generated in the lab using dust source materials from Mine 28, quartz percentage was determined using Equation 10:

$$Q_{RD} = 100\% \times \frac{M_{Q\_2PC}(\mu g)}{M_{RD}\ (mg)} \times \frac{mg}{1000\ \mu g} \qquad \text{Equation 10}$$

2.4 Results and Discussion

A summary of the gravimetric and DOF FTIR analysis on the Mine 28 filter samples (i.e., collected with the CMDPSUs) is given in Table A2, and a summary of the CPDM data is given in Table A3. For three sample sets (n = 9 filter samples)—all of which were collected in the section intake (Location 4 per Figure 2.4)—the post-weight measurements on all filters indicated negligible sample mass (i.e., M_{RCMD_filter} < 10 µg). Thus, these filters were excluded from further analysis (i.e., yielding a total of 63 filter samples in 21 sets). Notably, the CPDM data from these sample sets also indicated negligible dust concentration in the sampling environment (see Table A3). Several other CPDM data logs showed error or warning messages (also in Table A3): HIGH FILTER LOAD (n=1), which occurs when the TEOM filter is nearing its maximum capacity; MASS OFFSET (n=6), which occurs in response to rapid weight gain/loss from the TEOM filter; and POWER LOW (n=2), which occurs when the CPDM battery is low (Thermo Fisher Scientific, 2016). Except when the CPDM powered off before 50% of the CMDPSU sampling duration (n=1), data in these instances were still used to estimate C_{RCMD_CPDM} (using the CPDMs sampling time as *t*) and results are marked in presentation of the results. For the two CPDMs that had POWER LOW errors (CPDM 8 and 10 in Event 9, Location 1), the time interval used to calculate C_{RCMD_CPDM} was determined by subtracting the triplicate CMDPSUs start time from the CPDM shutoff time. The dust concentration values that were calculated from CPDM 8 and 10 were found to be similar and averaged in the same way as Events 3 through 10.

As mentioned, the filter samples in Mine 28 were collected with the cyclone-cassette assembly shown in Figure 2.3f at 2.0 L/min (i.e., standard for RCMD sampling with the CMDPSU). However, since no *FAST* model exists for these conditions, the model shown in Figure 2.3c was used to generate quartz mass values. To interpret these results, a correction was established by comparing the *FAST*-output values to the reference measurements (i.e., Method 7603 analysis) for the subset of 10 samples analyzed by both methods (Table A4). Figure 2.7 shows the correlation plot. There is a clear linear relationship with little scatter (coefficient of determination, R^2, is 0.95) and a minimal y-intercept (about 3 µg). These results provide further evidence that the sample handling and transport did not appreciably affect quartz measurements. However, the trendline slope in Figure 2.7 is approximately 1.6, meaning that the *FAST* model used here tends to overpredict quartz mass by a factor of 1.6×. This is attributed to the fact that the *FAST* model assumes a sampling flow rate of 1.7 L/min. The higher flow rate used in this study should yield a deposition pattern that is somewhat heavier than the filter center, which is the scan location for the DOF FTIR analysis. The *FAST* model extrapolates data from this location to the entire filter area based on expected deposition pattern; so, if more of the total dust is within the scan area than expected, the model prediction will be too high. Nevertheless, Figure 2.7 demonstrates that the *FAST*-output quartz mass can be reasonably corrected by a factor of 1.6×, over the mass range represented by filter samples collected for this field study. Thus, Equation 6 was modified to Equation 11 to incorporate the correction factor.

$$C'_{Q_{FAST}}\left(\frac{\mu g}{mg^3}\right) = \frac{1.38 \times M_{Q\_FAST}\ (\mu g)}{1.6 \times 2.0\left(\frac{L}{min}\right) \times t\ (min)} \times \frac{1000\ L}{m^3} \qquad \text{Equation 11}$$

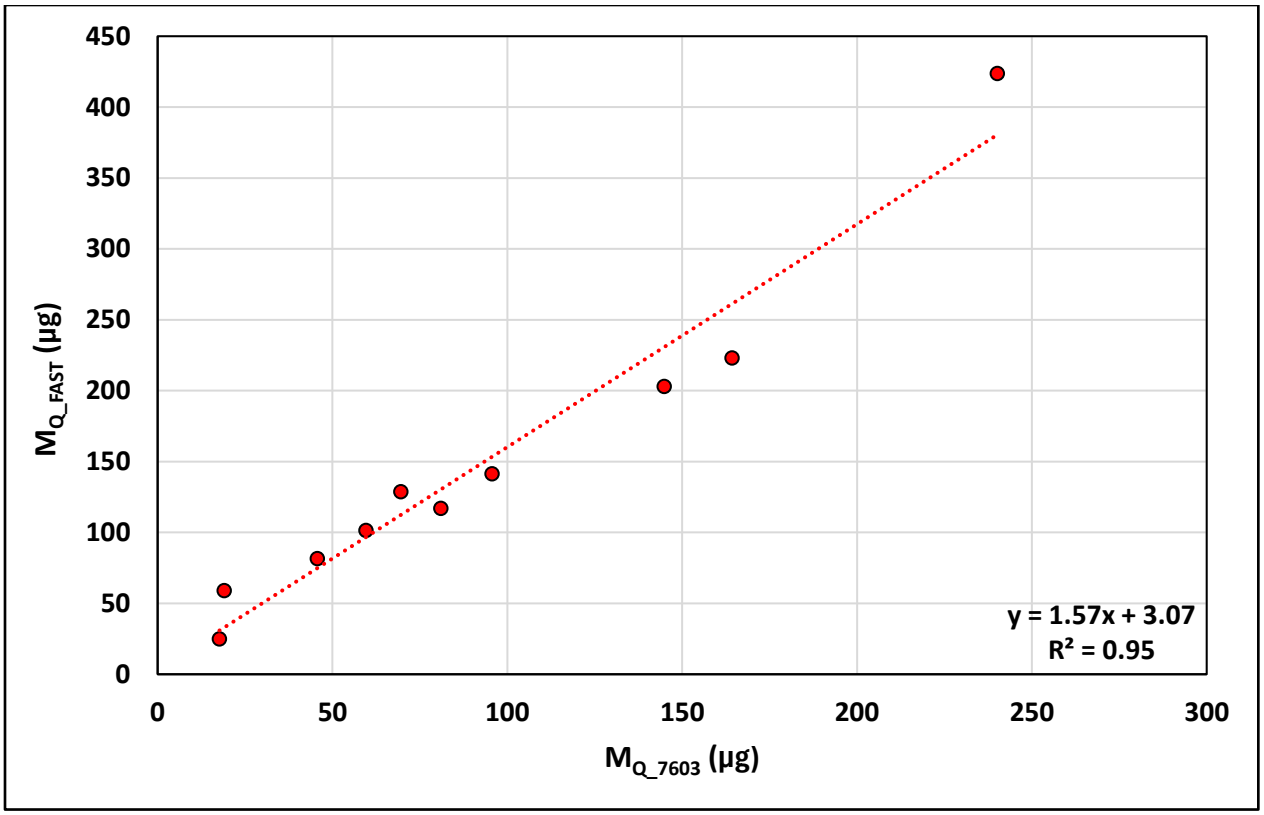

Figure 2.7: *FAST*-derived quartz mass vs. NIOSH 7603 quartz mass.

2.4.1 Trends in Quartz Concentration and Percentage in Study Mine

Figure 2.8 shows the quartz concentration ($C'_{Q_{FAST}}$) in each sampling event and location (n = 21 sample sets). As mentioned, the samples collected in the intake location (L4) did not have enough mass for analysis in either MMU. Regarding the other samples, it should be reiterated that these were collected in fixed locations—including in areas that mine personnel are generally not expected to be working in regularly or for long durations (i.e., just downwind of the continuous miner or in the section return). Thus, results presented here should not be construed as representative of typical exposures. Rather, this sort of sampling scheme could be used for collection of routine non-regulatory samples, for example, to track trends in quartz concentration with mining or geological conditions.

Figure 2.8 shows no discernable trends among samples collected in L1, L2 and L3. For instance, in Events 2, 3, 7 and 10, the quartz concentration was clearly higher downwind the continuous miner (L1) than in the section return (L2) and/or just downwind the bolter (L3), but the opposite is true for Events 1 and 6. Similarly, there was not a consistent trend between L2 and L3. In general, the quartz concentration increased with event number in both mine sections sampled—although there is no specific explanation for this in terms of the activities or conditions in the mine (e.g., production, ventilation, strata conditions, etc.)

Nevertheless, Figure 2.8 shows that the quartz concentration was higher on average in MMU3 than in MMU1 (i.e., 180.3 µg/m³ versus 79.8 µg/m³, respectively); a Student's t-test comparing group means (α=0.05, assuming unequal variances) indicated the difference was significant (P = .02). This finding was unexpected based on the observation that MMU3 was mining relatively little roof rock along with the

coal seam, whereas substantial rock was being taken in MMU1 (see Table A1). For context, the average height of roof rock being mined represented about 27% of the total mining height during the four sampling events in MMU1, but only about 7% during the six events in MMU3. However, analysis of the dust source materials helps explain the results: the respirable dust generated from the coal being mined in MMU3 contained about 7.4% quartz, whereas this value was only about 0.9% for the coal in MMU1. For the respirable dust samples representing the roof rock strata, results indicated quartz content was about 19.3% in MMU1 and 15.1% in MMU3. (The rock dusting product, which was used in both sections, was found to have a quartz content of about 2.5%. However, based on field observations, the rock dusting product was not expected to be a substantial source of the RCMD in locations sampled for this study.)

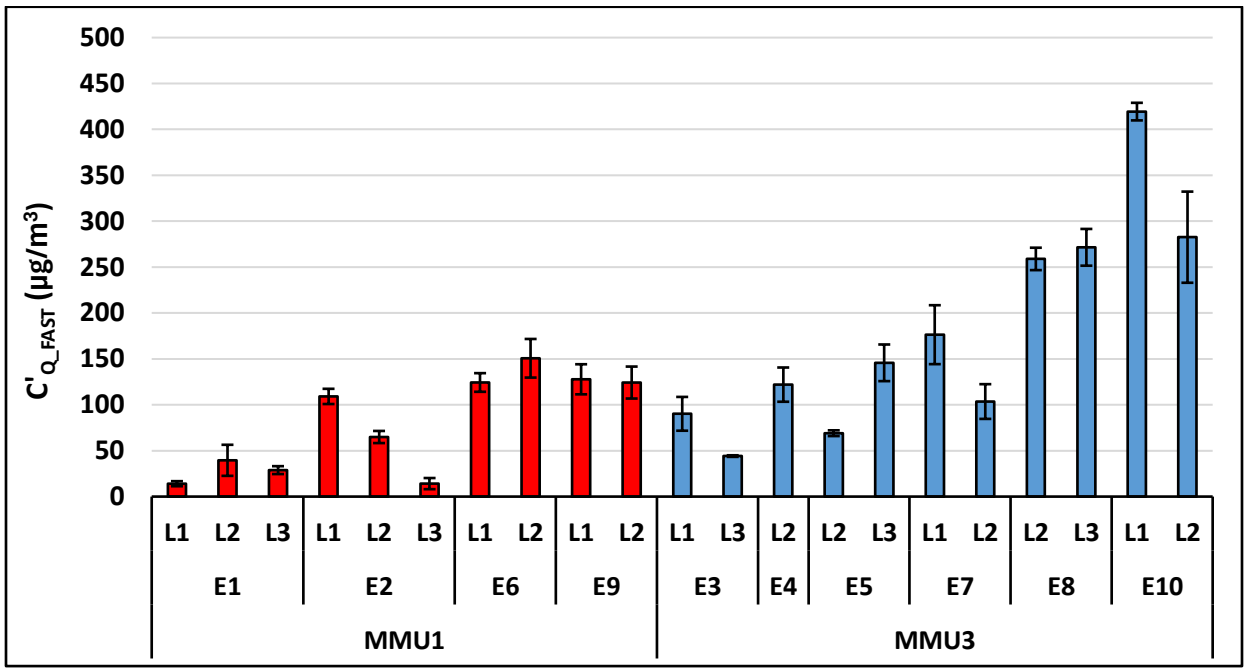

Figure 2.8: Quartz concentration determined from the DOF FTIR analysis of the filter samples and corrected by the 1.6x factor.

To put the quartz concentration data into context, Figure 2.9 plots this data along with the total RCMD concentration (C_{RCMD_filter}) and quartz percentage (Q_{RCMD}), determined using only the filter samples (i.e., not considering the CPDM data). While samples from MMU1 generally indicated lower quartz concentrations than in MMU3, they indicated slightly higher RCMD concentrations (i.e., average of 2.7 mg/m^3 versus 2.2 mg/m^3, respectively), but the difference was not found to be statistically significant (P = 0.65). Prior studies have found that, with continuous mining, cutting rock—which is generally much harder than the target coal seam—can produce substantially more respirable dust than cutting coal (Jaramillo et al., 2022). However, the personnel in Mine 28 noted that the coal seam in both sections was particularly hard, which could limit relative differences in the amount of dust being generated from cutting the roof rock versus the coal.

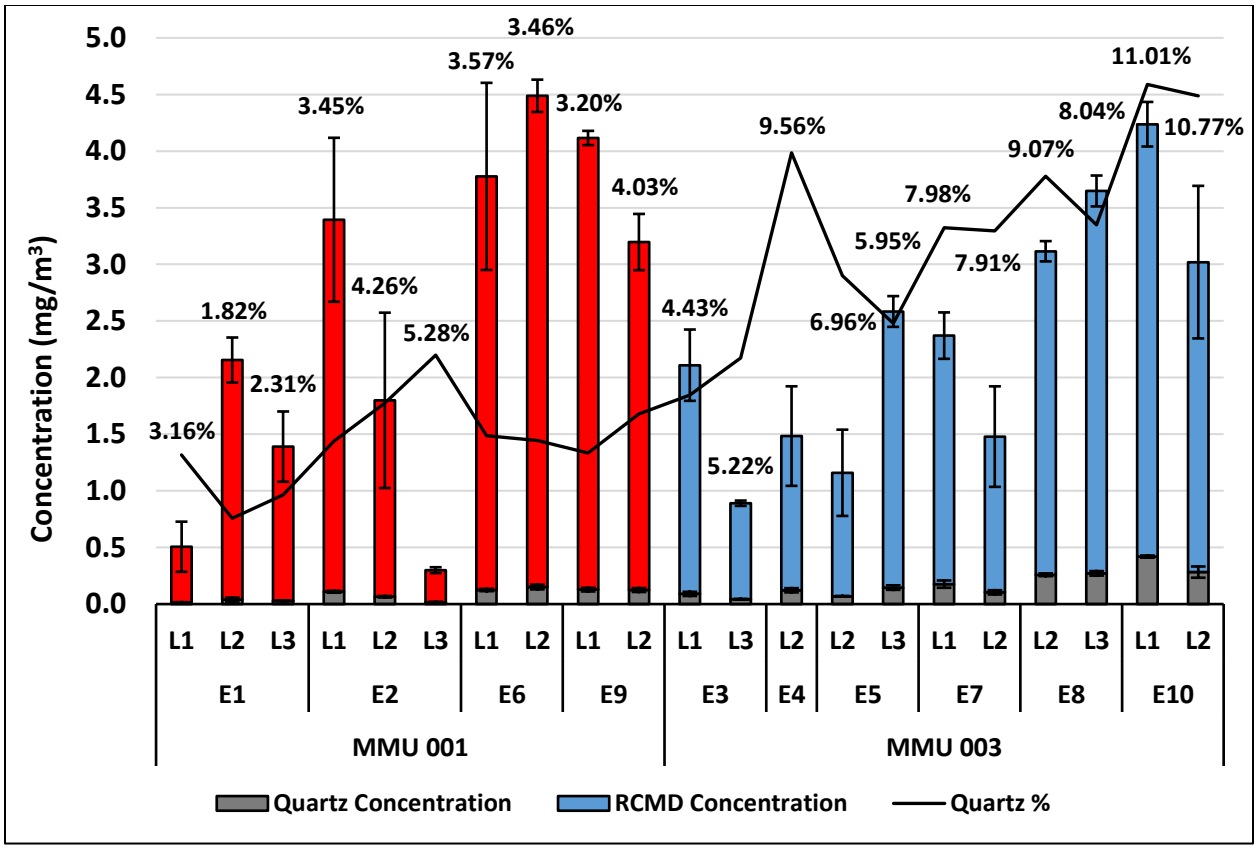

Figure 2.9: RCMD, quartz concentration, and quartz percentage by MMU.

Still, Figure 2.9 shows that the *percentage* of quartz in the RCMD (Q_{RCMD}) was higher in MMU3 than in MMU1 (i.e., 7.9% versus 3.9%, respectively) and this difference was found to be statistically significant (P<0.001). Again, this is attributed to the relatively high quartz content of the coal being mined in MMU3 during the field study. A very simple source apportionment exercise is illustrated in Table 2.1, considering only the average heights of coal and roof rock being mined in each section and the quartz content of those strata (i.e., based on the analysis of respirable dust generated from the grab samples of source materials). Assuming that during the field study (a) the continuous miner operation was the predominant source of RCMD, (b) the coal and rock strata produced similar amounts of RCMD, and (c) the respirable quartz content of these strata was represented by the samples generated in the lab, the predicted Q_{RCMD} would be about 5.8% in MMU1 and 7.9% in MMU3. Despite the simplicity of this exercise, the relative results are consistent with observations based on the RCMD filter sample analysis. Indeed, this sort of sampling approach (i.e., collecting dust-source materials along with RCMD samples) could be useful for mines aiming to identify and understand variability in RCS sources.

Table 2.1: Predicted RCMD quartz content per MMU section based on MMU dimensions and quartz content.

Section	Stratum Height (ft)		Quartz Content (%)		Predicted Q_{RCMD} (%)
	Coal (H_{coal})	Rock (H_{rock})	Coal (Q_{RD_coal})	Rock (Q_{RD_rock})	$= \frac{(H_{coal} \times Q_{RD\_coal}) + (H_{rock} \times Q_{RD\_rock})}{(H_{coal} + H_{rock})}$
MMU1	5	1.8	0.9	19.3	5.8
MMU3	7.8	0.5	7.4	15.1	7.9

2.4.2 Estimating Quartz Percentage with CPDM Data

In Figure 2.9, the quartz percentage data is based solely on analysis of the CMDPSU filter samples, including post-weighing the filters to determine RCMD mass concentration (i.e., C_{RCMD_filter} per Equation 2). However, this approach is impractical in the field since a microbalance is unlikely to be available. Figure 2.10 evaluates the option to instead use a paired CPDM instrument as a means to estimate the RCMD concentration for a filter sample (i.e., C_{RCMD_CPDM} per Equation 4). Figure 2.10a compares the CPDM- versus filter sample-derived RCMD concentration for each sample set (i.e., one or two CPDMs and three CMDPSUs per set; n = 20 sets per Table A3). (It is reiterated that, for both measures, the values represent MRE-equivalent TWA concentration.) Excluding just one datapoint which appears to be an outlier (i.e., greater than the third quartile by more than 1.5x the inter-quartile range), there is a strong correlation between the two measures (R^2 = 0.73). This is expected since the CPDM was developed using standard CMDPSU sampling as the reference (Page et al. 2008). Notably, the linear trendline of best fit for this dataset has a slope of 0.78 and a y-intercept of 0.74 mg/m^3, which implies the CPDM would measure non-trivial RCMD concentration even when a filter sample indicates negligible mass. If the trendline is constrained to a y-intercept of 0 (as suggested by Page 2008 for comparing CPDM to gravimetric analysis of filter samples), the slope is 1.04.

In Figure 2.10b, the quartz percentage for each sample set (i.e., Q_{RCMD} per Equation 9) is compared for values derived using the CPDM versus filter sample analysis. Again, the correlation is strong (R^2 = 0.79) and the line of best fit has a slope of 0.96 and y-intercept of -0.004. The negative intercept in this case has no practical meaning (i.e., Q_{RCMD} cannot be less than 0), but is an artifact of the positive intercept in Figure 2.10a. If the trendline in Figure 2.10b is constrained to a y-intercept of 0, the slope is 0.94.

Taken together, the trends shown in Figure 2.10 suggest that, on average, the CPDM instruments used in Mine 28 slightly overestimated the RCMD concentration, which resulted in a slight underestimation of the quartz percentage (i.e., due to the inverse relationship between Q_{RCMD} and C_{RCMD}). Assuming that CPDMs are maintained and calibrated (as they were in Mine 28), these results suggest that the paired CPDM approach could work well to enable quartz percentage estimates in the field for non-regulatory monitoring purposes.

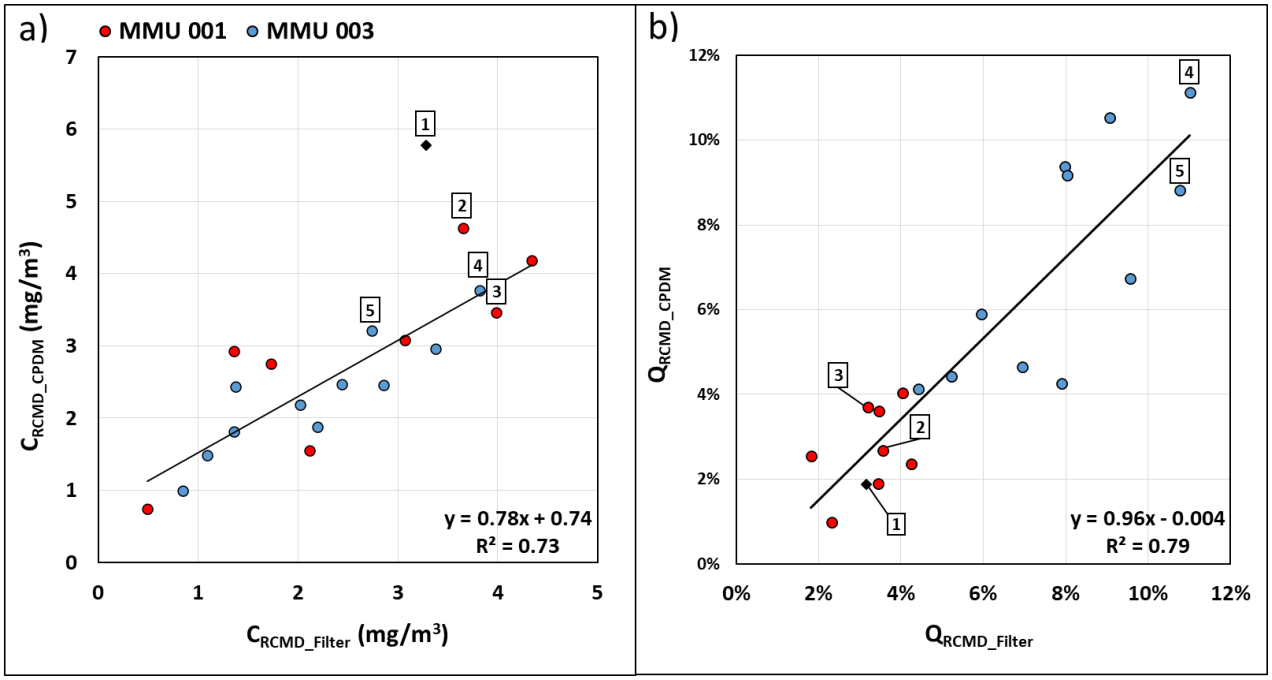

Figure 2.10: Comparison of CPDM RCMD concentration vs CMDPSU RCMD concentration (left) and CPDM quartz content vs CMDPSU quartz content (right). Five averaged CPDM samples contained function errors during the data collection in the field. Box 1 represents Event 2, Location 1, with CPDM 12 containing a HIGH FILTER LOAD error. Box 2 represents Event 6, Location 1, with CPDMs 11 and 13 containing MASS OFFSET errors. Box 3 represents Event 9, Location 1, with CPDMs 8 and 10 containing POWER LOW errors. Box 4 represents Event 10, Location 1, with CPDMs 8 and 10 containing MASS OFFSET errors. Box 5 represents Event 10, Location 2, with CPDMs 12 and 19 containing MASS OFFSET errors.

2.4.3 Feedback from Mine Personnel

During the sampling campaign for the field study, a demonstration of the DOF FTIR was conducted with the mine engineers and the health and safety team at Mine 28, including sample handling (i.e., transferring the sample filter from the 3-piece cassette to the analysis cassette); FTIR analysis of the sample filter (and blank); baseline and blank correction of the sample spectrum (i.e., in the OPUS software that goes with the Bruker FTIR instrument used in this study); download of the sample data from the FTIR software and upload to *FAST* software; and use of *FAST* to generate quartz results. (With the exception of the sample handling step needed for this study (i.e., due to the choice to demonstrate 3-piece rather than the special 4-piece sampling cassettes), these steps are all explained in detail in NIOSH's guide for the DOF-FTIR method (NIOSH, 2022).

Immediate feedback from the mine personnel was generally positive, with specific points being the efficiency and convenience of the DOF FTIR method. A main point of concern was the need to use CMDPSUs for sampling. Like many mines, Mine 28 has generally not collected filter samples since the CPDM was mandated for operator-conducted RCMD sampling in 2016; and, in fact, Mine 28 did not still have any CMDPSUs on site. The mine personnel expressed interest in capabilities for field analysis of CPDM samples, though no such method presently exists—and a DOF FTIR approach appears improbable with the current CPDM filter assembly, which includes borosilicate glass fiber material that directly interferes with the quartz spectral peak area (Tuchman et al., 2008; Chow et al., 2022).

In follow-up discussions with the mine partner (i.e., Mine 28 operator), they expressed interest in using the DOF FTIR method for non-regulatory RCS monitoring—and there is a sense of urgency given the

reduced PEL set by the 'new silica rule' (Lowering Miners' Exposure, 2014]. For example, this mine partner has interest to collect baseline quartz concentration data under different mining/geologic conditions and to test new or modified dust control conditions (i.e., beyond what is required by their current ventilation plans). The partner has made clear that their interest would be to conduct such studies using area samples in order to isolate test variables and avoid personal-sampling factors that could confound observations (e.g., specific positioning or actions of individual workers).

While not specifically raised during the demonstration at Mine 28 or in follow-up discussions with the mine partner, there are several other factors that must be considered for use of the DOF FTIR method for field analysis of RCS. Firstly, personnel responsible for conducting the analysis must be knowledgeable of the underlying principles, which is important for reliable FTIR data generation, effective use of *FAST*, detecting or troubleshooting problems, and communicating results. Again, there is available guidance from NIOSH (2022), and the current study illustrates how some deviations from the standardized method published by NIOSH might be handled (e.g., to use generic 3-piece styrene cassettes with an expandable cyclone-cassette holder apparatus with a CMDPSU). Indeed, the approach taken here to collect reference measurements on a subset of sample filters would be advisable as a preliminary or periodic check on DOF FTIR measurements for new users or under non-standardized conditions. Moreover, users must consider the availability of suitable space for housing the FTIR instrument and conducting the analysis; in general, this space should be relatively free of dust and climate controlled (i.e., to limit humidity). Care must also be taken during sample handling to minimize the potential for sample loss or contamination. That said, the current study demonstrates that this is possible, even using the 3-piece styrene cassettes which require the filter sample to be transferred to a separate cassette for analysis. Notably, the researcher performing the DOF FTIR sample analysis here had no prior experience with collecting or handling such filter samples.

2.5 Conclusion

The use of CPDMs for RCMD compliance leaves MSHA with the use of CMDPSUs for regulatory quartz monitoring through certified labs. Because of the delay between sampling collection, sample shipping, and lab analysis, there can be a significant wait time on quartz exposure data for mine operators. There is a need for fast and efficient forms of non-regulatory monitoring by mine operators to understand quartz exposure. DOF FTIR spectroscopy has strong potential for rapid, end-of-shift quartz examination by these mine operators for research and engineering studies. MSHA's proposed 2024 silica rule halving the PEL of quartz concentrations has further pushed the need for nonregulatory monitoring in mines of all commodities.

DOF FTIR is a cost-effective analysis method with versatility for mine operators to be able to pick, choose, and adapt the analysis based on the type of sampling equipment available at hand or within budget. Though 4-piece cassettes are expensive, DOF FTIR allows for the use of more inexpensive and widely available consumables such as 3-piece cassettes. It also allows for the use of sampling equipment that is available off-the-shelf such as the expandable cyclone-cassette holder, which can hold 2- or 3-piece cassettes. The simplicity of the portable FTIR scanning process and data importation into NIOSH's *FAST* software makes quartz determination easy to learn and quick to perform. Mine operators may be interested in the quartz percentages more than the quartz masses or concentrations, and if so, there are potential workarounds for a microbalance if one is not easily accessible. Pairing a CPDM with a

gravimetric sampling unit could provide an alternative method to determine dust mass, allowing for an estimated quartz percentage to be calculated.

This field study demonstrated the DOF FTIR analysis method with the above considerations. Expandable cassette-holders with three-piece cassettes were able to be used as they were inexpensive. Sampling at an alternative flowrate outside of *FAST* recommendations was also easily corrected for these sampling conditions through the use of a subset of samples being analyzed at a contract lab. Since the 4-piece cassettes were not used in the DOF FTIR analysis, the filters had to be handled and placed into a holder similar to a 4-piece cassette. The handling process was not found to be overly burdensome or prone to sample loss and contamination.

2.6 Acknowledgements

The authors would like to express their gratitude to the National Institute of Occupational Safety and Health for funding this research. We would also like to thank August Greth for his aid and support in the Mine 28 sampling, lab experiments, and data analyzation. Gratitude is additionally given to the Mine 28 engineers, health and safety team, and miners for their support in the dust sampling process and data collection.

2.7 References

Sarver, E., Keleş, Ç., & Afrouz, S. G. (2021). Particle size and mineralogy distributions in respirable dust samples from 25 US underground coal mines. *International Journal of Coal Geology*, *247*, 103851.

NIOSH (2002). Health effects of occupational exposure to respirable crystalline silica.

Hall, N. B., Blackley, D. J., Halldin, C. N., & Laney, A. S. (2019). Current review of pneumoconiosis among US coal miners. *Current environmental health reports*, *6*, 137-147.

Cohen, R. A., Rose, C. S., Go, L. H., Zell-Baran, L. M., Almberg, K. S., Sarver, E. A., ... & Green, F. H. (2022). Pathology and mineralogy demonstrate respirable crystalline silica is a major cause of severe pneumoconiosis in US coal miners. *Annals of the American Thoracic Society*, *19*(9), 1469-1478.

Lowering Miners' Exposure to Respirable Crystalline Silica and Improving Respiratory Protection, 89 F.R. 28218-28485 (April 18, 2024). https://www.federalregister.gov/documents/2023/08/14/2023-17370/lowering-miners-exposure-to-respirable-crystalline-silica-and-improving-respiratory-protection#:~:text=On%20July%2013%2C%202023%2C%20MSHA,Protection%20(88%20FR%2044852).

Department of Labor, Mine Safety and Health Administration. (2013). Infrared Determination of Quartz in Respirable Coal Mine Dust, MSHA Method P-7. https://arlweb.msha.gov/Techsupp/pshtcweb/MSHA%20P7.pdf

Health. Division of Physical Sciences. (2020). *NIOSH, Manual of Analytical Methods (NMAM), 5th Edition*. US Department of Health and Human Services, Public Health Service, Centers for Disease Control and

Prevention, National Institute for Occupational Safety and Health, Division of Physical Sciences and Engineering.

National Academies of Sciences, Medicine Division, Division on Earth, Life Studies, Board on Health Sciences Policy, Board on Environmental Studies, ... & Committee on the Study of the Control of Respirable Coal Mine Dust Exposure in Underground Mines. (2018). Monitoring and sampling approaches to assess underground coal mine dust exposures.

Miller, A. L., Drake, P. L., Murphy, N. C., Noll, J. D., & Volkwein, J. C. (2012). Evaluating portable infrared spectrometers for measuring the silica content of coal dust. *Journal of Environmental Monitoring*, *14*(1), 48-55.

Cauda, E., Miller, A., & Drake, P. (2016). Promoting early exposure monitoring for respirable crystalline silica: Taking the laboratory to the mine site. *Journal of occupational and environmental hygiene*, *13*(3), D39-D45.

Ashley, E. L., Cauda, E., Chubb, L. G., Tuchman, D. P., & Rubinstein, E. N. (2020). Performance comparison of four portable FTIR instruments for direct-on-filter measurement of respirable crystalline silica. *Annals of Work Exposures and Health*, *64*(5), 536-546.

Cauda, E., Chubb, L., Britton, J., Fritz, J., & Cole, G. (2018). *CDC - Mining - FAST - Field Analysis of Silica Tool - NIOSH*. Centers for Disease Control and Prevention. https://www.cdc.gov/niosh/mining/works/coversheet2056.html

Miller, A. L., Drake, P. L., Murphy, N. C., Cauda, E. G., LeBouf, R. F., & Markevicius, G. (2013). Deposition uniformity of coal dust on filters and its effect on the accuracy of FTIR analyses for silica. *Aerosol Science and Technology*, *47*(7), 724-733.

NIOSH (2022). Direct-on-filter analysis for respirable crystalline silica using a portable FTIR instrument. By Chubb LG, Cauda EG. Pittsburgh PA: U.S. Department of Health and Human Services, Centers for Disease Control and Prevention, National Institute for Occupational Safety and Health, DHHS (NIOSH) Publication No. 2022–108, IC 9533. https://doi.org/10.26616/NIOSHPUB2022108

Chubb, L. G., & Cauda, E. G. (2021). A novel sampling cassette for field-based analysis of respirable crystalline silica. *Journal of occupational and environmental hygiene*, *18*(3), 103-109.

Pampena, J. D., Cauda, E. G., Chubb, L. G., & Meadows, J. J. (2020). Use of the field-based silica monitoring technique in a coal mine: A case study. *Mining, metallurgy & exploration*, *37*(2), 717-726.

Miller, A. L., Weakley, A. T., Griffiths, P. R., Cauda, E. G., & Bayman, S. (2017). Direct-on-filter α-quartz estimation in respirable coal mine dust using transmission Fourier transform infrared spectrometry and partial least squares regression. *Applied spectroscopy*, *71*(5), 1014-1024.

Lowering Miners' Exposure to Respirable Coal Mine Dust, Including Continuous Personal Dust Monitors, 79 F.R. 24814-24994 (May 1, 2014). https://arlweb.msha.gov/regs/fedreg/final/2014finl/2014-09084.asp

Pokhrel, N., Agioutanti, E., Keles, C., Afrouz, S., & Sarver, E. (2022). Comparison of respirable coal mine dust constituents estimated using FTIR, TGA, and SEM–EDX. *Mining, Metallurgy & Exploration*, *39*(2), 291-300.

Keles, C., Pokhrel, N., & Sarver, E. (2022). A study of respirable silica in underground coal mines: Sources. *Minerals*, *12*(9), 1115.

Thermo Fisher Scientific. (2016). Model PDM3700 personal dust monitor. EPM-manual-PDM3700.pdf (thermofisher.com)

Jaramillo, L., Agioutanti, E., Ghaychi Afrouz, S., Keles, C., & Sarver, E. (2022). Thermogravimetric analysis of respirable coal mine dust for simple source apportionment. *Journal of Occupational and Environmental Hygiene*, *19*(9), 568-579.

Page, S. J., Volkwein, J. C., Vinson, R. P., Joy, G. J., Mischler, S. E., Tuchman, D. P., & McWilliams, L. J. (2008). Equivalency of a personal dust monitor to the current United States coal mine respirable dust sampler. *Journal of Environmental Monitoring*, *10*(1), 96–101. https://doi.org/10.1039/b714381h

Tuchman, D. P., Volkwein, J. C., & Vinson, R. P. (2008). Implementing infrared determination of quartz particulates on novel filters for a prototype dust monitor. *Journal of environmental monitoring*, *10*(5), 671-678.

Chow, J. C., Watson, J. G., Wang, X., Abbasi, B., Reed, W. R., & Parks, D. (2022). Review of filters for air sampling and chemical analysis in mining workplaces. *Minerals*, *12*(10), 1314.

3 Chapter 3: Preliminary investigation of CPDM sample recovery method to enable quartz analysis by FTIR

Garek Elie, Emily Sarver

3.1 Abstract

Respirable coal mine dust (RCMD) in conjunction with respirable crystalline silica (RCS) can lead to debilitating health conditions in miners. Since 2016, mine operators have transitioned from coal mine dust personal sampling units (CMDPSUs) to continuous personal dust monitors (CPDMs) for compliance. CPDMs can sample for RCMD compliance in real time however, lack the capabilities to monitor for quartz. With the 2016 transition, quartz analysis has primarily been reserved to the Mine Safety and Health Administration (MSHA), who use the CMDPSUs to collect filter samples and send them to official labs for the MSHA Method P-7 analysis. The use of direct-on-filter (DOF) Fourier transform infrared (FTIR) analysis paired with a CPDM filter stub redeposition method could provide mine operators with an alternative analysis method for research or engineering studies in quartz data. CPDM filters will need to undergo a redeposition process due to the material makeup of the filters interfering with infrared (IR) analysis. The CPDM filter can be shaken in IPA and the dust-laden IPA can be deposited onto a polyvinylchloride (PVC) filter for the DOF FTIR analysis. Due to the CPDM filter stub easily deteriorating, corrections can be applied to the determined quartz and dust mass to remove interference from the CPDM filter.

3.2 Introduction

Beginning in the late 1990's, there has been an alarming uptick in the number of cases of Coal Worker's Pneumoconiosis (CWP, or "Black Lung") in the United States, primarily focused around central Appalachia (Hall et al., 2019). CWP is caused by overexposure to respirable coal mine dust (RCMD), which can also include respirable crystalline silica (RCS); in coal mines, the predominant form of RCS is alpha-quartz (termed simply "quartz" from here). RCS, in particular, is linked to the most severe form of CWP, called progressive massive fibrosis (Hall et al., 2019, Cohen et al., 2022). In 2014, the Mine Safety and Health Administration (MSHA) finalized a 'new dust rule', which reduced the permissible exposure limit (PEL) for RCMD and mandated the continuous personal dust monitor (CPDM) for all mine operator-conducted sampling (Lowering Miners' Exposure, 2014). Further, in 2024, MSHA finalized a 'new silica rule' to reduce the PEL for RCS specifically (Lowering Miners' Exposure, 2024). The new RCS PEL is 50 $\mu g/m^3$ for all miners, with an action level at 25 $\mu g/m^3$. These limits are applied as an 8-hour time-weighted average (TWA) to samples collected over a full shift of work.

In coal mines, before the CPDM was required, all respirable dust sampling was done using a Coal Mine Dust Personal Sampling Unit (CMDPSU). This unit collects a physical sample on a polyvinyl chloride (PVC) filter that can be used to determine the RCMD concentration by gravimetric analysis; and the sample can also be analyzed for RCS by Fourier transform infrared spectroscopy (FTIR) using quartz as a surrogate analyte. For regulatory compliance demonstration, the RCS analysis is conducted using the standard MSHA Method P7 (MSHA P-7, 2013). Briefly, the sample is ashed to remove combustible matter (i.e., coal dust and the PVC filter itself); the residue is deposited onto a new filter; and that filter is analyzed to determine quartz mass, which can be converted to mass concentration knowing the sampling flowrate and duration. However, since Method P7 must be performed in a lab, there can be substantial delays between sampling and results reporting.

When the 2014 'new dust rule' was fully implemented, MSHA took over all compliance sampling for RCS in coal mines, and many mines got rid of their CMDPSUs since they were only required to use CPDMs. Moving forward with the 'new silica rule', it appears MSHA will still be responsible for RCS sampling, and will use their own lab (as has been the case heretofore) or a contract lab for the Method P7 analysis. However, especially in light of the reduced RCS PEL and action level, mines need more data—and more timely data—to better understand their RCS sources and the effectiveness of their controls.

To enable more timely RCS data, researchers at the National Institute of Occupational Safety and Health (NIOSH) have developed a standardized method for direct-on-filter (DOF) FTIR analysis (Ashely, 2003, Miller et al., 2012, Cauda et al., 2016). It uses the same PVC filter samples as would be collected for the Method P7 analysis, but no sample preparation is required. Thus, with a portable FTIR instrument, the DOF method can be done in the field to enable rapid (e.g., end-of-shift) results. Nevertheless, a main challenge for widespread adoption of the DOF FTIR method is that many mines are no longer using—and do not even possess—the CMDPSUs needed for filter sampling. Rather, coal mines have moved almost exclusively to the CPDM for RCMD sampling. The CPDM is worn by a miner and allows for real-time RCMD concentration monitoring (National Academies, 2018). While it does collect a physical RCMD sample, at present there is no analytical method to enable RCS determination in that sample.

While FTIR analysis of CPDM samples has previously been considered, a main barrier is the makeup of the CPDM's filter stub assembly. It consists of a borosilicate glass fiber and polytetrafluoroethylene (PTFE) filter, with a woven glass backing mounted to a polypropylene (PP) stub (Chow et al., 2022). The

glass materials directly interfere with the IR spectral peaks of the target quartz analyte, which prevents typical DOF analysis that relies on IR absorbance or transmission (Tuchman, 2008); and attempts to use diffuse reflectance IR have also been unsuccessful (Miller et al., 2015). However, a method that includes a simple dust recovery step, followed by deposition of the recovered dust onto a PVC filter might represent a feasible workaround. Figure 3.1 presents a conceptual illustration of such a method.

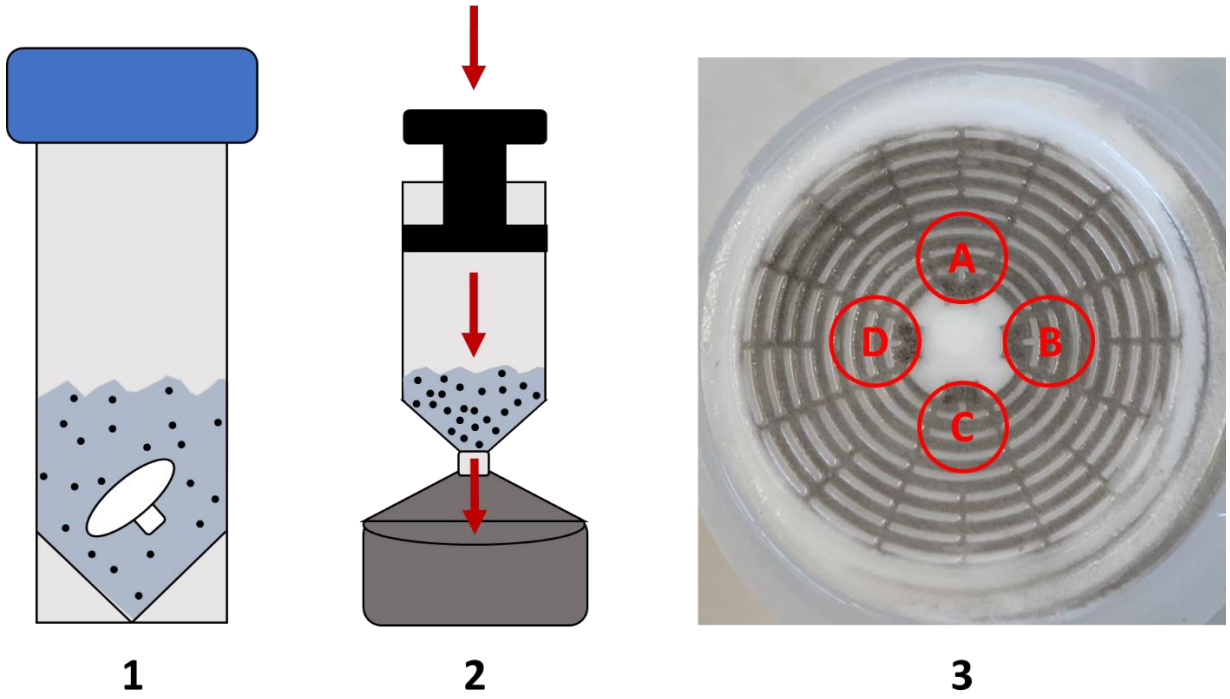

Figure 3.1: Conceptual illustration of a method to enable FTIR analysis of CPDM samples, wherein **(**1) CPDM filter stub is placed in tube with IPA and shaken to remove dust; (2) the dust-IPA suspension is deposited onto a clean 25-mm PVC filter using an in-line PP syringe filter apparatus; and (3) the PVC filter is scanned by the FTIR in four center-offset locations, represented by circles A, B, C, and D (90 degrees apart).

To this end, recent work in the author's research group has focused on the deposition and FTIR analysis steps shown in Figure 3.1 (Greth and Sarver, n.d.) Starting with representative respirable dust suspensions in IPA, that work determined that a simple syringe filter apparatus (i.e., 50 mL syringe with Leur Lock® outlet and 25 mm in-line PP filter holder) can be used to deposit the dust onto a clean 25 mm PVC filter—with a characteristic deposition pattern that is repeatable (i.e., same pattern on each filter). IPA was chosen for the redeposition process due to its quick evaporation, allowing samples to dry and be scanned the next day. Once dry, this enables the filter to be scanned by FTIR, and the resulting spectrum can be used to determine quartz mass. This is essentially the same way that quartz mass is determined via the DOF method, except that the FTIR analysis location on the filter is changed. For the DOF method (i.e., 37 mm PVC filters with RCMD collected directly from the mine atmosphere), a single analysis point in the center of the filter can be used. But, for the 25 mm PVC filters with IPA-recovered dust, the previous work showed that an average of data from four analysis locations (offset from the filter center at 90 degrees from one another) yields more accurate results (Greth and Sarver, n.d.) This is due the characteristic deposition pattern yielded by the 25 mm in-line filter holder (see Figure 3.1).

Though the previous work addressed deposition and FTIR analysis of recovered dust, it did not address the actual recovery procedure—nor the possible contamination of the sample that might result from the CPDM filter stub materials. These were the subject of the current study. Here, a simple procedure that includes shaking the CPDM filter stub in IPA for a short duration was tested, and the recovered material was deposited and analyzed using the previously established procedures (i.e., per Figure 3.1 and as detailed in Greth and Sarver, n.d.) Experiments were conducted in three phases with three different sample types: (1) samples generated from blank CPDM filter-stubs ("blank CPDM"), which were used to observe the range of residue that might be expected from the CPDM filter stubs themselves and establish corrections for their contribution to total sample mass and quartz mass; (2) samples generated from blank CPDM filters spiked with respirable dust of known quartz content, which were used to test the CPDM residue corrections; and (3) samples generated from field CPDM filters, which were used to evaluate the three-step method shown in Figure 3.1 by comparison to reference analysis on paired CMDPSU filter samples.

3.3 Methods and Materials

3.3.1 Sample Preparation

All samples were prepared using 25-mm PVC filters (Zefon International, Ocala, FL), which were pre-weighed using a Cubis MSE6.6S microbalance (Sartorius, Gottingen, Germany) with a readability of 2 µg. After pre-weighing, each filter was loaded into PP in-line syringe filter holder (Sterlitech Corporation, Auburn, WA) along with a cellulose backing pad. The filter holders have Luer Lock® inlets and were used with 50 mL sterile syringes (BD, Franklin Lakes, NJ). Following sample deposition onto the filter, it was allowed to dry completely and then post-weighed using the same microbalance. Sample mass was determined using Equation 1:

$$\mathrm{M}=F_2 - F_1 \qquad \text{Equation 1}$$

where, F_1 and F_2 are the filter pre- and post-weigh respectively.

3.3.1.1 Blank CPDM Samples

A total of 20 samples were prepared from blank CPDM filter stubs (Thermo Scientific, Waltham, MA). For this, clean stainless steel tweezers were used to transfer a blank CPDM filter into a clean 50 mL test tube, and then 5mL of IPA was added to completely submerge the filter stub. Care was taken to handle the filter stubs by holding the PP stub to prevent damaging the filter itself. Test tubes were capped and placed into a holder that was secured to a shaker table (Thermolyne, Dubuque, IA) using zip ties. The shaker table was turned on for 1 minute (350 RPM), and then the tubes were uncapped and the CPDM filter stubs were carefully removed using tweezers. Then, the tubes were recapped to minimize IPA evaporation before each CPDM residue suspension could be deposited onto a PVC filter.

To deposit the suspensions onto the prepared PVC filters, each suspension was transferred into a syringe with an attached filter holder (i.e., already loaded with the pre-weighed PVC filter). Then, the syringe plunger used to push the IPA through the filter. After that, the filter holder was opened and the filter was carefully transferred to a two-piece cassette (inlet and outlet plugs removed) and allowed to dry completely in a clean fume hood (at least 12 hours).

3.3.1.2 Spiked CPDM Samples

A total of 20 samples were prepared using blank CPDM filter stubs spiked with respirable dust of known quartz content. These samples were prepared using the same procedure described above to shake a blank CPDM filter stub in IPA. However, after the stub was removed from the test tube, a small mass of respirable dust from one of two sources was also added to the tube to create a suspension that included the CPDM residue and dust.

The respirable dust was collected from a bulk source of either 'Mine 10 bolter dust' or 'Mine 15 roof rock'. The former had been taken directly from the dust collection system of a roof bolter machine at a partner mine (Mine 10), and the latter was created by pulverizing raw roof rock material that had been taken from the production belt in another partner mine (Mine 15). Respirable dust was collected from each of these source materials using the following procedure: A small mass of the material was placed in a small enclosure and aerosolized using compressed air, and CMDPSUs (i.e., 10 mm nylon cyclone with air pump at 2.0 L/min) were used to collect the respirable dust directly onto 37-mm PTFE filters in closed two-piece cassettes. The filters were pre-and post-weighed to estimate the total mass of respirable dust collected, and a total of 10 filters were collected for each material having mass in the range of about 0.1 to 2.0 mg to simulate realistic CPDM sample masses that might be expected in the field. Notably, in the previous work, the same procedure was used to generate respirable dust samples of these same two materials on 37-mm PVC filters; these were sent to a contract lab (RJLee Group, Pittsburgh, PA) for quartz analysis using the standard NIOSH Method 7603 (i.e., analogous to MSHA Method P7). Results showed that the respirable quartz content in the Mine 10 bolter dust was 9.51% and that of the Mine 15 roof rock was 10.45%.

To spike the CPDM residue suspensions (n = 20) with respirable dust, one of the loaded PTFE filters was added to each test tube and submerged in the IPA (n = 10 for Mine 10 bolter dust and n = 10 for Mine 15 roof rock). Then, the tubes were capped and placed into a sonic bath at 32 degrees Celsius for three minutes to dislodge the dust from the filters. Finally, the filters were removed from the tubes and the tubes were recapped until the suspensions were deposited onto the prepared 25-mm PVC filters. For that, the same procedure described above was followed.

3.3.1.3 Field Samples

A total of ten field CPDM samples were available from a previous study in a partner mine (Mine 28, see Chapter 2). The CPDM samples had been collected in sets with paired RCMD samples collected directly onto 37-mm PVC filters using CMDPSUs. No sampling equipment was placed onto a miner, with only area studies performed, generally downwind of the continuous miner and roof bolter. Following sampling in the field, each CPDM filter stub was carefully removed from the CPDM instrument and placed into a clean test tube (i.e., identical to those used in the lab), and then these were transported to the Virginia Tech lab and kept capped until this study.

Each CPDM used in the sampling process at Mine 28 had its data sheet downloaded and the dust mass deposited onto the TEOM filter (mg) was calculated through Equation 2:

$$M_{CPDM} = M_2 - M_1 \qquad \text{Equation 2}$$

where, M_1 is the filter mass at the start of the CPDM sampling (mg) and M_2 is the filter mass at the end of the CPDM sampling (mg).

To prepare the CPDM samples for FTIR analysis, the same recovery and dust deposition procedures described above for the blank CPDM filter stubs were used: The CPDM filter stubs were placed into a clean test tube, 5 mL of IPA was added to each test tube, the tube was shaken for 1 minute (350 RPM), and the filter stub was removed. Then, the recovered dust was deposited onto a prepared 25-mm PVC filter using the syringe-filter apparatus, and the filter was allowed to dry completely before FTIR analysis.

For each of the ten CPDM samples used here, there was a paired PVC filter sample (i.e., n = 10 PVC filters). These filters had been pre-weighed prior to sampling and were post-weighed to determine total sample mass per Equation 1. (They were also analyzed by the DOF FTIR method, though these results are not relevant to the current study). The 10 PVC filter samples were then sent to the contract lab for quartz analysis by NIOSH Method 7603. Prior to the 7603 analysis, the lab also weighed the filters—and these results confirmed that sample mass loss or contamination was unlikely.

3.3.2 FTIR Analysis

An Alpha II Compact spectrometer paired with the OPUS software (Bruker Optics, Billerica, MA) was used to scan each of the samples following the mass determination. The filter needed to be removed from its cassette and placed into a custom 3-D printed analysis cassette to be secured and aligned in the instrument's scanning compartment, shown in Figure 3.2. The analysis cassette is square in shape with dimensions such that the center of a 25-mm filter to be aligned with the 6-mm diameter IR beam. For this study, a 4-mm spacer was placed under the cassette such that the beam was offset from the filter center by a distance 4-mm (per Figure 3.2). The FTIR analysis was conducted at four 4-mm offset locations (90 degrees apart) by simply rotating the cassette four times.

Figure 3.2: 3-D printed 25mm filter holder (above) and 4mm offset spacer.

Each filter was analyzed three times, on three separate days (events), and since the filter was placed into and removed from the analysis cassette for each event, the actual scan locations most certainly varied

between events (i.e., due to the relative rotation of the filter within the cassette). For each event, the spectrum from each analysis location was used to obtain the integrated spectral peak areas in two ranges: 767cm^{-1}-816cm^{-1} refers to the quartz doublet peak area and 900 cm^{-1}-930 cm^{-1} refers to the primary kaolinite peak. Notably, kaolinite has a secondary peak that overlaps with the quartz peak, but the primary and secondary kaolinite peaks occur in near constant ratio. Thus, the primary kaolinite peak area was used to correct the quartz peak area per Equation 3:

$$P'_Q = (P_Q - \frac{P_K}{3.8}) \qquad \text{Equation 3}$$

where, P'_Q is the corrected integrated quartz peak area (arbitrary units); P_Q is the integrated quartz area (arbitrary units); P_K is the integrated kaolinite area (arbitrary units); and 3.8 is the constant ratio between the primary and secondary kaolinite peak areas (Pokhrel et al., 2022).

For each event, the four values of P'_Q were averaged and then Equation 4 was used to compute quartz mass on the sample filter. This equation represents a model established in the previous work by Greth and Sarver (n.d.), for the "4-mm offset, 4-pt" analysis pattern on a 25-mm PVC filter with dust deposition using the same procedure as used for this study.

$$Q = P'_{Q_{avg}}/9.3482 \qquad \text{Equation 4}$$

where, Q is quartz mass (µg), $P'_{Q_{avg}}$ is the mean integrated quartz area (arbitrary units); and 9.3482 is the calibration factor determined by (Greth and Sarver., (n.d)).

Finally, the Q values from each event were averaged to obtain a mean Q and standard deviation for each sample.

3.4 Results and Discussion

3.4.1 Blank CPDM Sample Data

Each 25-mm PVC filter was post-weighed and the dust mass was calculated through Equation 1. Then the filter was analyzed by FTIR (i.e., three scanning events, each collecting data from four 4-mm offset locations). Corrected quartz spectral peak and quartz mass were determined using Equation 3 and Equation 4, respectively, with the results shown in Table B1. (Table B2, Table B3, and Table B4 show the spectral peaks for each of the four scan locations for the three different events.) Figure 3.3. shows that the quartz mass had a relatively low correlation with the CPDM residue mass. Due to this low correlation, the median CPDM residue mass and median quartz mass were determined to be 0.019mg and 0.002mg respectively, and used for corrections to account for contributions to a CPDM sample arising from the CPDM filter assembly itself.

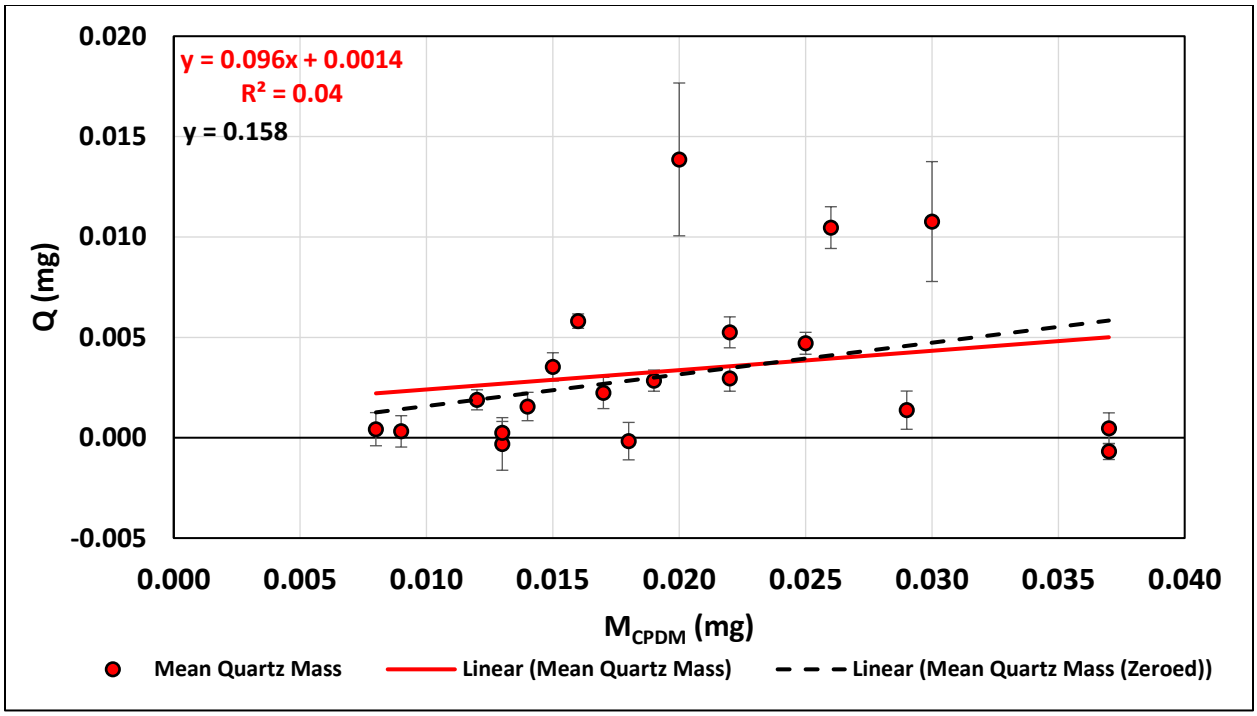

Figure 3.3: Mean quartz mass and CPDM residue from blank CPDM filters.

The corrected dust mass and corrected quartz mass were calculated using Equation 5 and Equation 6 respectively:

$$M' = M - 0.0185 \qquad \text{Equation 5}$$

$$Q' = Q - 0.00214 \qquad \text{Equation 6}$$

where, M is the total sample mass, attributed to the dust (mg) plus CPDM residue; 0.0185 is the median CPDM residue mass (mg) determined from the CPDM blank experiments; Q is the total quartz mass (mg) in the sample, attributed to the dust plus CPDM residue; and 0.00214 is the median quartz mass from the CPDM residue determined from the CPDM blank experiments.

As previously mentioned, the median quartz mass and CPDM residue were used rather than the mean due to this low correlation. Presumably, the quartz mass is due to just the blank CPDM filter deterioration from the vigorous shaking process, but there could be other factors related to the procedure affecting this value such as the IPA. Depending on the type of deposition solution used, there may be varying results of quartz content from the FTIR (Greth and Sarver., (n.d)).

3.4.2 Spiked CPDM Sample Data

The Mine 10 bolter dust showed strong correlations between the quartz mass and dust mass for both the uncorrected and predicted values. Seen in Figure 3.4, the two slopes can be used in comparison to the previously established 7603 analysis quartz content of 9.51%. The uncorrected and predicted quartz content are both seen to be lower at 7.56%, with the mass data shown in Table B5, and the spectra of each event scan in Table B6, Table B7, and Table B8. The slope being equal values between the uncorrected and predicted quartz values could suggest that correcting for CPDM residue interference

may not be necessary when redepositing from a CPDM filter if the same shaking and redeposition method is followed.

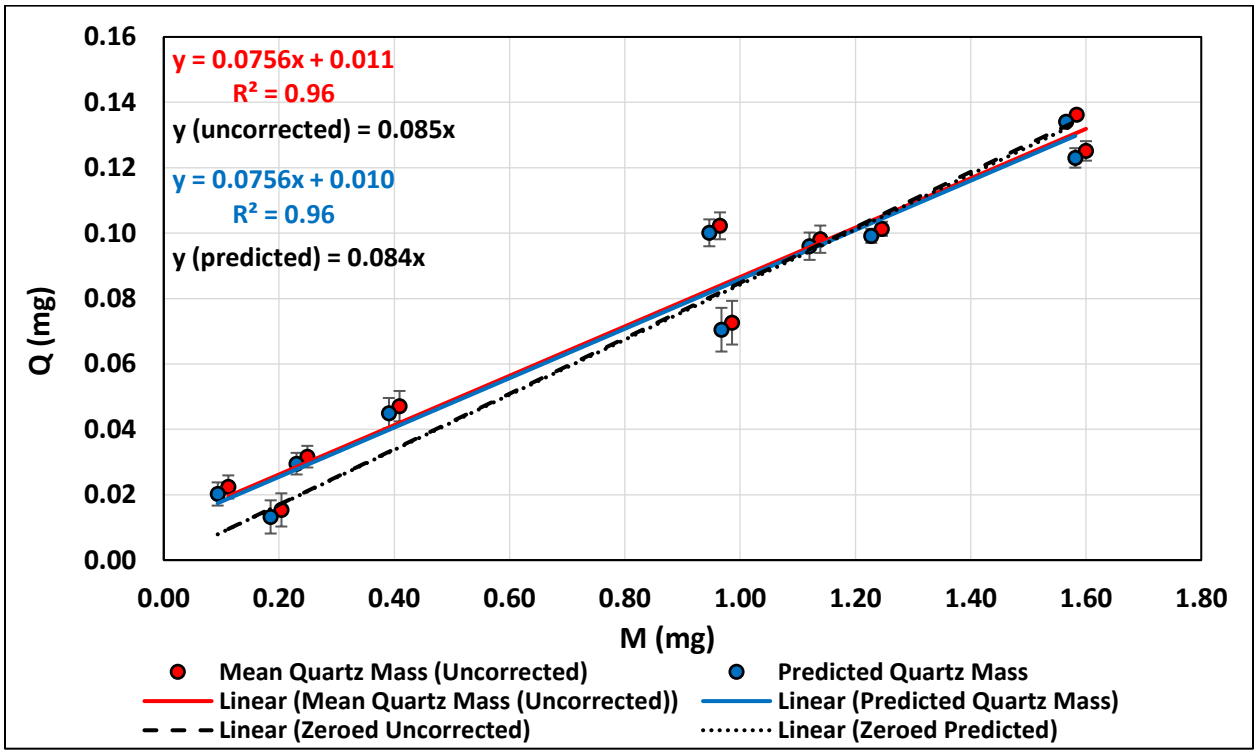

Figure 3.4: Mine 10 bolter dust uncorrected and predicted quartz masses against uncorrected and predicted dust masses.

The Mine 15 roof rock had a similar trend to the bolter dust, with strong correlations seen between the dust masses and quartz masses of the uncorrected and predicted values. From the Method 7603 analysis, the quartz content of the roof rock was found to be 10.45%. While the bolter dust was lower than its respective 7603 quartz content, the Mine 15 roof rock was nearly identical. The slopes of the uncorrected and predicted values in Figure 3.5 show the quartz percentages being equal at 9.62%, with Table B9 showing the masses and Table B10, Table B11, and Table B12 displaying the spectra data respectively. Again, since there were no calculated differences between the uncorrected and predicted quartz percentages, correction using the blank CPDM residue mass and quartz mass may not be necessary in the calculation if the same method of redeposition is followed.

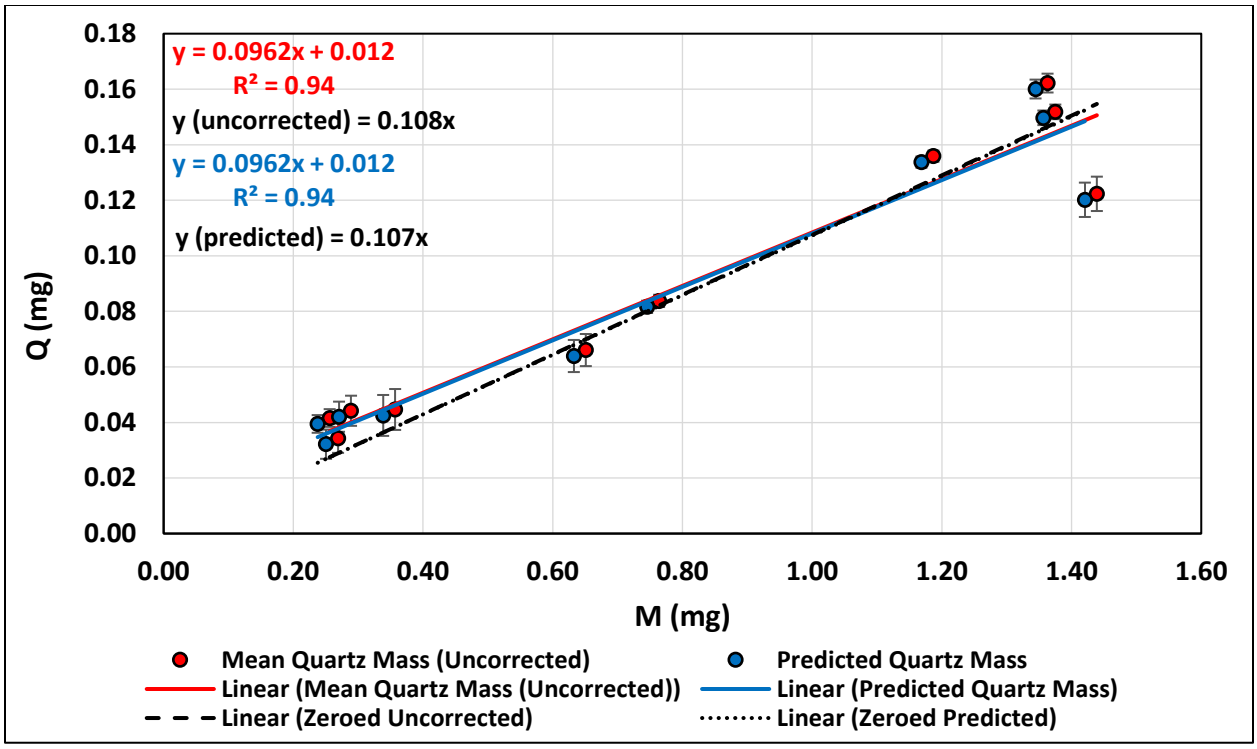

Figure 3.5: Mine 15 roof rock uncorrected and predicted quartz masses against uncorrected and predicted dust masses.

In both the bolter dust and roof rock materials, it is seen that the samples with lower dust masses generally overpredict quartz masses. Shown by the slopes and y-intercepts in Figure 3.4 and Figure 3.5, at a dust mass of zero, there will be a positive quartz mass prediction. The uncorrected quartz masses are shown to overpredict slightly more than the predicted quartz masses, however this difference is not significant. Additionally, though the slope of the trendlines for the spiked materials do not match the NIOSH Method 7603 materials quartz percentages, it should be noted that the generated samples may not be homogenous. The dust was scooped out of a plastic bag holding the respective materials, but the Method 7603 percentages may not be representative of the entire bag sample, where quartz percentages may vary depending on which spots were chosen to be scooped from.

Greth et al. (TBD) found that the Mine 10 bolter dust had a quartz to kaolinite ratio of 0.999 while the Mine 15 roof rock had a quartz to kaolinite ratio of 1.507. Using these factors, the expected quartz mass (mg) could be obtained as shown in Equation 7 and 8, and used to compare against the predicted values previously calculated using the methods from Equation 6. The expected quartz masses of the bolter dust are displayed in Table B5, with the expected quartz masses of the roof rock shown in Table B9.

$$Q_{exp} = P_{k\_avg} * \frac{0.999}{9.3482} \qquad \text{Equation 7}$$

$$Q_{exp} = P_{k\_avg} * \frac{1.507}{9.3482} \qquad \text{Equation 8}$$

Where, P_{k_avg} is the mean of the 12 peak kaolinite areas (arbitrary units); 0.999 is the Mine 10 bolter dust quartz to kaolinite ratio; 1.507 is the Mine 15 roof rock quartz to kaolinite ratio; and 9.3482 is the 4-mm offset mean determined by (Greth and Sarver., (n.d)).

Though the predicted quartz content for the Mine 10 bolter dust is a couple percentage points lower than the 7603 quartz content, when plotting between the predicted quartz mass and expected quartz mass, determined from the kaolinite peaks, it shows a very strong correlation with a near 1:1 slope seen in Figure 3.6. Figure 3.7 shows the Mine 15 roof rock also demonstrating a near 1:1 slope despite the predicted quartz content being about a percentage point lower than what was determined in the 7603 analysis. The predicted and expected values are seen to have a very strong correlation for both the bolter dust and roof rock at 0.98 and 0.97 respectively.

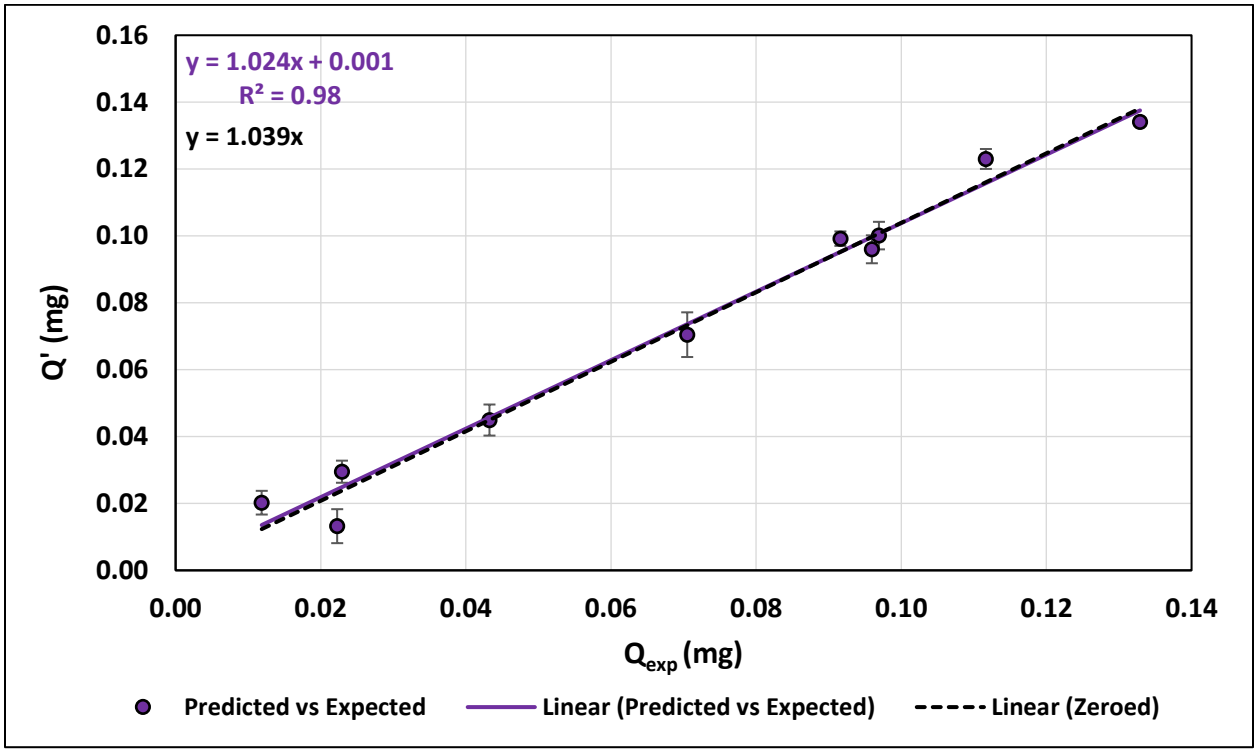

Figure 3.6: Predicted quartz mass versus expected quartz mass for Mine 10 bolter dust.

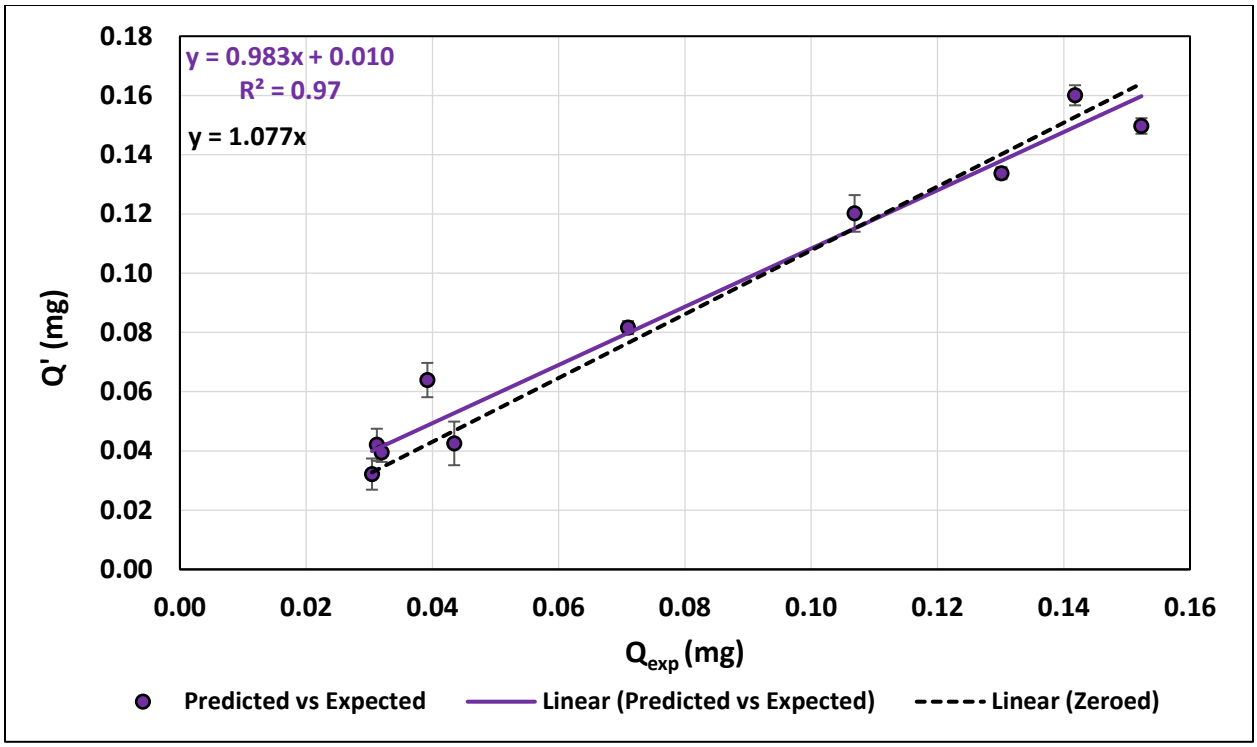

Figure 3.7: Predicted quartz mass versus expected quartz mass for Mine 15 roof rock.

3.4.3 Field Sample Data

The analysis methods of the Mine 28 field samples differed slightly from the methods used for the lab samples. Since the CPDM sample collection occurred in different sections of Mine 28 on different days, the CPDM contained dust of varying compositions and masses. Due to this variation, the quartz mass was not directly analyzed against the dust mass on the filter as the quartz content would vary depending on the type of dust on the filter.

The quartz mass of the samples was determined using Equation 3 and Equation 4, and then corrected to obtain the predicted quartz mass and predicted dust mass through Equation 5 and Equation 6. The expected quartz mass was obtained differently from the Mine 10 and Mine 15 materials. Each CPDM field sample had a paired 37-mm PVC filter triplicate sample taken in tandem at Mine 28. The paired PVC filter was analyzed by a contract lab which performed the NIOSH Method 7603 analysis and the resulting quartz data were used to calculate the expected quartz masses (mg) from the field samples. The quartz percentage from the 7603 analysis was multiplied by the respective Mine 28 CPDM dust mass deposited onto the 25-mm filter as shown in Equation 9:

$$Q_{exp} = M' * Q_{7603} \qquad \text{Equation 9}$$

where, M' is the corrected dust mass of the filter; and Q_{7603} is the NIOSH 7603 determined quartz percentage for the respective CPDM sample.

The predicted quartz percentages of the CPDM samples were determined by Equation 10 to be compared to the expected NIOSH 7603 percentages.

$$Q\% = \frac{Q'}{M'} \times 100 \qquad \text{Equation 10}$$

Where, Q' is the corrected quartz mass (mg) and M' is the corrected dust mass (mg).

Using the mass of the respirable dust collected on the CPDM filter, the estimated percentage of dust removed from the original filter onto the 25-mm PVC filter was calculated using Equation 11:

$$\mathrm{R\%} = \frac{M'}{M_{CPDM}} \times \frac{100}{1.38} \qquad \text{Equation 11}$$

where, M' is the corrected dust mass of the 25-mm PVC filter (mg), M_{CPDM} is the mass of dust on the original CPDM filter (mg), and 1.38 is the MRE conversion factor.

Since the CPDMs are programmed to automatically report MRE-equivalent values, the filter mass must be divided by 1.38 to convert it to non-MRE form. The quartz masses and dust masses were not corrected to the MRE-equivalent values during the study. Since the quartz percentage calculation involved dividing a quartz mass by a dust mass to obtain a ratio, multiplying by the 1.38 MRE factor in the numerator and denominator was not necessary.

The predicted and expected quartz mass was compared in Figure 3.8, where the correlation was seen to be very strong. However, there was a data point that created more significant weight to the slope due to its much higher quartz mass. The slope of the line was 0.744, showing that the predicted quartz masses were generally lower than the expected quartz masses. The Mine 28 dust and quartz masses are shown in Table B13 and the scanned spectra data from the FTIR are shown in Table B14, Table B15, and Table B16.

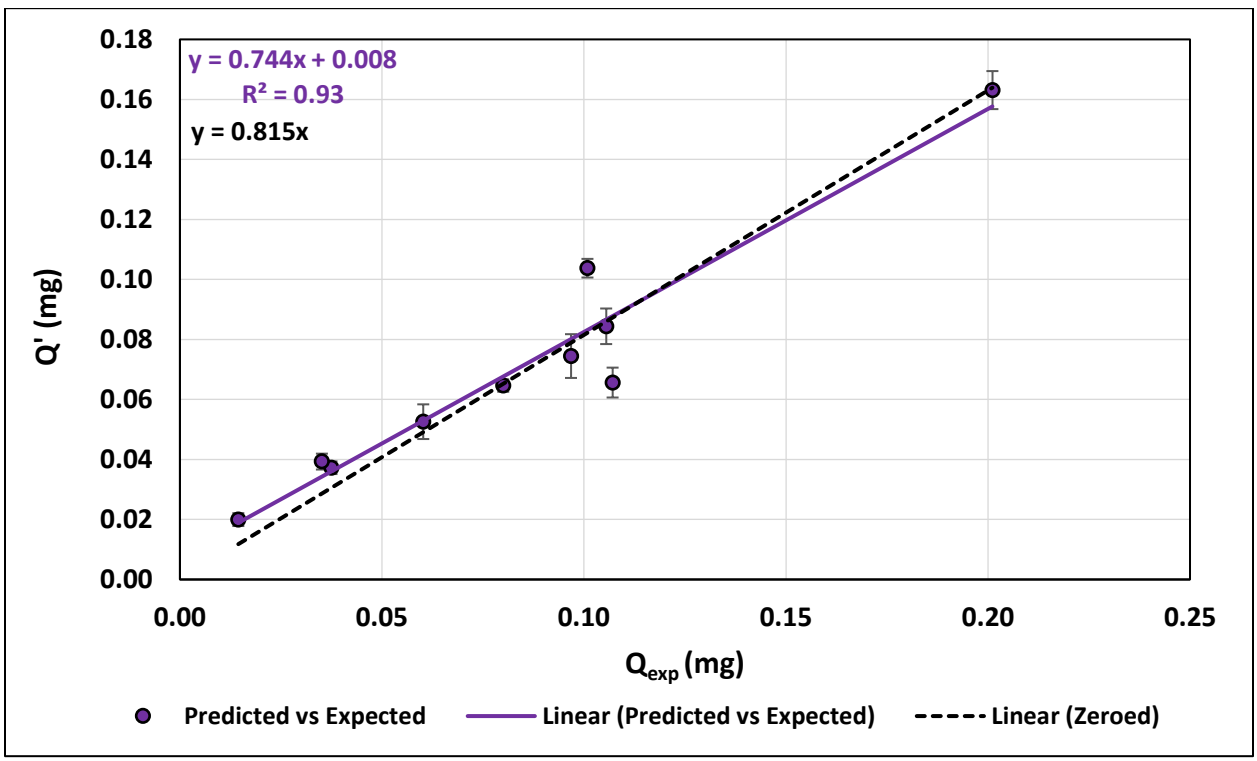

Figure 3.8: Predicted quartz mass versus expected quartz mass for Mine 28 field samples.

There is a similar case when it comes to the quartz percentages of the samples, shown in Figure 3.9. The slope of the quartz percentages of the predicted and expected values is similar to the slope of the

predicted vs. expected quartz masses in Figure 3.8 at 0.744, where the predicted quartz percentages are underpredicted compared to the 7603 values.

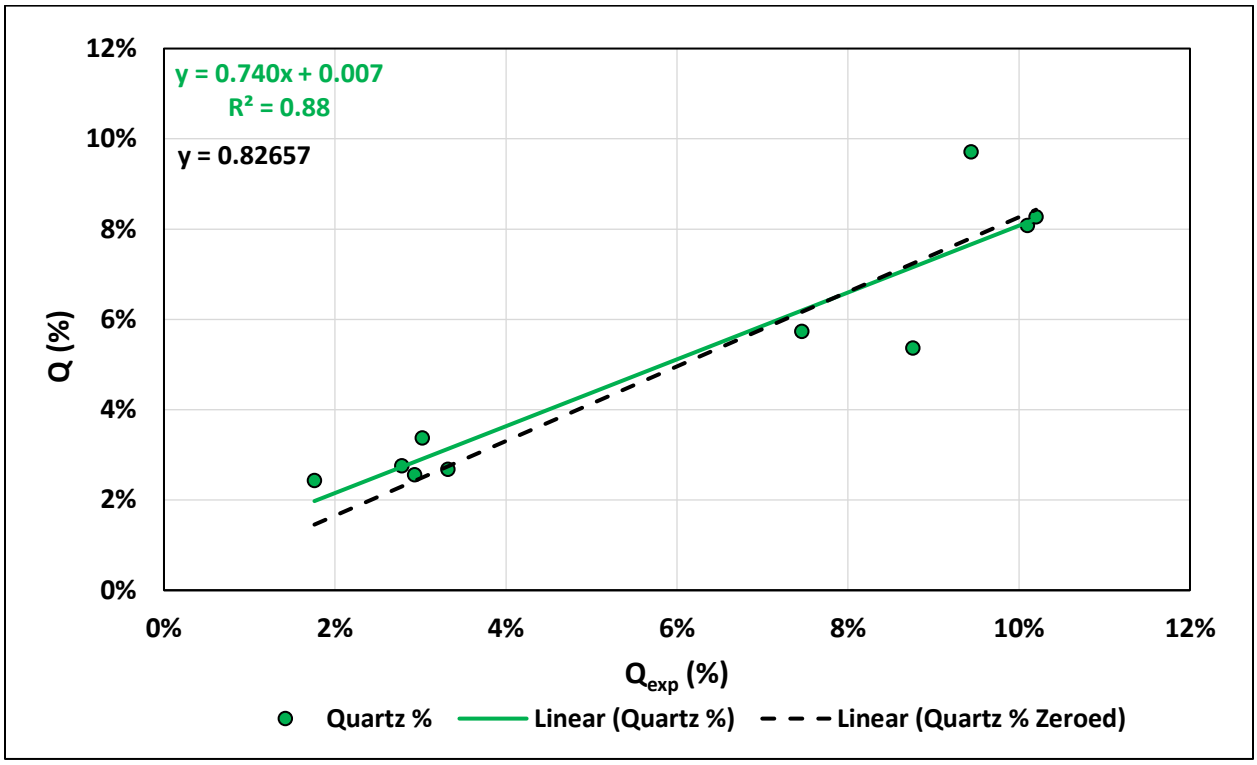

Figure 3.9: Mine 28 quartz percentages from CPDM filter redeposition versus quartz percentages from Mine 28 gravimetric field sample analyzed under the NIOSH Method 7603 analysis.

For each CPDM, the data file was collected, and the mass of the dust collected onto the TEOM filter was determined over the time period of the triplicate sampling. Table 3.1 displays the accumulated dust mass data before, during, and after the paired CMDPSU sampling period. It's seen that the majority of the dust deposited onto the CPDM filter was during the time that the CPDM was sampling alongside the CMDPSUs, with some additional dust collected outside of that time interval. Table 3.2 compares the total dust mass accumulated on the CPDM filter during its entire sampling period and the dust mass deposited onto the 25mm PVC filter, as well as the recovery. A mean of 84.89% of dust mass from the original filters were able to be removed and redeposited onto the 25-mm filter, assuming that the recovery process retained 100 percent of the dust through all stages. Figure 3.10 displays a box and whisker plot showing the spread of the mass percent of dust removed from the original CPDM filter. The median is slightly skewed right at a value of 84.44% with the lowest recovery at 75.43% and the highest recovery at 101.44%. The mass recovery above 100% for Sample 1 was likely due to a higher than normal filter deterioration of the original CPDM filter, with there being additional CPDM residue deposited onto its respective 25mm filter. The CPDM filter with the lowest recovery had the greatest measured corrected dust mass and CPDM filter mass. The CPDM non-MRE filter dust masses were seen to be greater than the redeposited 25mm filter dust masses (exception of Sample 1 shown in Table 3.2). Each CPDM was sampled in tandem with triplicate CMDPSUs however, the CPDMs were programmed for a set sampling time, causing the CPDMs to collect respirable dust particles onto its filter stub outside of the sampling time the CMDPSUs operated. Additionally, the collected CPDM filters likely had dust loss into

the test tube it resided in due to transportation and handling. For samples with greater dust mass, the dust adheres to other dust particles rather than the filter when no surface area of the filter is available. This causes the dust to be easily disturbed and fall off if not carefully handled. When redepositing the CPDM filter dust, the filters were placed into a second test tube for the process, meaning any dust left in the original test tube was not deposited onto the 25mm, PVC filter, potentially resulting in reduced dust recovery.

Table 3.1: CPDM sampling times and respirable dust mass accumulation before, during, and after CMDPSU operating time. *The CPDM shut off before the end of the CMDPSU samplers.

			CPDM Sampling Before CMDPSU Start Time		CPDM Sampling During CMDPSU Sampling Time		CPDM Sampling After CMDPSU End Time	
MMU	Event and Location	Sample ID	CPDM Sampling Time (min)	Non-MRE CPDM Accumulated Mass (mg)	CPDM Sampling Time (min)	Non-MRE CPDM Accumulated Mass (mg)	CPDM Sampling Time (min)	Non-MRE CPDM Accumulated Mass (mg)
3	E5-L3	S1	104	0.070	257	1.060	239	0.149
1	E6-L1	S2	104	0.346	291	2.235	145	0.143
3	E7-L2	S3	76	0.139	287	0.956	177	0.185
3	E8-L2	S4	100	0.114	256	1.038	64	0.066
3	E10-L1	S5	66	0.668	326	1.876	28	0.020
1	E1-L2	S6	150	0.090	281	0.695	169	0.162
1	E2-L1	S7	103	0.083	312	2.873	162	0.106
1	E2-L2	S8	110	0.174	307	1.345	163	0.105
3	E8-L3	S9	90	0.075	268	1.251	62	0.090
1	E9-L1	S10	118	0.073	213	1.224	*	0.000

Table 3.2: Recovery percentages from total CPDM accumulated mass and recovered dust mass.

Sample ID	Total Non-MRE CPDM Filter Dust Mass (mg)	PVC Filter Mass (mg)	Corrected Dust Mass (mg)	Percent of Mass Removed
S1	1.279	1.316	1.298	101.44%
S2	2.725	2.074	2.056	75.43%
S3	1.280	1.241	1.223	95.53%
S4	1.218	1.063	1.045	85.73%
S5	2.564	1.990	1.972	76.89%
S6	0.947	0.840	0.822	86.74%
S7	3.062	2.429	2.411	78.72%
S8	1.623	1.368	1.350	83.14%
S9	1.416	1.087	1.069	75.47%
S10	1.296	1.182	1.164	89.75%
			Average	84.89%

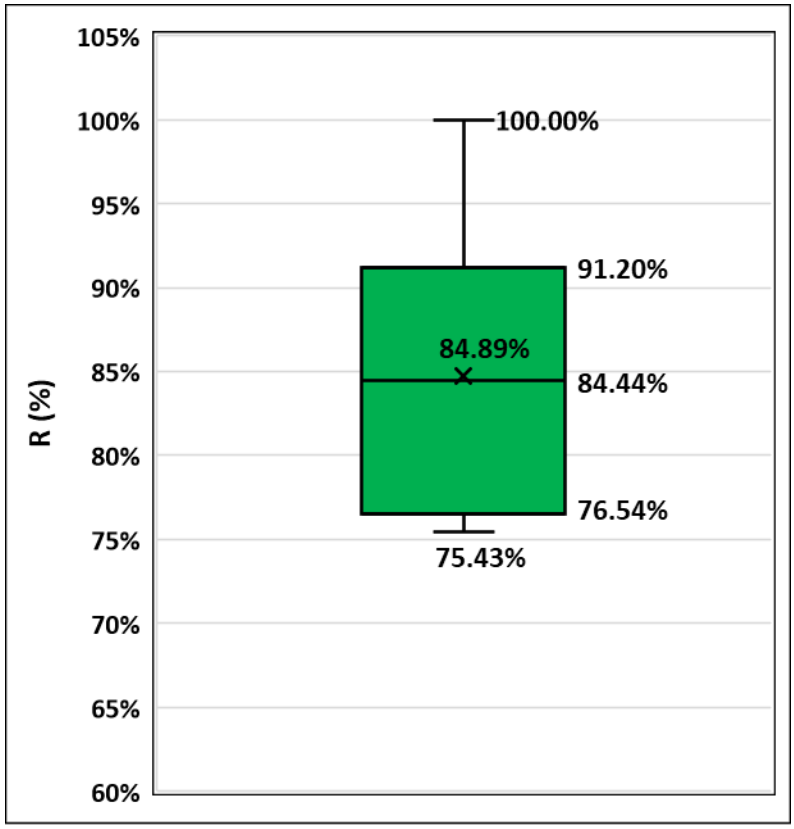

Figure 3.10: Recovery percentages of the Mine 28 CPDM field samples.

Due to the dust mass recovered from the CPDM filters ranging from 75.43% to 101.44%, a consistent mass recovery value is not obtainable, and variations in the determined quartz masses will be present. In Figure 3.10, despite the Sample 1 recovery being 101.44%, the max mass recovery percentage displayed was 100% as Sample 1 was the only one exceeding this value and a mass recovery past 100% could be due to excessive CPDM filter deterioration. The variation allows for a possible range of quartz masses which can be translated into quartz mass concentrations as long as the CPDM sampling time and flow rate are known. The quartz mass concentration (mg/m^3) can be calculated through Equation 12:

$$C_{Q\_CPDM} = \frac{Q\prime}{2.2 \times t} \times \frac{1000\ \mathrm{L}}{\mathrm{m}^3} \qquad \text{Equation 12}$$

An example quartz range determination for a CPDM sampled at 2.2 L/min for 480 minutes is shown in Figure 3.11, displaying the range of quartz mass concentrations given a specific quartz mass output obtained from this study's redeposition procedure. For example, if a quartz mass of 50 µg was observed, then it would be expected that the quartz concentration would range approximately between 35 µg/m^3 (75.43% recovery) and 50 µg/m^3 (100% recovery).

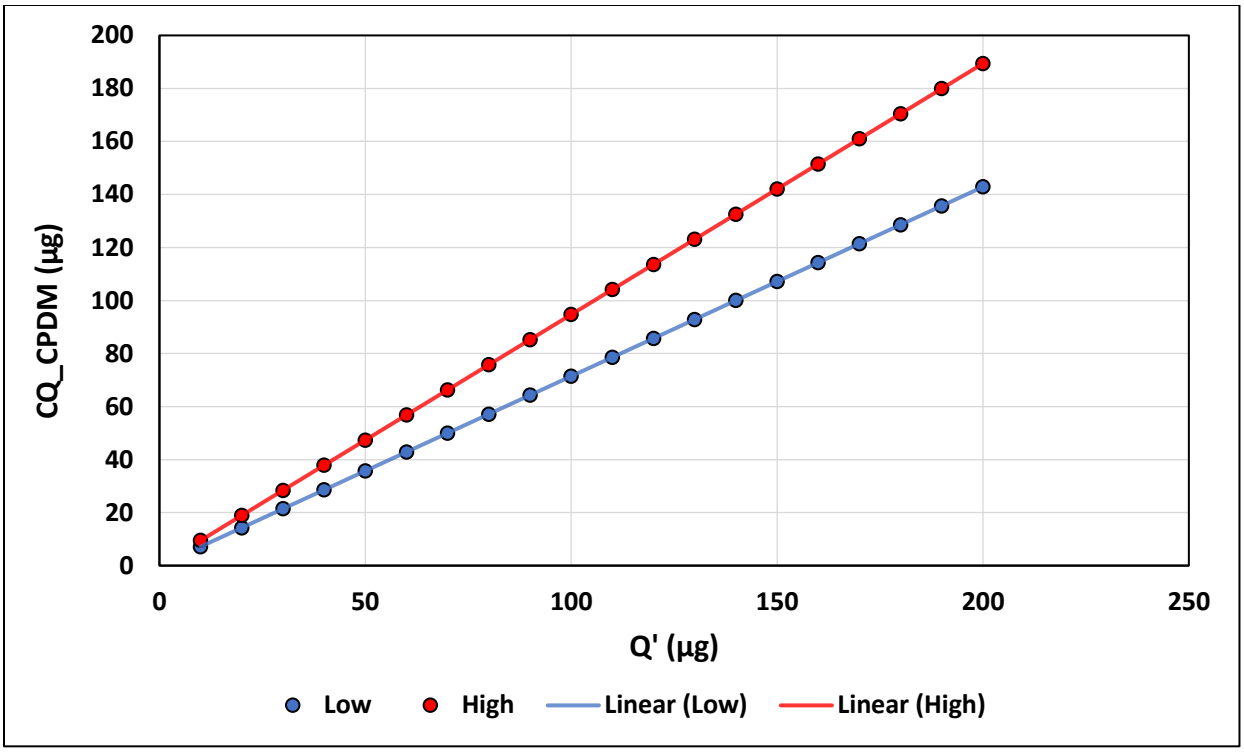

Figure 3.11: Mine 28 example expected high (100% recovery) and low (75.43% recovery) quartz concentrations for a CPDM running at 2.2 L/min for 480 minutes.

Since CPDMs were mandated in 2016, gravimetric pumps are primarily reserved to MSHA for quartz monitoring, leaving mine operators with little availability to CMDPSUs. This restricts the ability for mine operators to perform their own studies since the CPDMs are used for RCMD monitoring and lack the ability to be used to determine quartz concentrations. The process to redeposit dust from a field CPDM filter onto a 25-mm PVC filter is simple with the used equipment being relatively cheap. Due to its simplicity, mine operators may potentially be able to perform the process paired with portable FTIR for quartz analysis in research or engineering studies, such as in the case of the above methods. A contract lab would be necessary to perform the NIOSH Method 7603 analyses for the comparison to the CPDM samples and could potentially be used as a calibration. The near 1:1 slope of the Mine 10 and 15 materials (Figure 3.6 and Figure 3.7) suggest that the DOF FTIR analysis is accurate in the determination of the quartz content of the Mine 28 field samples. For the Mine 28 field samples, the correlations between the predicted and expected values are high however, the slope of 0.82 shows the predicted values being lower than the expected quartz percentages from the 7603 analyses. There could be potential for the CPDM quartz values to be calibrated by this slope in order to match the 7603 results. Calibration could also be performed by having reference measurements performed on the redeposited samples for confirmation. Though not done in this study, the 25mm filters can be sent to a contract lab for the NIOSH Method 7603 analysis, and the returned lab data can be compared against the DOF FTIR analysis. If there are any differences in the quartz values, the ratio or slope between the two different analysis types can provide a calibration factor.

A range of dust masses was deposited onto the 25mm PVC filters with the target dust masses being between 0.1 and 2.0mg. The masses obtained on the CPDM filter stubs and 25mm filters are generally much greater than what would be seen when dust sampling is performed on a miner. The greater dust

mass with more center heavy loading on a smaller filter could potentially block the beam pass-through in the IR analysis. The limit for what the beam can pass through has not been analyzed in this study and future analysis of a maximum dust loading mass could be done.

The strong correlations and near 1:1 slope of the lab generated samples may suggest that the correction using the CPDM residue mass and quartz mass may not be necessary. The residue and quartz masses are also much smaller in value in comparison to the dust and quartz masses deposited onto the filters and may be negligible if rougher estimations of quartz content are sought after.

The use of the term “blank” for CPDM samples was used throughout this study for CPDM filters containing no dust or contamination. Though this holds true for the filter itself, the use of IPA to saturate the filter may not mean the CPDM filter is “blank” anymore as it has been contaminated with the IPA. In the use of the portable FTIR, before a sample is scanned, a background scan must be performed to eliminate filter interference by using a new, dry 37-mm PVC filter. Though not tested in this study, the use of IPA on a filter could possibly cause interference in the filter scans. Further studies into using a PVC filter saturated in IPA for a background scan could potentially provide different results.

In this study, a shaker table was used for consistent shaking and repeatability of the process for all of the test tubes. Mine operators would be required to purchase a shaker table if they are to perform the same method of sample preparation. Investigations into shaking a test tube by hand to remove dust from a CPDM could allow for the mine operators to redeposit samples at a lower expense, but consistency of shaking may create large deviations in results.

3.5 Conclusion

When using IPA to redeposit dust from a CPDM filter for DOF FTIR analysis, the filter residue mass contamination is minimal and very little quartz mass is likewise determined. The Mine 10 bolter dust and Mine 15 roof rock presented strong correlations and near 1:1 slopes of the predicted quartz values against the expected. However, in the predicted quartz masses for both the bolter dust and roof rock are seen to be approximately 1 to 2 percentage points lower than the quartz percentage determined through the NIOSH Method 7603 analysis of the respective materials.

For the Mine 28 field samples, the quartz data was determined differently, but the analyzation process was generally easier to perform. The results differed slightly from the lab generated samples, with the slope of the predicted versus expected quartz masses being lower at 0.744. The predicted values generally underestimated the quartz masses, which was also seen in the comparison between the quartz percentages. The slope was nearly identical at 0.740, but a relatively strong correlation was seen on both comparisons. The near 1:1 slope of the predicted and expected quarts masses of the bolter dust and roof rock suggest that the lower slopes of the Mine 28 field samples are accurate, and therefore potentially requires calibration for more accurate results.

Though the redeposition process shown in this study is simple with relatively cost-effective materials, sending a set of PVC samples to a contract lab to undergo the NIOSH Method 7603 analysis would be required. The analysis of the PVC filters would provide a baseline quartz percentage that can be used to compare the redeposited CPDM filter quartz percentages, as well as provide potential calibration if the predicted values differ from the expected.

CPDM filter deterioration was not acutely seen in the redeposition process. The CPDM filters submerged in IPA were shaken somewhat vigorously to attempt to remove filter material for analysis but as previously stated, the mass of material removed was nearly negligible. The amount of material removed could change depending on if the filters were shaken more aggressively or if poorly handled, potentially varying quartz mass interference results.

3.6 Acknowledgements

The authors would like to express their gratitude to the National Institute of Occupational Safety and Health for funding this research. We would also like to thank August Greth for his aid and support in the Mine 28 sampling, lab experiments, and data analyzation. Gratitude is additionally given to the Mine 28 engineers, health and safety team, and miners for their support in the dust sampling process and data collection.

3.7 References

Hall, N. B., Blackley, D. J., Halldin, C. N., & Laney, A. S. (2019). Current review of pneumoconiosis among US coal miners. *Current environmental health reports*, *6*, 137-147.

Cohen, R. A., Rose, C. S., Go, L. H., Zell-Baran, L. M., Almberg, K. S., Sarver, E. A., ... & Green, F. H. (2022). Pathology and mineralogy demonstrate respirable crystalline silica is a major cause of severe pneumoconiosis in US coal miners. *Annals of the American Thoracic Society*, *19*(9), 1469-1478.

Lowering Miners' Exposure to Respirable Coal Mine Dust, Including Continuous Personal Dust Monitors, 79 F.R. 24814-24994 (May 1, 2014). https://arlweb.msha.gov/regs/fedreg/final/2014finl/2014-09084.asp

Lowering Miners' Exposure to Respirable Crystalline Silica and Improving Respiratory Protection, 89 F.R. 28218-28485 (April 18, 2024). https://www.federalregister.gov/documents/2023/08/14/2023-17370/lowering-miners-exposure-to-respirable-crystalline-silica-and-improving-respiratory-protection#:~:text=On%20July%2013%2C%202023%2C%20MSHA,Protection%20(88%20FR%2044852).

Department of Labor, Mine Safety and Health Administration. (2013). Infrared Determination of Quartz in Respirable Coal Mine Dust, MSHA Method P-7. https://arlweb.msha.gov/Techsupp/pshtcweb/MSHA%20P7.pdf

Ashley, K. (2003). Field-portable spectroscopy. *Applied Occupational and Environmental Hygiene*, *18*(1), 10-15.

Miller, A. L., Drake, P. L., Murphy, N. C., Noll, J. D., & Volkwein, J. C. (2012). Evaluating portable infrared spectrometers for measuring the silica content of coal dust. *Journal of Environmental Monitoring*, *14*(1), 48-55.

Cauda, E., Miller, A., & Drake, P. (2016). Promoting early exposure monitoring for respirable crystalline silica: Taking the laboratory to the mine site. *Journal of occupational and environmental hygiene*, *13*(3), D39-D45.

National Academies of Sciences, Medicine Division, Division on Earth, Life Studies, Board on Health Sciences Policy, Board on Environmental Studies, ... & Committee on the Study of the Control of Respirable Coal Mine Dust Exposure in Underground Mines. (2018). Monitoring and sampling approaches to assess underground coal mine dust exposures.

Chow, J. C., Watson, J. G., Wang, X., Abbasi, B., Reed, W. R., & Parks, D. (2022). Review of filters for air sampling and chemical analysis in mining workplaces. *Minerals*, *12*(10), 1314.

Tuchman, D. P., Volkwein, J. C., & Vinson, R. P. (2008). Implementing infrared determination of quartz particulates on novel filters for a prototype dust monitor. *Journal of environmental monitoring*, *10*(5), 671-678.

Miller, A. L., Murphy, N. C., Bayman, S. J., Briggs, Z. P., Kilpatrick, A. D., Quinn, C. A., ... & Griffiths, P. R. (2015). Evaluation of diffuse reflection infrared spectrometry for end-of-shift measurement of α-quartz in coal dust samples. *Journal of occupational and environmental hygiene*, *12*(7), 421-430.

Greth and Sarver (n.d.)

Pokhrel, N., Agioutanti, E., Keles, C., Afrouz, S., & Sarver, E. (2022). Comparison of respirable coal mine dust constituents estimated using FTIR, TGA, and SEM–EDX. *Mining, Metallurgy & Exploration*, *39*(2), 291-300.

4 Conclusions and Recommendations for Future Work

The studies performed in this thesis demonstrated the use of DOF FTIR for the estimation of RCS in coal mines. The first study details the use of portable FTIR paired with NIOSH's *FAST* software to easily determine quartz data using affordable sampling equipment. The second study provides a procedure to recover, redeposit, and analyze RCS from a CPDM filter sample. Both studies demonstrate the capabilities of DOF FTIR analysis at coal mines and its potential for non-regulatory research or engineering studies.

The dramatic resurgence of PMF and increasing need for non-regulatory RCS monitoring provides relevancy to the analysis methods used in this thesis. DOF FTIR analysis allows for rapid, end-of-shift, RCMD and RCS analysis for mine operators. NIOSH's *FAST* software makes RCS analysis easy, and for any inexpensive sampling equipment that is not readily modeled in *FAST*, the data can be calibrated for improved accuracy of results when compared to filter samples sent for official lab analysis. The shift to CPDMs for RCMD monitoring leaves mine operators with little availability of CMDPSUs. However, recovery of dust from a CPDM filter in IPA shows high recovery and little residue interference with strong results. There is potential for the future use of CPDM filters in DOF FTIR analysis through a redeposition method.

4.1 Discussion of Chapter 2

Chapter 2 details the use of portable FTIR paired with NIOSH's *FAST* software and affordable sampling equipment to determine RCMD and RCS data. The use of cheaper sampling equipment instead of the CMDPSUs with 4-piece cassettes used by MSHA can allow for the mine operators to perform sampling more often, but initial calibration would likely be required on a per-mine basis. NIOSH's *FAST* software is constrained by the preset sampling cyclones and cassette models in the program, which are modeled for specific flow rates and conditions. Like in this study, the closest preset model to the actual sampling conditions can be chosen for analysis, but calibration would be needed for more accurate results. This can be done through a third-party contract lab, where a subset of samples can be sent and compared between the FTIR and *FAST* results. This would allow for a reduced quantity of samples needed to be analyzed by a contract lab, reducing costs for the mine operators. Calibration of the *FAST* derived results would potentially need to be updated over time, especially if mining conditions change or a different area of the mine is opened, as these changes could result in different RCMD and quartz concentrations.

The process to calibrate the sampling data from a different sampling model than what is preset in *FAST* is shown in Figure 4.1. First, the sampling equipment is selected based on availability or budget with pre-weighed filters that can be sent to a contract lab for reference analysis. Once sampling has concluded, the filters can be post-weighed on a microbalance to determine the dust mass, and subsequently scanned in the portable FTIR unit. Using NIOSH's *FAST* software, the quartz mass and quartz concentrations of the samples can be determined. A selection of filter samples can be sent to undergo the NIOSH Method 7603 analysis and the results can be compared against the *FAST* derived data to determine a calibration factor. Using the calibration factor, the corrected quartz concentration can be found. In the sampling process, paired CPDMs can be placed with the CMDPSUs if a microbalance is not available for Step 2 shown in Figure 4.1. The mass data from the CPDM can then be used to determine a dust mass concentration and calculate an estimated quartz percentage shown in Step 7 of Figure 4.1.

There is potential for NIOSH to update and improve the *FAST* software for more versatile sampling conditions in the future as well, further increasing the range of use that portable FTIR and *FAST* could provide.

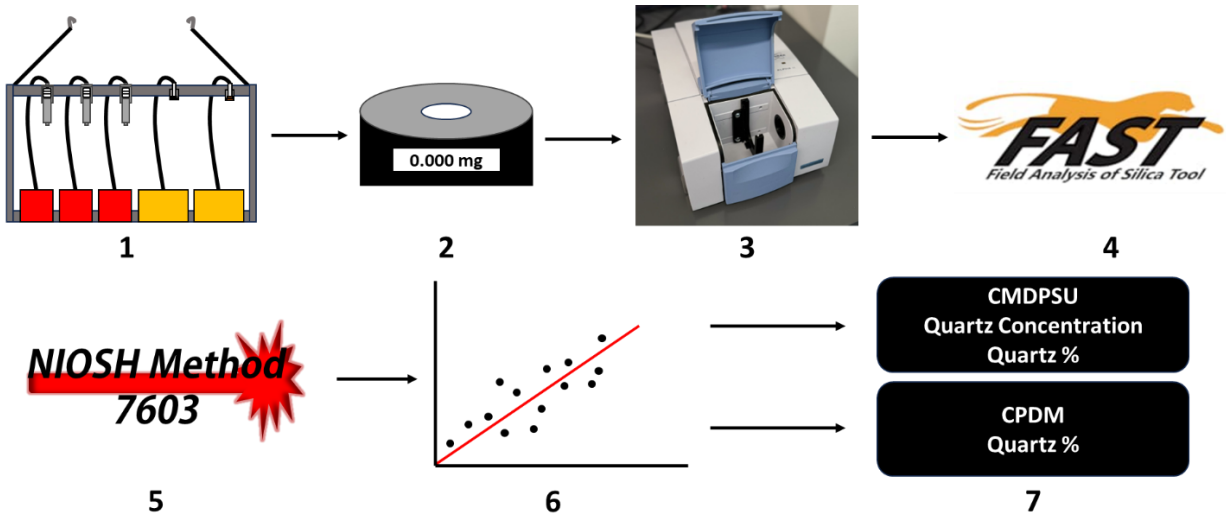

Figure 4.1: Sampling and calibration process. Steps involve 1) Perform sampling using available sampling equipment. 2) Post-weigh the PVC filters. 3) Scan in portable FTIR. 4) Analyze data in *FAST*. 5) Send select samples to undergo NIOSH Method 7603 analysis. 6) Determine the calibration factor for the *FAST* derived data by comparing the *FAST* derived and NIOSH method 7603 data. 7) Calculate the calibrated quartz concentrations and quartz percentages from CMDPSU data. If paired CPDMs were used, the estimated quartz percentages can be determined using CPDM mass concentration data.

Further, while the current study considers the potential for field-based DOF FTIR to support non-regulatory RCS monitoring, it should be noted that a plain text interpretation of the US federal regulations (30 CFR part 70) requires advanced notice to MSHA for any RCMD sampling outside of that used to demonstrate regulatory compliance.

4.2 Discussion of Chapter 3

Chapter 3 details a developed procedure to recover, redeposit, and analyze RCS from a CPDM filter sample. Due to the materials that make-up the CPDM filter interfering with DOF FTIR analysis, the CPDM filters cannot be placed directly into a portable FTIR. As a result, the dust needs to be removed from the CPDM filter and deposited onto a scannable PVC filter. The procedure performed in Chapter 3 uses IPA to remove and redeposit the dust onto a PVC filter. Based on the mass reported by the CPDM in its data sheet, high dust recovery was seen in the redeposition process. Additionally, it was seen that there was little CPDM filter deterioration from the shaking process, resulting in low interference of quartz data. To keep consistency in the procedure, a shaker table was used at a consistent shaking speed and duration. Because of the low deterioration and interference of the CPDM filter, a more cost-effective method of hand-shaking the test tubes could potentially be performed.

The results from Chapter 3 suggest that a similar calibration method used in Chapter 2 could be beneficial. The resulting quartz percentages of the lab-generated samples and field samples were seen to

be lower than the previously analyzed NIOSH Method 7603 percentages, so a subset of the redeposited samples could be sent to an official lab to have the Method 7603 analysis performed. Using a calibration, the redeposition methods and procedures for CPDM filters have potential to be used in DOF FTIR analysis.

4.3 Recommendations for Future Research

Future work into updating NIOSH's *FAST* software for more preset sampling models would allow for greater versatility in sampling equipment that mine operators can use in the DOF FTIR analysis process. It would allow for greater accuracy in quartz mass and quartz concentration data as well as reduce the number of samples required to be sent to an official lab for calibration. This would further reduce the cost of non-regulatory sampling and analysis, allowing for more affordable research and engineering studies.

Future studies into the potential interference of IPA in the CPDM filter recovery and redeposition process could provide benefits to the accuracy of the procedure. IPA could potentially cause interference with the DOF FTIR analysis, which was not studied in Chapter 3, and possibly had influence in the determined blank CPDM filter residue and quartz mass interference.

5 Appendix A

Table A1: Summary of sampling events in Mine 28. *Anemometer unavailable.

Event and MMU			Location	Date	Time		Duration (min)	CPDM Number	Average Mining height (ft)		Airway dimensions (ft)		Velocity (ft/min)	Airflow (ft^3/min)
					Start	End			Coal	Rock	Width	Height		
E1	1	L4	Entry 2, XC-65 Left	7/10/2023	16:42	21:35	293	CPDM 11	4.58	2.23	19.83	6.75	*	-
E1	1	L1	Entry 0, XC-64 Left	7/10/2023	16:47	21:40	293	CPDM 12			18.42	6.17	*	-
E1	1	L3	Entry 00, XC 64-65 Left	7/10/2023	16:54	21:38	284	CPDM 13			19.42	7.50	*	-
E1	1	L2	Entry 4, XC-63 Inby	7/10/2023	17:00	21:41	281	CPDM 14			16.50	7.67	*	-
E2	1	L3	Entry 1, XC-64 Outby	7/11/2023	16:26	21:28	302	NO CPDM	4.79	2.00	17.83	6.83	*	-
E2	1	L4	Entry 1, XC-64-65 Left	7/11/2023	16:01	21:22	321	CPDM 28			18.33	6.33	*	-
E2	1	L1	Entry 0000, XC-64 Inby	7/11/2023	16:13	21:25	312	CPDM 12			18.25	7.42	*	-
E2	1	L2	Entry 0, XC-64 Outby	7/11/2023	16:20	21:27	307	CPDM 11			18.50	6.58	190.0	23,140.4
E3	3	L3	Entry 1, XC-15 Outby	7/12/2023	16:00	21:10	310	CPDM 11, 13	7.58	1.04	18.75	7.83	42.0	6,168.8
E3	3	L1	Entry 0, XC 16 Outby	7/12/2023	16:07	21:12	305	CPDM 14, 27			17.83	9.42	183.0	30,459.3
E4	3	L4	Entry 4, XC-2 Outby	7/13/2023	16:07	20:51	284	CPDM 11, 13	7.67	0.33	18.25	7.67	357.0	49,950.3
E4	3	L2	Entry 1, XC-3 Outby	7/13/2023	15:58	20:49	291	CPDM 14, 27			17.75	8.33	180.0	26,625.0
E5	3	L3	Entry 1, XC-5 Left	7/14/2023	16:14	20:31	257	CPDM 11, 13	8.13	0.38	17.42	8.08	154.0	21,680.9
E5	3	L2	Entry 0, XC-3 Outby	7/14/2023	16:21	20:33	252	CPDM 14, 27			18.58	8.92	207.0	34,300.2
E6	1	L1	Entry 0000, XC-65 Inby	7/17/2023	9:14	14:05	291	CPDM 11, 13	4.79	1.88	19.83	6.92	69.0	9,465.5
E6	1	L2	Entry 000-0000, XC-64	7/17/2023	9:20	14:07	287	CPDM 14, 27			18.50	6.42	74.0	8,784.4
E7	3	L1	Entry 0, XC-3 Inby	7/18/2023	8:46	13:33	287	CPDM 11, 13	8.33	0.04	17.42	8.42	163.0	23,894.2
E7	3	L2	Entry 0, XC-5 Inby	7/18/2023	8:39	13:35	296	CPDM 14, 27			18.42	8.33	181.0	27,778.5
E8	3	L3	Entry 0-1, XC-7	7/19/2023	9:00	13:28	268	CPDM 8, 10	7.75	0.42	18.25	8.25	201.0	30,263.1
E8	3	L2	Entry 0, XC-5 Inby	7/19/2023	9:10	13:26	256	CPDM 12, 19			18.67	8.08	189.0	28,518.0
E9	1	L1	Entry 10, XC-67 Outby	7/20/2023	9:32	13:47	255	CPDM 8,10	6.00	0.50	17.50	6.08	220.0	23,420.8
E9	1	L2	Entry 10, XC-66 Outby	7/20/2023	9:23	13:46	263	CPDM 12, 19			17.33	6.92	243.0	29,133.0
E10	3	L1	Entry 0, XC-8 Inby	7/21/2023	8:36	14:02	326	CPDM 8,10	7.38	0.54	13.75	8.08	61.0	6,779.9
E10	3	L2	Entry 0, XC-7 Outby	7/21/2023	8:41	14:04	323	CPDM 12, 19			19.17	7.75	164.0	24,360.8

Table A2: Mine 28 CMDPSU Filter Sample Data

				RCMD				Quartz						
Event	**MMU**	**Location**	**Filter Number**	**M_{RCMD_filter} (mg)**	**Average M_{RCMD_filter} (mg)**	**C_{RCMD_filter} (mg/m³)**	**Average C_{RCMD_filter} (mg/m³)**	**M_{Q_FAST} (µg)**	**Average M_{Q_FAST} (µg)**	**$C_{Q\ FAST}$ (µg/m³)**	**$C'_{Q\ FAST}$ (µg/m³)**	**Average $C'_{Q\ FAST}$ (µg/m³)**	**Q_{RCMD} (%)**	**Average Q_{RCMD} (%)**
E1	1	L1	S1	0.166	0.281 (± 0.127)	0.290	0.492 (± 0.221)	9.853	12.765 (± 2.498)	17.347	10.842	14.047 (± 2.751)	5.95%	3.164% (± 0.689%)
			S2	0.218		0.386		12.489		21.983	13.740		5.73%	
			S3	0.458		0.800		15.953		28.097	17.561		3.48%	
		L2	S1	1.173	1.190 (± 0.113)	2.084	2.116 (± 0.198)	24.592	35.544 (± 15.217)	43.746	27.341	39.528 (± 16.925)	2.10%	1.818% (± 0.608%)
			S2	1.336		2.374		57.063		101.540	63.463		4.27%	
			S3	1.060		1.891		24.978		44.450	27.781		2.36%	
		L3	S1	1.027	0.796 (± 0.182)	1.753	1.362 (± 0.310)	22.715	27.043 (± 4.029)	38.750	24.219	28.839 (± 4.297)	2.21%	2.311% (± 0.872%)
			S2	0.781		1.339		25.999		44.367	27.729		3.33%	
			S3	0.581		0.994		32.416		55.310	34.569		5.58%	
		L4	S1	-0.035	-0.018 (± 0.012)	-	-	-	-	-	-	-	-	-
			S2	-0.015		-		-		-	-		-	
			S3	-0.005		-		-		-	-		-	
E2	1	L1	S1	1.423	2.050 (± 0.451)	2.277	3.284 (± 0.724)	97.594	108.941 (± 8.278)	156.395	97.747	109.118 (± 8.294)	6.86%	3.453% (± 0.595%)
			S2	2.262		3.629		112.125		179.690	112.306		4.96%	
			S3	2.466		3.947		117.107		187.680	117.300		4.75%	
		L2	S1	1.739	1.068 (± 0.475)	2.829	1.734 (± 0.774)	72.933	63.760 (± 6.488)	118.777	74.235	64.9 (± 6.603)	4.19%	4.258% (± 1.155%)
			S2	0.733		1.187		59.395		96.738	60.461		8.11%	
			S3	0.731		1.187		58.954		96.007	60.004		8.06%	
		L3	S1	0.146	0.172 (± 0.018)	0.248	0.285 (± 0.026)	21.901	13.676 (± 5.868)	36.266	22.667	14.15 (± 6.074)	14.97%	8.342% (± 2.777%)
			S2	0.184		0.304		10.516		17.402	10.876		5.73%	
			S3	0.186		0.304		8.611		14.255	8.910		4.62%	
		L4	S1	0.005	0.014 (± 0.010)	-	-	-		-	-	-	-	-
			S2	0.027		-		-		-	-		-	
			S3	0.009		-		-		-	-		-	

E3	3	L1	S1	0.980	1.232 (± 0.190)	1.601	2.019 (± 0.314)	64.004	88.012 (± 17.968)	104.921	65.576	90.174 (± 18.408)	6.53%	4.428% (± 0.239%)
			S2	1.437		2.360		107.226		175.771	109.857		7.46%	
			S3	1.281		2.098		92.805		152.145	95.091		7.25%	
		L3	S1	0.504	0.526 (± 0.016)	0.814	0.846 (± 0.023)	43.166	43.792 (± 0.846)	69.607	43.505	44.146 (± 0.858)	8.57%	5.218% (± 0.102%)
			S2	0.534		0.856		43.222		69.718	43.574		8.09%	
			S3	0.541		0.869		44.988		72.574	45.359		8.32%	
E4	3	L2	S1	1.104	0.794 (± 0.258)	1.891	1.362 (± 0.439)	135.019	113.574 (± 17.360)	231.992	144.995	121.969 (± 18.639)	12.23%	9.560% (± 1.924%)
			S2	0.473		0.814		92.501		158.948	99.343		19.54%	
			S3	0.805		1.380		113.201		194.511	121.569		14.07%	
		L4	S1	0.016	-0.004 (± 0.014)	-	-	-		-	-	-	-	-
			S2	-0.016		-		-		-	-		-	
			S3	-0.012		-		-		-	-		-	
E5	3	L2	S1	0.822	0.549 (± 0.193)	1.628	1.090 (± 0.380)	58.581	55.688 (± 2.520)	116.224	72.640	69.055 (± 3.125)	7.12%	6.956% (± 1.807%)
			S2	0.424		0.842		52.440		104.038	65.024		12.38%	
			S3	0.402		0.800		56.042		111.200	69.500		13.96%	
		L3	S1	1.261	1.253 (± 0.068)	2.456	2.438 (± 0.135)	116.582	119.839 (± 16.410)	226.831	141.769	145.722 (± 19.953)	9.24%	5.951% (± 0.493%)
			S2	1.332		2.594		141.367		275.034	171.896		10.62%	
			S3	1.165		2.263		101.568		197.602	123.501		8.72%	
E6	1	L1	S1	1.448	2.128 (± 0.481)	2.484	3.652 (± 0.826)	106.702	115.754 (± 9.459)	183.333	114.583	124.306 (± 10.158)	7.37%	3.571% (± 0.759%)
			S2	2.477		4.250		111.752		192.013	120.008		4.51%	
			S3	2.459		4.223		128.809		221.324	138.328		5.24%	
		L2	S1	2.527	2.49 (± 0.081)	4.402	4.338 (± 0.143)	127.940	138.363 (± 19.320)	222.898	139.311	150.662 (± 21.035)	5.06%	3.465% (± 0.399%)
			S2	2.567		4.471		165.448		288.241	180.150		6.45%	
			S3	2.378		4.140		121.702		212.037	132.523		5.12%	
E7	3	L1	S1	1.213	1.300 (± 0.118)	2.042	2.194 (± 0.204)	138.041	167.063 (± 30.400)	233.179	145.737	176.378 (± 32.099)	11.38%	7.978% (± 0.715%)
			S2	1.467		2.484		209.042		353.128	220.705		14.25%	
			S3	1.219		2.056		154.105		260.309	162.693		12.65%	
		L2	S1	0.524	0.788 (± 0.253)	0.911	1.375 (± 0.443)	81.613	95.114 (± 17.366)	142.181	88.863	103.563 (± 18.906)	15.56%	7.910% (± 1.343%)
			S2	0.712		1.242		84.097		146.515	91.572		11.81%	
			S3	1.129		1.973		119.632		208.408	130.255		10.60%	
E8	3	L2	S1	1.504		2.939		226.030		441.462	275.914		15.03%	

			S2	1.486	1.463 (± 0.046)	2.898	2.857 (± 0.089)	203.053	212.097 (± 9.997)	396.584	247.865	258.908 (± 12.202)	13.66%	9.066% (± 0.366%)
			S3	1.398		2.732		207.207		404.713	252.945		14.82%	
		L3	S1	1.842	1.811 (± 0.073)	3.436	3.376 (± 0.136)	223.174	232.875 (± 17.166)	416.374	260.234	271.544 (± 20.012)	12.11%	8.038% (± 0.399%)
			S2	1.710		3.188		218.454		407.569	254.731		12.78%	
			S3	1.881		3.505		256.997		479.467	299.667		13.66%	
E9	1	L1	S1	2.040	2.034 (± 0.032)	4.002	3.988 (± 0.063)	101.402	104.273 (± 13.361)	198.817	124.260	127.782 (± 16.377)	4.97%	3.199% (± 0.362%)
			S2	1.991		3.905		89.534		175.550	109.719		4.50%	
			S3	2.070		4.057		121.882		238.988	149.368		5.89%	
		L2	S1	1.511	1.616 (± 0.128)	2.870	3.073 (± 0.248)	103.541	104.549 (± 14.660)	196.843	123.027	124.226 (± 17.418)	6.85%	4.031% (± 0.348%)
			S2	1.797		3.422		122.986		233.813	146.133		6.84%	
			S3	1.541		2.926		87.119		165.628	103.517		5.65%	
E10	3	L1	S1	2.360	2.491 (± 0.127)	3.616	3.818 (± 0.196)	447.079	437.478 (± 9.982)	685.694	428.559	419.365 (± 9.563)	18.95%	11.012% (± 0.622%)
			S2	2.663		4.085		441.641		677.373	423.358		16.58%	
			S3	2.450		3.754		423.715		649.883	406.177		17.30%	
		L2	S1	1.163	1.771 (± 0.434)	1.794	2.737 (± 0.673)	251.712	292.063 (± 51.303)	389.657	243.536	282.572 (± 49.636)	21.64%	10.772% (± 2.222%)
			S2	2.150		3.326		364.458		564.185	352.616		16.95%	
			S3	2.000		3.091		260.020		402.505	251.565		13.00%	

Table A3: Mine 28 CPDM Data

				RCMD				
Event	**MMU**	**Location**	**CPDM Number**	**Mass (mg)**	**Average Mass (mg)**	**Concentration (mg/m³)**	**Average Concentration (mg/m³)**	**CPDM Errors**
E1	1	L1	13	0.468	0.468	0.749	0.749	
		L2	14	0.959	0.959	1.551	1.551	
		L3	12	1.886	1.886	2.926	2.926	
		L4	11	0.021	-	-	-	
E2	1	L1	12	3.965	3.965	5.777	5.777	HIGH FILTER LOAD
		L2	11	1.856	1.856	2.748	2.748	
		L3	-	-	-	-	-	
		L4	28	0.085	-	-	-	
E3	3	L1	14	1.462	1.465	2.179	2.183	
			27	1.467		2.186		
		L3	11	0.731	0.680	1.072	0.996	
			13	0.628		0.921		
E4	3	L2	14	1.157	1.161	1.807	1.813	
			27	1.164		1.818		
		L4	11	0.000	-	-	-	
			13	0.000		-		
E5	3	L2	14	0.823	0.825	1.484	1.487	
			27	0.826		1.490		
		L3	11	1.463	1.399	2.588	2.473	
			13	1.334		2.359		
E6	1	L1	11	3.085	2.965	4.819	4.631	MASS OFFSET
			13	2.845		4.444		MASS OFFSET
		L2	14	2.702	2.644	4.279	4.188	
			27	2.586		4.096		
E7	3	L1	14	1.217	1.224	1.869	1.880	
			27	1.231		1.890		

		L2	11	1.319	1.268	2.089	2.008	
			13	1.217		1.927		
E8	3	L2	12	1.433	1.384	2.544	2.457	
			19	1.335		2.370		
		L3	8	1.726	1.744	2.927	2.958	
			10	1.762		2.988		
E9	1	L1	8	1.689	1.310	4.625	3.587	POWER LOW
			10	0.931		2.549		POWER LOW
		L2	12	1.844	1.785	3.187	3.085	
			19	1.726		2.983		
E10	3	L1	8	2.589	2.702	3.610	3.767	MASS OFFSET
			10	2.815		3.925		MASS OFFSET
		L2	12	2.368	2.279	3.332	3.207	MASS OFFSET
			19	2.190		3.082		MASS OFFSET

Table A4: NIOSH Method 7603 results for 10 samples.

				RCMD		Quartz		
Event	**MMU**	**Location**	**Filter Number**	**MRE Mass (mg)**	**MRE Concentration (mg/m^3)**	**MRE Mass (mg)**	**MRE Concentration (mg/m^3)**	**Quartz %**
E1	1	L2	S3	1.006	1.794	0.018	0.031	1.76%
E2	1	L1	S3	2.443	3.905	0.081	0.130	3.32%
E2	1	L2	S3	0.686	1.116	0.019	0.031	2.78%
E5	3	L3	S2	1.282	2.498	0.096	0.186	7.46%
E6	1	L1	S3	2.374	4.085	0.070	0.120	2.93%
E7	3	L2	S1	0.522	0.909	0.046	0.080	8.76%
E8	3	L2	S2	1.435	2.788	0.145	0.283	10.10%
E8	3	L3	S1	1.739	3.243	0.164	0.305	9.44%
E9	1	L1	S1	1.973	3.878	0.060	0.117	3.02%
E10	3	L1	S3	2.360	3.616	0.240	0.368	10.20%

Table A5: Summary of data for respirable dust samples lab-generated from Mine 28 dust source materials.

MMU	Material Type	Filter Number	Filter Mass (mg)	Average Mass (mg)	Filter Mass Std. Dev (mg)	Quartz Mass (mg)	Average Quartz Mass (mg)	Quartz Mass Std. Dev (mg)	Quartz %	Average Quartz %	Quartz % Std. Dev
1	Coal	S1	0.774	0.737	0.060	0.006	0.006	0.004	0.78%	0.88%	0.69%
		S2	0.652			0.012			1.77%		
		S3	0.784			0.001			0.10%		
	Shale (Roof Rock)	S1	2.204	2.143	0.166	0.466	0.413	0.038	21.16%	19.32%	1.66%
		S2	1.916			0.377			19.67%		
		S3	2.31			0.396			17.14%		
3	Coal	S1	1.485	1.188	0.344	0.091	0.082	0.008	6.12%	7.40%	1.84%
		S2	1.373			0.083			6.07%		
		S3	0.706			0.071			10.00%		
	Bolter Dust (Roof Rock)	S1	1.177	0.972	0.222	0.151	0.144	0.024	12.84%	15.14%	1.68%
		S2	0.664			0.111			16.78%		
		S3	1.075			0.170			15.82%		
1 and 3	Rock Dust	S1	0.886	1.135	0.176	0.040	0.026	0.016	4.56%	2.50%	1.78%
		S2	1.255			0.034			2.70%		
		S3	1.263			0.003			0.22%		

Table A6: CMDPSU filter-derived and CPDM-derived quartz percentages for samples collected in Mine 28.

MMU	Sample ID	Q_{RCMD_filter} (%)	Q_{RCMD_CPDM} (%)	Ratio of Q_{RCMD_filter} (%) to Q_{RCMD_CPDM} (%)
1	E1-L3	2.311%	0.985%	2.345
	E1-L1	3.164%	1.875%	1.687
	E1-L2	1.818%	2.549%	0.713
	E2-L3	3.453%	1.889%	1.828
	E2-L1	4.258%	2.362%	1.803
	E2-L2	3.571%	2.684%	1.330
	E6-L1	3.465%	3.598%	0.963
	E6-L2	3.199%	3.693%	0.866
	E9-L1	4.031%	4.027%	1.001
3	E3-L3	5.218%	4.430%	1.178
	E3-L1	4.428%	4.132%	1.072
	E4-L2	9.560%	6.729%	1.421
	E5-L3	5.951%	5.892%	1.010
	E5-L2	6.956%	4.642%	1.498
	E7-L2	7.910%	4.257%	1.858
	E7-L1	7.978%	9.384%	0.850
	E8-L3	8.038%	9.179%	0.876
	E8-L2	9.066%	10.536%	0.860
	E10-L1	11.013%	11.132%	0.989
	E10-L2	10.772%	8.811%	1.222

6 Appendix B

Table B1: Blank CPDM PVC filter data.

Sample ID	Filter Pre-Weigh	Filter Post-Weigh	Dust Mass (mg)	Mean Corrected Quartz Spectral Peak	Mean Kaolinite Spectral Peak	Mean Quartz Mass (mg)	Corrected Quartz Spectral Peak Std Dev	Kaolinite Spectral Peak Std Dev	Quartz Mass Std Dev (mg)
S1	7.112	7.142	0.030	0.1007	0.0053	0.0108	0.0392	0.0023	0.0030
S2	7.706	7.726	0.020	0.1296	0.0071	0.0139	0.0597	0.0017	0.0038
S3	7.767	7.789	0.022	0.0491	0.0088	0.0053	0.0185	0.0016	0.0008
S4	7.642	7.658	0.016	0.0543	0.0069	0.0058	0.0197	0.0022	0.0004
S5	6.990	6.999	0.009	0.0030	0.0047	0.0003	0.0088	0.0019	0.0008
S6	6.665	6.691	0.026	0.0978	0.0030	0.0105	0.0478	0.0021	0.0010
S7	6.874	6.899	0.025	0.0440	0.0033	0.0047	0.0100	0.0016	0.0005
S8	6.864	6.886	0.022	0.0276	0.0031	0.0030	0.0176	0.0026	0.0006
S9	6.920	6.937	0.017	0.0208	0.0033	0.0022	0.0140	0.0021	0.0008
S10	6.992	7.004	0.012	0.0176	0.0041	0.0019	0.0118	0.0020	0.0005
S11	6.865	6.894	0.029	0.0128	0.0039	0.0014	0.0122	0.0013	0.0010
S12	6.529	6.548	0.019	0.0266	0.0016	0.0028	0.0136	0.0027	0.0005
S13	7.572	7.585	0.013	-0.0029	0.0079	-0.0003	0.0305	0.0018	0.0013
S14	6.574	6.589	0.015	0.0330	0.0015	0.0035	0.0126	0.0015	0.0007
S15	7.359	7.372	0.013	0.0023	0.0072	0.0002	0.0112	0.0009	0.0006
S15	6.952	6.989	0.037	0.0044	0.0048	0.0005	0.0105	0.0006	0.0008
S17	7.616	7.653	0.037	-0.0064	0.0084	-0.0007	0.0091	0.0013	0.0004
S18	6.881	6.895	0.014	0.0145	0.0032	0.0016	0.0113	0.0010	0.0007
S19	6.990	6.998	0.008	0.0040	0.0046	0.0004	0.0170	0.0011	0.0008
S20	6.994	7.012	0.018	-0.0016	0.0049	-0.0002	0.0115	0.0012	0.0009

Table B2: Blank CPDM Event 1 spectral data and average quartz mass.

Event 1													
	Scan 1			Scan 2			Scan 3			Scan 4			
Sample ID	Quartz Peak Area	Kaolinite Peak Area	Corrected Quartz Peak Area	Quartz Peak Area	Kaolinite Peak Area	Corrected Quartz Peak Area	Quartz Peak Area	Kaolinite Peak Area	Corrected Quartz Peak Area	Quartz Peak Area	Kaolinite Peak Area	Corrected Quartz Peak Area	Quartz Mass (mg)
S1	0.1218	0.0072	0.1200	0.0450	0.0077	0.0430	0.0913	0.0068	0.0895	0.1312	0.0082	0.1290	0.0102
S2	0.1119	0.0099	0.1093	0.2224	0.0069	0.2206	0.1766	0.0071	0.1747	0.0875	0.0090	0.0852	0.0158
S3	0.0637	0.0108	0.0608	0.0202	0.0102	0.0175	0.0369	0.0110	0.0340	0.0462	0.0112	0.0433	0.0042
S4	0.0400	0.0096	0.0374	0.0877	0.0075	0.0857	0.0550	0.0101	0.0524	0.0288	0.0100	0.0262	0.0054
S5	-0.0010	0.0073	-0.0029	-0.0101	0.0062	-0.0118	-0.0095	0.0060	-0.0111	0.0036	0.0051	0.0023	-0.0006
S6	0.1520	0.0037	0.1510	0.1070	0.0062	0.1053	0.0665	0.0049	0.0652	0.0415	0.0060	0.0399	0.0097
S7	0.0483	0.0052	0.0469	0.0327	0.0055	0.0313	0.0551	0.0042	0.0540	0.0498	0.0040	0.0487	0.0048
S8	0.0100	0.0051	0.0086	0.0166	0.0084	0.0144	0.0487	0.0025	0.0481	0.0222	0.0027	0.0215	0.0025
S9	0.0087	0.0059	0.0072	0.0268	0.0060	0.0252	0.0304	0.0057	0.0289	-0.0107	0.0057	-0.0122	0.0013
S10	0.0039	0.0068	0.0021	0.0015	0.0053	0.0001	0.0250	0.0065	0.0233	0.0264	0.0070	0.0246	0.0013
S11	0.0029	0.0045	0.0017	0.0034	0.0041	0.0023	0.0065	0.0024	0.0059	-0.0072	0.0067	-0.0089	0.0000
S12	0.0446	0.0028	0.0439	0.0400	0.0014	0.0396	0.0311	0.0017	0.0306	0.0150	0.0094	0.0125	0.0034
S13	-0.0142	0.0090	-0.0166	-0.0136	0.0085	-0.0158	-0.0100	0.0085	-0.0122	0.0942	0.0023	0.0936	0.0013
S14	0.0250	0.0033	0.0241	0.0222	0.0005	0.0220	0.0316	0.0036	0.0306	0.0316	0.0036	0.0306	0.0029
S15	-0.0050	0.0072	-0.0068	0.0056	0.0076	0.0036	0.0098	0.0082	0.0076	0.0045	0.0077	0.0025	0.0002
S16	0.0037	0.0048	0.0024	-0.0096	0.0049	-0.0109	-0.0050	0.0060	-0.0066	0.0096	0.0055	0.0081	-0.0002
S17	-0.0082	0.0079	-0.0103	-0.0110	0.0109	-0.0139	-0.0032	0.0100	-0.0059	-0.0076	0.0088	-0.0099	-0.0011
S18	0.0135	0.0042	0.0124	0.0064	0.0050	0.0051	0.0091	0.0041	0.0080	0.0335	0.0024	0.0329	0.0016
S19	0.0063	0.0054	0.0049	-0.0097	0.0049	-0.0110	-0.0060	0.0057	-0.0075	-0.0070	0.0058	-0.0085	-0.0006
S20	-0.0170	0.0060	-0.0186	-0.0007	0.0041	-0.0017	-0.0050	0.0077	-0.0070	-0.0004	0.0063	-0.0021	-0.0008

Table B3: Blank CPDM Event 2 spectral data and average quartz mass.

Event 2													
	Scan 1			Scan 2			Scan 3			Scan 4			
Sample ID	Quartz Peak Area	Kaolinite Peak Area	Corrected Quartz Peak Area	Quartz Peak Area	Kaolinite Peak Area	Corrected Quartz Peak Area	Quartz Peak Area	Kaolinite Peak Area	Corrected Quartz Peak Area	Quartz Peak Area	Kaolinite Peak Area	Corrected Quartz Peak Area	Quartz Mass (mg)
S1	0.1220	0.0062	0.1203	0.1423	0.0061	0.1407	0.1824	0.0043	0.1812	0.1084	0.0070	0.1066	0.0147
S2	0.1811	0.0063	0.1794	0.0970	0.0069	0.0952	0.1239	0.0105	0.1211	0.2512	0.0044	0.2500	0.0173
S3	0.0366	0.0080	0.0345	0.0726	0.0080	0.0705	0.0566	0.0078	0.0545	0.0578	0.0090	0.0554	0.0057
S4	0.0470	0.0078	0.0449	0.0443	0.0073	0.0424	0.0512	0.0073	0.0493	0.0805	0.0060	0.0789	0.0058
S5	0.0128	0.0041	0.0117	0.0017	0.0051	0.0003	0.0049	0.0051	0.0036	-0.0026	0.0073	-0.0046	0.0003
S6	0.2258	0.0034	0.2249	0.0961	0.0046	0.0949	0.0540	0.0025	0.0533	0.0739	0.0031	0.0731	0.0119
S7	0.0348	0.0053	0.0334	0.0485	0.0031	0.0477	0.0313	0.0028	0.0305	0.0381	0.0036	0.0372	0.0040
S8	0.0138	0.0031	0.0130	0.0110	0.0057	0.0095	0.0226	0.0046	0.0214	0.0512	0.0019	0.0507	0.0025
S9	0.0334	0.0036	0.0325	0.0157	0.0014	0.0154	0.0105	0.0037	0.0095	0.0245	0.0048	0.0232	0.0022
S10	0.0342	0.0047	0.0329	0.0132	0.0046	0.0120	0.0077	0.0039	0.0067	0.0154	0.0023	0.0148	0.0018
S11	0.0142	0.0044	0.0131	0.0355	0.0035	0.0346	0.0238	0.0011	0.0236	0.0083	0.0044	0.0071	0.0021
S12	0.0495	-0.0005	0.0496	0.0263	-0.0017	0.0267	0.0145	-0.0005	0.0146	0.0223	0.0015	0.0218	0.0030
S13	-0.0193	0.0071	-0.0212	-0.0229	0.0072	-0.0247	-0.0183	0.0093	-0.0207	-0.0023	0.0082	-0.0044	-0.0019
S14	0.0571	-0.0007	0.0572	0.0341	-0.0008	0.0343	0.0179	0.0018	0.0174	0.0594	-0.0001	0.0594	0.0045
S15	0.0089	0.0062	0.0073	0.0082	0.0059	0.0066	-0.0174	0.0083	-0.0196	-0.0079	0.0055	-0.0094	-0.0004
S16	0.0112	0.0035	0.0103	-0.0052	0.0044	-0.0064	-0.0015	0.0048	-0.0028	0.0020	0.0049	0.0007	0.0000
S17	-0.0209	0.0064	-0.0226	-0.0094	0.0092	-0.0119	0.0165	0.0073	0.0146	-0.0101	0.0077	-0.0121	-0.0009
S18	-0.0044	0.0046	-0.0056	0.0172	0.0014	0.0169	0.0180	0.0029	0.0173	-0.0021	0.0029	-0.0029	0.0007
S19	-0.0109	0.0039	-0.0119	-0.0085	0.0035	-0.0094	0.0426	0.0033	0.0418	-0.0033	0.0037	-0.0043	0.0004
S20	0.0030	0.0027	0.0023	-0.0004	0.0050	-0.0018	-0.0091	0.0046	-0.0104	-0.0214	0.0052	-0.0228	-0.0009

Table B4: Blank CPDM Event 3 spectral data and average quartz mass.

Event 3													
	Scan 1			Scan 2			Scan 3			Scan 4			
Sample ID	Quartz Peak Area	Kaolinite Peak Area	Corrected Quartz Peak Area	Quartz Peak Area	Kaolinite Peak Area	Corrected Quartz Peak Area	Quartz Peak Area	Kaolinite Peak Area	Corrected Quartz Peak Area	Quartz Peak Area	Kaolinite Peak Area	Corrected Quartz Peak Area	Quartz Mass (mg)
S1	0.0451	0.0033	0.0442	0.0878	0.0032	0.0869	0.0589	0.0023	0.0583	0.0884	0.0007	0.0882	0.0074
S2	0.0732	0.0061	0.0715	0.0729	0.0064	0.0712	0.0613	0.0065	0.0596	0.1187	0.0052	0.1174	0.0086
S3	0.0610	0.0076	0.0590	0.0252	0.0079	0.0232	0.0545	0.0070	0.0526	0.0855	0.0065	0.0837	0.0058
S4	0.0576	0.0043	0.0565	0.0890	0.0032	0.0881	0.0599	0.0047	0.0587	0.0324	0.0051	0.0311	0.0063
S5	0.0141	0.0019	0.0136	0.0095	0.0040	0.0085	0.0132	0.0024	0.0126	0.0138	0.0017	0.0134	0.0013
S6	0.1199	0.0004	0.1198	0.0723	0.0004	0.0722	0.0920	0.0008	0.0918	0.0828	0.0003	0.0827	0.0098
S7	0.0479	0.0022	0.0473	0.0659	0.0013	0.0655	0.0368	0.0012	0.0365	0.0489	0.0009	0.0487	0.0053
S8	0.0639	-0.0012	0.0643	0.0375	-0.0010	0.0378	0.0269	0.0021	0.0263	0.0164	0.0039	0.0154	0.0038
S9	0.0327	0.0008	0.0325	0.0144	0.0011	0.0142	0.0350	0.0008	0.0348	0.0391	0.0007	0.0389	0.0032
S10	0.0331	0.0002	0.0330	0.0365	0.0014	0.0361	0.0169	0.0033	0.0160	0.0111	0.0036	0.0101	0.0025
S11	0.0208	0.0032	0.0200	0.0117	0.0047	0.0105	0.0140	0.0041	0.0129	0.0324	0.0041	0.0313	0.0020
S12	0.0407	0.0009	0.0405	0.0173	0.0001	0.0173	0.0053	0.0023	0.0047	0.0175	0.0013	0.0172	0.0021
S13	0.0082	0.0083	0.0060	-0.0100	0.0082	-0.0122	-0.0073	0.0092	-0.0097	0.0057	0.0095	0.0033	-0.0003
S14	0.0303	0.0014	0.0300	0.0248	0.0021	0.0243	0.0397	0.0019	0.0392	0.0271	0.0012	0.0268	0.0032
S15	0.0195	0.0073	0.0176	-0.0042	0.0067	-0.0060	0.0035	0.0079	0.0015	0.0251	0.0078	0.0231	0.0010
S16	0.0237	0.0050	0.0224	0.0137	0.0049	0.0125	0.0018	0.0046	0.0006	0.0235	0.0042	0.0224	0.0015
S17	-0.0020	0.0083	-0.0042	0.0006	0.0093	-0.0019	0.0069	0.0081	0.0047	-0.0019	0.0064	-0.0036	-0.0001
S18	0.0310	0.0024	0.0304	0.0215	0.0033	0.0206	0.0197	0.0029	0.0189	0.0210	0.0022	0.0204	0.0024
S19	0.0071	0.0036	0.0062	0.0351	0.0049	0.0338	0.0161	0.0071	0.0143	0.0004	0.0038	-0.0006	0.0014
S20	0.0158	0.0045	0.0146	0.0186	0.0044	0.0174	0.0068	0.0047	0.0055	0.0064	0.0038	0.0054	0.0011

Table B5: Mine 10 bolter dust PVC filter data.

Mine 10 Bolter Dust														
Sample ID	Filter Pre-Weigh	Filter Post-Weigh	Dust Mass (mg)	Corrected Dust Mass (mg)	Mean Corrected Quartz Spectral Peak	Mean Kaolinite Spectral Peak	Quartz Peak from Kaolinite	Mean Quartz Mass (mg)	Corrected Quartz Mass (Predicted)	Quartz Mass from Kaolinite (Expected)	Corrected Quartz Spectral Peak Std Dev	Kaolinite Spectral Peak Std Dev	Quartz Mass Std Dev (mg)	Expected Quartz Mass Std Dev (mg)
S1	7.007	7.119	0.112	0.0935	0.2091	0.1110	0.1110	0.0224	0.0202	0.0119	0.0716	0.0088	0.0035	0.0006
S2	7.360	7.609	0.249	0.2305	0.2958	0.2144	0.2143	0.0316	0.0295	0.0229	0.0715	0.0515	0.0033	0.0016
S3	6.971	7.380	0.409	0.3905	0.4401	0.4046	0.4043	0.0471	0.0449	0.0433	0.0546	0.0361	0.0046	0.0008
S4	6.865	7.069	0.204	0.1855	0.1435	0.2083	0.2082	0.0154	0.0132	0.0223	0.0503	0.0150	0.0051	0.0009
S5	7.088	8.074	0.986	0.9675	0.6788	0.6595	0.6591	0.0726	0.0705	0.0705	0.0667	0.0223	0.0067	0.0005
S6	6.751	7.716	0.965	0.9465	0.9557	0.9067	0.9061	0.1022	0.1001	0.0969	0.0565	0.0479	0.0041	0.0012
S7	7.359	8.498	1.139	1.1205	0.9175	0.8976	0.8970	0.0981	0.0960	0.0959	0.0638	0.0720	0.0042	0.0009
S8	7.515	9.115	1.600	1.5815	1.1699	1.0445	1.0439	0.1252	0.1230	0.1117	0.0523	0.0783	0.0030	0.0009
S9	7.230	8.476	1.246	1.2275	0.9472	0.8569	0.8564	0.1013	0.0992	0.0916	0.0312	0.0355	0.0022	0.0004
S10	6.933	8.517	1.584	1.5655	1.2738	1.2432	1.2424	0.1363	0.1341	0.1329	0.0696	0.1204	0.0013	0.0037

Table B6: Mine 10 bolter dust Event 1 spectral data and quartz mass.

Event 1														
	Scan 1			Scan 2			Scan 3			Scan 4				
Sample ID	Quartz Peak Area	Kaolinite Peak Area	Corrected Quartz Peak Area	Quartz Peak Area	Kaolinite Peak Area	Corrected Quartz Peak Area	Quartz Peak Area	Kaolinite Peak Area	Corrected Quartz Peak Area	Quartz Peak Area	Kaolinite Peak Area	Corrected Quartz Peak Area	Quartz Mass (mg)	Expected Quartz Mass (mg)
S1	0.6168	0.2618	0.5479	0.6552	0.2648	0.5856	0.7087	0.2426	0.6449	0.7936	-0.0220	0.7994	0.0689	0.0301
S2	0.3844	0.1775	0.3377	0.3647	0.1774	0.3180	0.4274	0.1892	0.3776	0.4098	0.1919	0.3593	0.0372	0.0297
S3	0.4949	0.1906	0.4447	0.4457	0.1954	0.3943	0.4835	0.1870	0.4343	0.5190	0.1912	0.4687	0.0466	0.0308
S4	0.5164	0.2770	0.4435	0.5589	0.2716	0.4874	0.5472	0.2538	0.4804	0.5265	0.2605	0.4579	0.0500	0.0428
S5	1.3516	0.6410	1.1830	1.3411	0.6548	1.1687	1.3819	0.6974	1.1984	1.3118	0.6287	1.1464	0.1256	0.1057
S6	0.3590	0.2020	0.3058	0.5159	0.2143	0.4595	0.4131	0.1825	0.3651	0.3020	0.1685	0.2577	0.0371	0.0309
S7	0.8170	0.4135	0.7082	0.8909	0.4291	0.7780	0.8708	0.4489	0.7527	0.8974	0.4539	0.7780	0.0807	0.0703
S8	1.9144	1.0258	1.6444	1.7108	0.8833	1.4783	1.6516	0.8067	1.4393	1.6376	0.8286	1.4196	0.1600	0.1428
S9	1.5717	0.9285	1.3274	1.6425	0.9730	1.3865	1.6622	0.9563	1.4106	1.6626	0.9398	1.4153	0.1481	0.1530
S10	1.4126	0.7814	1.2070	1.5236	0.8359	1.3036	1.4258	0.7918	1.2174	1.4761	0.8331	1.2569	0.1333	0.1307

Table B7: Mine 10 bolter dust Event 2 spectral data and quartz mass.

Event 2														
	Scan 1			Scan 2			Scan 3			Scan 4				
Sample ID	Quartz Peak Area	Kaolinite Peak Area	Corrected Quartz Peak Area	Quartz Peak Area	Kaolinite Peak Area	Corrected Quartz Peak Area	Quartz Peak Area	Kaolinite Peak Area	Corrected Quartz Peak Area	Quartz Peak Area	Kaolinite Peak Area	Corrected Quartz Peak Area	Quartz Mass (mg)	Expected Quartz Mass (mg)
S1	0.5954	0.2821	0.5212	0.6362	0.2683	0.5656	0.6925	0.3191	0.6085	0.5459	0.2741	0.4738	0.0580	0.0461
S2	0.2757	0.1848	0.2271	0.2791	0.1860	0.2302	0.3382	0.1981	0.2860	0.3164	0.2003	0.2637	0.0269	0.0310
S3	0.4175	0.1904	0.3674	0.3416	0.2001	0.2889	0.3821	0.2015	0.3290	0.4419	0.2063	0.3876	0.0367	0.0322
S4	0.3891	0.2735	0.3171	0.3843	0.2648	0.3146	0.3864	0.2771	0.3135	0.4112	0.2857	0.3360	0.0343	0.0444
S5	1.2280	0.6563	1.0553	1.2288	0.6540	1.0567	1.2255	0.6627	1.0511	1.2737	0.7096	1.0869	0.1137	0.1081
S6	0.5121	0.1924	0.4614	0.3914	0.1895	0.3416	0.4319	0.2243	0.3729	0.5092	0.2063	0.4549	0.0436	0.0327
S7	0.9146	0.4520	0.7957	0.9115	0.4339	0.7974	0.9068	0.4337	0.7927	0.9424	0.4677	0.8193	0.0857	0.0720
S8	1.9719	1.0290	1.7011	1.7715	0.8792	1.5401	1.7415	0.8298	1.5232	1.7024	0.8448	1.4801	0.1670	0.1444
S9	1.6295	0.9304	1.3846	1.7079	0.9785	1.4504	1.7170	0.9596	1.4645	1.7041	0.9307	1.4591	0.1540	0.1531
S10	1.4080	0.7442	1.2121	1.5141	0.7989	1.3039	1.4499	0.7762	1.2457	1.5524	0.8532	1.3279	0.1361	0.1279

Table B8: Mine 10 bolter dust Event 3 spectral data and quartz mass.

Event 3														
	Scan 1			Scan 2			Scan 3			Scan 4				
Sample ID	Quartz Peak Area	Kaolinite Peak Area	Corrected Quartz Peak Area	Quartz Peak Area	Kaolinite Peak Area	Corrected Quartz Peak Area	Quartz Peak Area	Kaolinite Peak Area	Corrected Quartz Peak Area	Quartz Peak Area	Kaolinite Peak Area	Corrected Quartz Peak Area	Quartz Mass (mg)	Expected Quartz Mass (mg)
S1	0.7569	0.2800	0.6832	0.6798	0.2523	0.6134	0.7374	0.2423	0.6736	0.7612	0.2518	0.6949	0.0713	0.0414
S2	0.4324	0.1950	0.3811	0.3576	0.1736	0.3119	0.3931	0.1964	0.3414	0.4676	0.1937	0.4166	0.0388	0.0306
S3	0.5254	0.1859	0.4765	0.4540	0.1851	0.4053	0.4924	0.1901	0.4423	0.5732	0.1977	0.5212	0.0493	0.0306
S4	0.5323	0.2650	0.4625	0.5465	0.2700	0.4755	0.5181	0.2701	0.4470	0.5464	0.2651	0.4766	0.0498	0.0431
S5	1.2624	0.6017	1.1040	1.4392	0.7123	1.2518	1.3019	0.6208	1.1385	1.4696	0.7164	1.2811	0.1277	0.1068
S6	0.5391	0.1987	0.4868	0.4141	0.1823	0.3661	0.4070	0.1967	0.3552	0.4989	0.2211	0.4407	0.0441	0.0322
S7	0.9417	0.4603	0.8206	0.8597	0.4006	0.7542	0.9397	0.4431	0.8231	0.8959	0.4480	0.7780	0.0849	0.0706
S8	1.8388	0.9445	1.5902	1.7832	0.8939	1.5480	1.6519	0.8087	1.4391	1.5977	0.7803	1.3924	0.1596	0.1381
S9	1.6435	0.9317	1.3983	1.7190	0.9860	1.4596	1.6434	0.8939	1.4082	1.7137	0.9294	1.4691	0.1534	0.1508
S10	1.5129	0.8135	1.2988	1.4913	0.8039	1.2797	1.4825	0.8006	1.2718	1.5432	0.8550	1.3182	0.1382	0.1319

Table B9: Mine 15 roof rock PVC filter data.

Mine 15 Roof Rock														
Sample ID	Filter Pre-Weigh	Filter Post-Weigh	Dust Mass (mg)	Corrected Dust Mass (mg)	Mean Corrected Quartz Spectral Peak	Mean Kaolinite Spectral Peak	Quartz Peak from Kaolinite	Mean Quartz Mass (mg)	Corrected Quartz Mass (Predicted)	Quartz Mass from Kaolinite (Expected)	Corrected Quartz Spectral Peak Std Dev	Kaolinite Spectral Peak Std Dev	Quartz Mass Std Dev (mg)	Expected Quartz Mass Std Dev (mg)
S1	6.623	7.274	0.651	0.6325	0.6177	0.2431	0.3663	0.0661	0.0639	0.0392	0.0846	0.0824	0.0058	0.0067
S2	7.883	8.152	0.269	0.2505	0.3209	0.1887	0.2843	0.0343	0.0322	0.0304	0.0576	0.0085	0.0053	0.0006
S3	6.814	7.103	0.289	0.2705	0.4133	0.1934	0.2915	0.0442	0.0421	0.0312	0.0624	0.0064	0.0054	0.0007
S4	7.211	7.568	0.357	0.3385	0.4177	0.2695	0.4061	0.0447	0.0425	0.0434	0.0701	0.0081	0.0074	0.0007
S5	7.838	9.277	1.439	1.4205	1.1435	0.6630	0.9991	0.1223	0.1202	0.1069	0.0733	0.0365	0.0062	0.0010
S6	6.970	7.226	0.256	0.2375	0.3890	0.1982	0.2987	0.0416	0.0395	0.0320	0.0681	0.0159	0.0032	0.0008
S7	7.015	7.779	0.764	0.7455	0.7831	0.4404	0.6637	0.0838	0.0816	0.0710	0.0319	0.0185	0.0022	0.0007
S8	7.762	9.125	1.363	1.3445	1.5163	0.8796	1.3255	0.1622	0.1601	0.1418	0.0899	0.0788	0.0034	0.0027
S9	7.008	8.383	1.375	1.3565	1.4195	0.9448	1.4238	0.1518	0.1497	0.1523	0.0409	0.0253	0.0026	0.0011
S10	6.547	7.734	1.187	1.1685	1.2703	0.8073	1.2166	0.1359	0.1337	0.1301	0.0405	0.0315	0.0020	0.0017

Table B10: Mine 15 roof rock Event 1 spectral data and quartz mass.

Event 1														
	Scan 1			Scan 2			Scan 3			Scan 4				
Sample ID	Quartz Peak Area	Kaolinite Peak Area	Corrected Quartz Peak Area	Quartz Peak Area	Kaolinite Peak Area	Corrected Quartz Peak Area	Quartz Peak Area	Kaolinite Peak Area	Corrected Quartz Peak Area	Quartz Peak Area	Kaolinite Peak Area	Corrected Quartz Peak Area	Quartz Mass (mg)	Expected Quartz Mass (mg)
S1	0.6168	0.2618	0.5479	0.6552	0.2648	0.5856	0.7087	0.2426	0.6449	0.7936	-0.0220	0.7994	0.0689	0.0301
S2	0.3844	0.1775	0.3377	0.3647	0.1774	0.3180	0.4274	0.1892	0.3776	0.4098	0.1919	0.3593	0.0372	0.0297
S3	0.4949	0.1906	0.4447	0.4457	0.1954	0.3943	0.4835	0.1870	0.4343	0.5190	0.1912	0.4687	0.0466	0.0308
S4	0.5164	0.2770	0.4435	0.5589	0.2716	0.4874	0.5472	0.2538	0.4804	0.5265	0.2605	0.4579	0.0500	0.0428
S5	1.3516	0.6410	1.1830	1.3411	0.6548	1.1687	1.3819	0.6974	1.1984	1.3118	0.6287	1.1464	0.1256	0.1057
S6	0.3590	0.2020	0.3058	0.5159	0.2143	0.4595	0.4131	0.1825	0.3651	0.3020	0.1685	0.2577	0.0371	0.0309
S7	0.8170	0.4135	0.7082	0.8909	0.4291	0.7780	0.8708	0.4489	0.7527	0.8974	0.4539	0.7780	0.0807	0.0703
S8	1.9144	1.0258	1.6444	1.7108	0.8833	1.4783	1.6516	0.8067	1.4393	1.6376	0.8286	1.4196	0.1600	0.1428
S9	1.5717	0.9285	1.3274	1.6425	0.9730	1.3865	1.6622	0.9563	1.4106	1.6626	0.9398	1.4153	0.1481	0.1530
S10	1.4126	0.7814	1.2070	1.5236	0.8359	1.3036	1.4258	0.7918	1.2174	1.4761	0.8331	1.2569	0.1333	0.1307

Table B11: Mine 15 roof rock Event 2 spectral data and quartz mass.

Event 2														
	Scan 1			Scan 2			Scan 3			Scan 4				
Sample ID	Quartz Peak Area	Kaolinite Peak Area	Corrected Quartz Peak Area	Quartz Peak Area	Kaolinite Peak Area	Corrected Quartz Peak Area	Quartz Peak Area	Kaolinite Peak Area	Corrected Quartz Peak Area	Quartz Peak Area	Kaolinite Peak Area	Corrected Quartz Peak Area	Quartz Mass (mg)	Expected Quartz Mass (mg)
S1	0.5954	0.2821	0.5212	0.6362	0.2683	0.5656	0.6925	0.3191	0.6085	0.5459	0.2741	0.4738	0.0580	0.0461
S2	0.2757	0.1848	0.2271	0.2791	0.1860	0.2302	0.3382	0.1981	0.2860	0.3164	0.2003	0.2637	0.0269	0.0310
S3	0.4175	0.1904	0.3674	0.3416	0.2001	0.2889	0.3821	0.2015	0.3290	0.4419	0.2063	0.3876	0.0367	0.0322
S4	0.3891	0.2735	0.3171	0.3843	0.2648	0.3146	0.3864	0.2771	0.3135	0.4112	0.2857	0.3360	0.0343	0.0444
S5	1.2280	0.6563	1.0553	1.2288	0.6540	1.0567	1.2255	0.6627	1.0511	1.2737	0.7096	1.0869	0.1137	0.1081
S6	0.5121	0.1924	0.4614	0.3914	0.1895	0.3416	0.4319	0.2243	0.3729	0.5092	0.2063	0.4549	0.0436	0.0327
S7	0.9146	0.4520	0.7957	0.9115	0.4339	0.7974	0.9068	0.4337	0.7927	0.9424	0.4677	0.8193	0.0857	0.0720
S8	1.9719	1.0290	1.7011	1.7715	0.8792	1.5401	1.7415	0.8298	1.5232	1.7024	0.8448	1.4801	0.1670	0.1444
S9	1.6295	0.9304	1.3846	1.7079	0.9785	1.4504	1.7170	0.9596	1.4645	1.7041	0.9307	1.4591	0.1540	0.1531
S10	1.4080	0.7442	1.2121	1.5141	0.7989	1.3039	1.4499	0.7762	1.2457	1.5524	0.8532	1.3279	0.1361	0.1279

Table B12: Mine 15 roof rock Event 3 spectral data and quartz mass.

Event 3														
	Scan 1			Scan 2			Scan 3			Scan 4				
Sample ID	Quartz Peak Area	Kaolinite Peak Area	Corrected Quartz Peak Area	Quartz Peak Area	Kaolinite Peak Area	Corrected Quartz Peak Area	Quartz Peak Area	Kaolinite Peak Area	Corrected Quartz Peak Area	Quartz Peak Area	Kaolinite Peak Area	Corrected Quartz Peak Area	Quartz Mass (mg)	Expected Quartz Mass (mg)
S1	0.7569	0.2800	0.6832	0.6798	0.2523	0.6134	0.7374	0.2423	0.6736	0.7612	0.2518	0.6949	0.0713	0.0414
S2	0.4324	0.1950	0.3811	0.3576	0.1736	0.3119	0.3931	0.1964	0.3414	0.4676	0.1937	0.4166	0.0388	0.0306
S3	0.5254	0.1859	0.4765	0.4540	0.1851	0.4053	0.4924	0.1901	0.4423	0.5732	0.1977	0.5212	0.0493	0.0306
S4	0.5323	0.2650	0.4625	0.5465	0.2700	0.4755	0.5181	0.2701	0.4470	0.5464	0.2651	0.4766	0.0498	0.0431
S5	1.2624	0.6017	1.1040	1.4392	0.7123	1.2518	1.3019	0.6208	1.1385	1.4696	0.7164	1.2811	0.1277	0.1068
S6	0.5391	0.1987	0.4868	0.4141	0.1823	0.3661	0.4070	0.1967	0.3552	0.4989	0.2211	0.4407	0.0441	0.0322
S7	0.9417	0.4603	0.8206	0.8597	0.4006	0.7542	0.9397	0.4431	0.8231	0.8959	0.4480	0.7780	0.0849	0.0706
S8	1.8388	0.9445	1.5902	1.7832	0.8939	1.5480	1.6519	0.8087	1.4391	1.5977	0.7803	1.3924	0.1596	0.1381
S9	1.6435	0.9317	1.3983	1.7190	0.9860	1.4596	1.6434	0.8939	1.4082	1.7137	0.9294	1.4691	0.1534	0.1508
S10	1.5129	0.8135	1.2988	1.4913	0.8039	1.2797	1.4825	0.8006	1.2718	1.5432	0.8550	1.3182	0.1382	0.1319

Table B13: Mine 28 field sample PVC filter data.

Mine 28 Field Samples														
Sample ID	Filter Pre-Weigh	Filter Post-Weigh	Dust Mass (mg)	Corrected Dust Mass (mg)	Mean Corrected Quartz Spectral Peak	Mean Kaolinite Spectral Peak	Mean Quartz Mass (mg)	Corrected Quartz Mass (Predicted)	Expected Quartz Mass from 7603 % (mg)	NIOSH Method 7603 Quartz %	Quartz % from CPDM Samples	Corrected Quartz Spectral Peak Std Dev	Kaolinite Spectral Peak Std Dev	Quartz Mass Std Dev (mg)
S1	6.927	8.243	1.316	1.2975	0.7161	0.4554	0.0766	0.0745	0.0968	7.46%	5.74%	0.0854	0.0247	0.0073
S2	6.917	8.991	2.074	2.0555	0.5117	0.6296	0.0547	0.0526	0.0602	2.93%	2.56%	0.0578	0.0472	0.0058
S3	7.041	8.282	1.241	1.2225	0.6336	0.3152	0.0678	0.0656	0.1071	8.76%	5.37%	0.0516	0.0127	0.0050
S4	7.152	8.215	1.063	1.0445	0.8089	0.3904	0.0865	0.0844	0.1055	10.10%	8.08%	0.0708	0.0214	0.0059
S5	7.514	9.504	1.990	1.9715	1.5448	0.7038	0.1653	0.1631	0.2011	10.20%	8.27%	0.1486	0.0712	0.0063
S6	6.846	7.686	0.840	0.8215	0.2067	0.2480	0.0221	0.0200	0.0145	1.76%	2.43%	0.0436	0.0161	0.0021
S7	6.938	9.367	2.429	2.4105	0.6243	0.8360	0.0668	0.0646	0.0800	3.32%	2.68%	0.0596	0.0778	0.0021
S8	7.019	8.387	1.368	1.3495	0.3682	0.4623	0.0394	0.0372	0.0375	2.78%	2.76%	0.0337	0.0109	0.0021
S9	7.818	8.905	1.087	1.0685	0.9899	0.4615	0.1059	0.1037	0.1009	9.44%	9.71%	0.0423	0.0247	0.0031
S10	7.236	8.418	1.182	1.1635	0.3874	0.5142	0.0414	0.0393	0.0351	3.02%	3.38%	0.0294	0.0199	0.0026

Table B14: Mine 28 field samples Event 1 spectral data and quartz mass.

Event 1														
	Scan 1			Scan 2			Scan 3			Scan 4				
Sample ID	Quartz Peak Area	Kaolinite Peak Area	Corrected Quartz Peak Area	Quartz Peak Area	Kaolinite Peak Area	Corrected Quartz Peak Area	Quartz Peak Area	Kaolinite Peak Area	Corrected Quartz Peak Area	Quartz Peak Area	Kaolinite Peak Area	Corrected Quartz Peak Area	Quartz Mass (mg)	Expected Quartz Mass (mg)
S1	0.8265	0.4497	0.7082	0.8768	0.4532	0.7575	0.9307	0.4692	0.8072	0.7653	0.3984	0.6604	0.0784	0.0968
S2	0.7454	0.5781	0.5933	0.6982	0.6629	0.5238	0.7190	0.6490	0.5482	0.7126	0.6058	0.5531	0.0593	0.0602
S3	0.7400	0.3224	0.6552	0.7288	0.2916	0.6521	0.7604	0.3236	0.6753	0.7260	0.3051	0.6457	0.0703	0.1071
S4	0.9072	0.3834	0.8063	1.0263	0.4154	0.9170	0.9180	0.3765	0.8189	0.9175	0.3751	0.8188	0.0899	0.1055
S5	1.6021	0.6202	1.4389	1.7215	0.6626	1.5471	1.7872	0.7052	1.6016	2.0027	0.8071	1.7904	0.1706	0.2011
S6	0.2955	0.2315	0.2346	0.2205	0.2717	0.1490	0.1959	0.2430	0.1320	0.2635	0.2470	0.1985	0.0191	0.0145
S7	0.9209	0.9383	0.6740	0.8248	0.8991	0.5882	0.7081	0.7221	0.5181	0.8321	0.8432	0.6102	0.0639	0.0800
S8	0.5249	0.4730	0.4005	0.4429	0.4787	0.3170	0.4462	0.4547	0.3266	0.4403	0.4619	0.3187	0.0364	0.0375
S9	1.0482	0.4502	0.9297	1.0784	0.4843	0.9510	1.1037	0.4533	0.9844	1.0448	0.4366	0.9299	0.1015	0.1009
S10	0.5235	0.5553	0.3774	0.4838	0.5357	0.3428	0.4694	0.5105	0.3350	0.4930	0.5265	0.3544	0.0377	0.0351

Table B15: Mine 28 field samples Event 2 spectral data and quartz mass.

Event 2														
	Scan 1			Scan 2			Scan 3			Scan 4				
Sample ID	Quartz Peak Area	Kaolinite Peak Area	Corrected Quartz Peak Area	Quartz Peak Area	Kaolinite Peak Area	Corrected Quartz Peak Area	Quartz Peak Area	Kaolinite Peak Area	Corrected Quartz Peak Area	Quartz Peak Area	Kaolinite Peak Area	Corrected Quartz Peak Area	Quartz Mass (mg)	Expected Quartz Mass (mg)
S1	0.8273	0.4757	0.7021	0.6591	0.4080	0.5517	0.7251	0.4694	0.6016	0.7686	0.4655	0.6461	0.0669	0.0968
S2	0.5891	0.7104	0.4022	0.6064	0.6377	0.4386	0.6141	0.6783	0.4356	0.6068	0.5366	0.4656	0.0466	0.0602
S3	0.6620	0.3255	0.5764	0.6768	0.3297	0.5900	0.6755	0.3256	0.5898	0.5978	0.3028	0.5181	0.0608	0.1071
S4	0.8281	0.3933	0.7246	0.8101	0.3890	0.7077	0.8046	0.4012	0.6990	0.9056	0.4275	0.7931	0.0782	0.1055
S5	1.4738	0.6308	1.3078	1.6013	0.6921	1.4192	1.6065	0.6953	1.4235	1.9142	0.8307	1.6956	0.1563	0.2011
S6	0.2665	0.2779	0.1933	0.2414	0.2441	0.1772	0.3045	0.2494	0.2388	0.3411	0.2179	0.2838	0.0239	0.0145
S7	0.8870	0.8325	0.6679	0.8056	0.8259	0.5882	0.7728	0.7349	0.5794	0.9425	0.9348	0.6965	0.0677	0.0800
S8	0.4972	0.4725	0.3729	0.4916	0.4447	0.3746	0.4859	0.4730	0.3614	0.5249	0.4495	0.4066	0.0405	0.0375
S9	1.0839	0.4320	0.9702	1.1224	0.4557	1.0024	1.1971	0.5097	1.0630	1.1329	0.4562	1.0128	0.1083	0.1009
S10	0.5270	0.5053	0.3940	0.5274	0.4857	0.3995	0.5513	0.5021	0.4192	0.5522	0.5318	0.4123	0.0435	0.0351

Table B16: Mine 28 field samples Event 3 spectral data and quartz mass.

Event 3														
	Scan 1			Scan 2			Scan 3			Scan 4				
Sample ID	Quartz Peak Area	Kaolinite Peak Area	Corrected Quartz Peak Area	Quartz Peak Area	Kaolinite Peak Area	Corrected Quartz Peak Area	Quartz Peak Area	Kaolinite Peak Area	Corrected Quartz Peak Area	Quartz Peak Area	Kaolinite Peak Area	Corrected Quartz Peak Area	Quartz Mass (mg)	Expected Quartz Mass (mg)
S1	0.8484	0.4641	0.7263	0.9697	0.4622	0.8481	0.9226	0.4730	0.7981	0.9119	0.4768	0.7864	0.0845	0.0968
S2	0.7034	0.6602	0.5297	0.7171	0.6487	0.5464	0.7027	0.6110	0.5419	0.7138	0.5769	0.5620	0.0583	0.0602
S3	0.7361	0.2948	0.6585	0.7711	0.3275	0.6849	0.7336	0.3143	0.6509	0.7902	0.3197	0.7060	0.0722	0.1071
S4	0.8698	0.3414	0.7799	0.9936	0.4052	0.8870	1.0164	0.3993	0.9113	0.9428	0.3772	0.8436	0.0915	0.1055
S5	1.7397	0.6901	1.5580	2.0124	0.8130	1.7984	1.5807	0.6192	1.4177	1.7181	0.6792	1.5394	0.1688	0.2011
S6	0.2891	0.2422	0.2253	0.2542	0.2648	0.1845	0.2582	0.2485	0.1928	0.3328	0.2379	0.2702	0.0233	0.0145
S7	0.8696	0.8663	0.6417	0.7731	0.7451	0.5771	0.8063	0.7561	0.6073	0.9886	0.9333	0.7430	0.0687	0.0800
S8	0.5533	0.4580	0.4327	0.4898	0.4714	0.3658	0.4900	0.4486	0.3720	0.4914	0.4617	0.3699	0.0412	0.0375
S9	1.0956	0.4512	0.9768	1.1824	0.5074	1.0489	1.1596	0.4636	1.0376	1.0869	0.4384	0.9716	0.1079	0.1009
S10	0.5697	0.5143	0.4344	0.5283	0.5198	0.3915	0.5128	0.4975	0.3819	0.5342	0.4861	0.4063	0.0432	0.0351